

POLITECNICO DI TORINO

Master's Degree
in Biomedical Engineering

Evaluation of low-cost optical motion capture systems for the
assessment of parameters in neurologic rating scales



Supervisor:
Prof.ssa Gabriella Olmo

Correlator:
Dr. Roberto Nerino, CNR-IEIIT
Dr.ssa Claudia Ferraris, CNR-IEIIT

Author:

Valerio Votta 245849

Limits, like fears, are often just an illusion.

Abstract

The neurologic diseases are very diffuse nowadays and, with their progression, the mobility is one of the most affected functions, condition that results very disabling for the patient. The evaluation of the kinematic parameters is thus fundamental in order to follow the progression of the illness and, different scales are utilized in order to evaluate the general condition of the patient. Their main limitation derives from the lack of physical quantities and the great inter-variability of the subjective evaluations of the physicians, but, giving a quantitative characterization of the loss of mobility is essential to set the correct therapy and make the quality life of the patient better. In this context, the aim of the work is to find a reliable and cheap system of human motion tracking, applied to neurologic scales, in order to extract the most important parameters for the clinical evaluation. Different systems have been evaluated: the software development kit (SDK) NuiTrack with three RGB-D cameras, the Intel D415, the Intel D435 and the Orbbec Astra Pro, juxtaposed to the Microsoft Kinect Azure and his own software for the 3D tracking. The first part of the thesis is focused on the implementation of different custom MATLAB code for the handling of the data provided by the different systems: check of the correctness of the data, representation of the human model reconstructed, analysis of the kinematic information provided. It have been made a statistical and qualitative evaluation of the three cameras interfaced with the SDK NuiTrack in order to have the best couple NuiTrack-camera, highlighting the Orbbec Astra Pro as the best camera to be used with NuiTrack, and the couple Azure Kinect-Kinect SDK as similar setup in terms of statistical rating. The validation of the systems has been made with the optoelectronic system BTS SMART-DX, considered the gold standard in motion capture. We have performed a set of tasks that allowed to show the behaviour in different exercises widely used in the clinic rating scales. The results showed that the Orbbec Astra Pro, joint with NuiTrack, allows to have highly correlated information with the BTS system, (mean Pearson's correlation coefficient near to 1), especially about the angles of the limbs, about time and frequency domain parameters, and a comparable statistical analysis of the Center of Pressure in the static exercise. The results of Kinect Azure, instead, showed that, during the synchronous acquisition with the BTS system, a destructive interference occurred, making the recovering of the joints coordinates impossible and, consequently, the validation of the camera. In conclusion, the Orbbec Astra Pro has turned out to be a reliable system for both motion capture and its parameters, but in order to confirm the possibility of using it as a system widely exploitable in the assessments of pathological subjects, further researches will be necessary, especially by testing directly on the patients.

Abstract

Le malattie neurologiche sono molto diffuse al giorno d'oggi e, con la loro progressione, la mobilità è una delle funzioni più colpite, condizione che risulta molto invalidante per il paziente. La valutazione dei parametri cinematici è quindi fondamentale per seguire la progressione della malattia e, diverse scale, vengono utilizzate per valutare le condizioni generali del paziente. La loro principale limitazione deriva dalla mancanza di quantità fisiche e dalla grande inter-variabilità delle valutazioni soggettive dei medici, ma, dare una caratterizzazione quantitativa della perdita di mobilità è essenziale per impostare la terapia corretta e rendere migliore la qualità di vita del paziente. In questo contesto, l'obiettivo del lavoro è trovare un sistema affidabile ed economico di tracciamento del movimento umano, applicato a scale neurologiche, al fine di estrarre i parametri più importanti per la valutazione clinica. Sono stati valutati diversi sistemi: il kit di sviluppo software (SDK) NuiTrack con tre telecamere RGB-D, la Intel D415, la Intel D435 e la Orbbec Astra Pro, giustapposti alla Microsoft Kinect Azure e il suo software per il tracciamento 3D. La prima parte della tesi è focalizzata sull'implementazione di diversi codici MATLAB personalizzati per la gestione dei dati forniti dai diversi sistemi: verifica della correttezza dei dati, ricostruzione del modello umano ricostruito, analisi delle informazioni cinematiche fornite. È stata fatta una valutazione statistica e qualitativa delle tre telecamere interfacciate con l'SDK NuiTrack al fine di avere la migliore coppia NuiTrack-telecamera, mettendo in evidenza la Orbbec Astra Pro come la migliore telecamera da utilizzare con NuiTrack e la coppia Azure Kinect- Kinect SDK come configurazione simile in termini di valutazione statistica. La validazione dei sistemi è stata effettuata con il sistema optoelettronico BTS SMART-DX, considerato lo standard di riferimento nella motion capture. Abbiamo eseguito una serie di attività che hanno permesso di mostrare il comportamento in diversi esercizi ampiamente utilizzati nelle scale di valutazione della clinica. I risultati hanno mostrato che Orbbec Astra Pro, unito a NuiTrack, consente di avere informazioni altamente correlate con il sistema BTS (coefficiente di correlazione di Pearson vicino a 1), in particolare sugli angoli degli arti e sui parametri del dominio del tempo e della frequenza, e un'analisi statistica comparabile del centro di massa nell'esercizio statico. I risultati di Kinect Azure, invece, hanno mostrato che, durante l'acquisizione sincrona con il sistema BTS, si è verificata un'interferenza distruttiva, rendendo impossibile il recupero delle coordinate articolari e, di conseguenza, la validazione della telecamera. In conclusione, Orbbec Astra Pro si è rivelato un sistema affidabile sia per la motion capture che per i suoi parametri, ma per confermare la possibilità di utilizzarlo come sistema ampiamente sfruttabile nelle valutazioni di soggetti patologici, saranno necessarie ulteriori ricerche, in particolare testando direttamente sui pazienti.

ACKNOWLEDGEMENT

Desidero ringraziare la Prof.ssa Olmo per la disponibilità nel seguire il lavoro di tesi durante i mesi e per il supporto ricevuto.

Un grande ringraziamento va al team del CNR, il Dr. Nerino, la Dr.ssa Ferraris, il Dr. Chimienti e il Dr. Pettiti per avermi permesso di lavorare a stretto contatto con loro nei laboratori del CNR, per avermi fornito tutto ciò di cui avevo bisogno durante questi mesi di tesi, e per avermi guidato nelle analisi che sono state condotte.

A Luca, Matteo, Beppe, Gian, Tony, un grande ringraziamento, per essere stati sempre presenti, per avermi fatto vivere degli anni fantastici, per avermi aiutato e per essere da sempre amici veri.

Ai miei genitori, non basteranno mai abbastanza ringraziamenti per avermi permesso di realizzare tutto ciò, per avermi sempre assecondato ed esser stati così presenti anche se lontani.

A Francesca, per essere stata la mia forza da quando è arrivata nella mia vita, per essermi stata accanto in ogni modo, per amarmi con tutta sé stessa ogni giorno, per avermi sostenuto in ogni momento e per aver condiviso con me questo periodo surreale e difficile, dandomi sempre conforto.

Table of contents

Introduction	1
1. Neurologic disorders	4
1.1 Cerebrovascular diseases	4
1.2 Parkinson's disease	4
1.3 Multiple sclerosis	8
2. Methodologies	10
2.1 Non-optical systems	10
2.1.1 Electromagnetic sensors.....	11
2.1.2 Inertial sensors.....	11
2.2 Optical systems	13
2.2.1 Marker-based optical systems	13
2.2.2 Marker-free optical systems	20
2.3 Experimental setup	22
2.3.1 Equipment	22
2.4 Data Handling.....	25
2.5 Experiments conducted.....	31
2.5.1 Preliminary tests	32
2.5.2 Validation of the system.....	34
2.6 Leg-agility Parameters.....	42
2.7 Kinect Azure Insight.....	46
3. Preliminary Results	48
3.1 Intel D415-D435	48
3.1.1 Static standing task in artificial light conditions.....	48
3.1.2 Static standing task in natural light conditions	50
3.1.3 Standing dynamic Task in artificial light conditions.....	52
3.1.4 Seated dynamic task in artificial light conditions	53
3.2 Intel D415-Orbbec Astra Pro	55
3.2.1 Static standing task in artificial light conditions.....	55
3.2.2 Static standing task in natural light conditions	57
3.2.3 Standing dynamic task.....	57
3.2.4 Seated dynamic task.....	58
3.3 Orbbec Astra Pro-Azure Kinect	59
3.3.1 Orbbec Astra Pro-Azure Kinect Static Standing task	59
3.3.2 Orbbec Astra Pro-Azure Kinect Standing dynamic task	61
3.3.3 Orbbec Astra Pro-Azure Kinect seated static task.....	61
4. Validation results	64
4.1 Orbbec Astra Pro results	64

4.1.1 Static standing task	64
4.1.2 Standing dynamic task:.....	70
4.1.3 Seated static task	73
4.1.4 Seated dynamic task.....	78
4.1.5 Increasing velocity task.....	78
4.1.6 Leg-agility.....	82
4.2 Kinect Azure results.....	88
4.2.1 IR Analysis: BTS Camera Area.....	90
4.2.1 Depth Analysis: BTS Camera Area	90
4.2.3 Depth Analysis: Wall Area.....	91
5. Conclusions.....	93
LIST OF SYMBOLS	95
BIBLIOGRAPHY.....	96

List of Tables

Table 1.1- Webster Gravity Valuation of Parkinson’s disease	5
Table 1.2- UPDRS Leg-agility	6
Table 1.3- UPDRS Get-up from the chair	6
Table 1.4- UPDRS Gait	7
Table 1.5- UPDRS Freezing.....	7
Table 1.6- UPDRS Posture.....	7
Table 1.7- UPDRS Bradykinesia.....	8
Table 1.8- TUG Typical Results	8
Table 1.9- Berg Test	9
Table 2.1- Davis protocol position markers	18
Table 2.2- Cast protocol markers	19
Table 2.3- Camera descriptions	22
Table 2.4- BTS SMART DX-400 Characteristics.....	34
Table 3.1- Static standing results Intel D415-D435 artificial light condition.....	48
Table 3.2- Static standing results Intel D415-D435 Natural light condition	50
Table 3.3- Standing dynamic task results Intel D415-D435 artificial light condition.....	52
Table 3.4- Pearson’s correlation coefficient standing dynamic task Intel D415-D435 artificial light condition	53
Table 3.5- Seated dynamic task results Intel D415-D435 artificial light condition.....	53
Table 3.6- Pearson’s correlation coefficient seated dynamic task Intel D415-D435 artificial light condition	54
Table 3.7- Standing static task results Intel D415-Orbbec artificial light condition	55
Table 3.8- Standing static task results Intel D415-Orbbec Natural light condition	57
Table 3.9- Standing static task results Intel D415-Orbbec artificial light condition	57
Table 3.10- Pearson’s correlation coefficient standing dynamic task Intel D415-Orbbec artificial light condition	58
Table 3.11- Seated static task results Intel D415-Orbbec artificial light condition	58
Table 3.12- Pearson’s correlation coefficient seated dynamic task Intel D415-Orbbec artificial light condition	58
Table 3.13- Pearson’s correlation coefficient standing dynamic task Azure-Orbbec artificial light condition	61
Table 3.14- Pearson’s correlation coefficient seated dynamic task Azure-Orbbec artificial light condition	63
Table 4.1- Variation coefficient BTS-Orbbec	69
Table 4.2- CoP BTS-Orbbec Mean Standard Deviation.....	70
Table 4.3- Pearson’s correlation coefficients standing dynamic task BTS-Orbbec	72
Table 4.4- CoP BTS-Orbbec CV Seated task	77
Table 4.5- CoP BTS-Orbbec Mean Standard Deviation Seated task	78
Table 4.6- Pearson’s correlation coefficients seated dynamic task BTS-Orbbec	78
Table 4.7- Pearson’s correlation coefficients increasing velocity dynamic task BTS-Orbbec.....	80
Table 4.8- Pearson’s correlation coefficients Leg-agility task BTS-Orbbec	83
Table 4.9- Kinematic results of the Leg-agility.....	85

List of Figures

Figure 2.1- Scheme of an accelerometer	11
Figure 2.2- Accelerometer electrical scheme	12
Figure 2.3- Gyroscopes scheme	13
Figure 2.4- DLT scheme	15
Figure 2.5- Marker Occlusion	17
Figure 2.6- Davis protocol markers	18
Figure 2.7- Time of flight camera	21
Figure 2.8- Depth image produced	21
Figure 2.9- Nuitrack joints	23
Figure 2.10- Kinect Azure Joints	24
Figure 2.11- Kinect Azure Mesh	24
Figure 2.12- Table of CoP weights [36]	25
Figure 2.13- Reference system	26
Figure 2.14- Framerate obtained from MATLAB	27
Figure 2.15- Skeleton recovered on MATLAB	28
Figure 2.16- Synchronization with the right elbow	29
Figure 2.17- Chebyshev order 1 low pass filter and example of filtering performed	30
Figure 2.18- CoP sway extracted from one acquisition	31
Figure 2.19- Orbbec and Kinect Azure positioning	32
Figure 2.20- Positions of the camera in the Laboratory	35
Figure 2.21- Markers positions	35
Figure 2.22- BTS skeleton recovered in MATLAB	36
Figure 2.23- Joints labeling BTS	36
Figure 2.24- Local reference systems BTS-Orbbec	38
Figure 2.25- Projections of the local reference systems.	40
Figure 2.26- Example of Boxplot	42
Figure 2.27- Leg agility task angle	43
Figure 2.28- Burg Parametric PSD	45
Figure 2.29- (a)Contour of the STFT (b)Mesh of the STFT	46
Figure 2.30- (a)Depth image of Kinect Azure (b) IR image of Kinect Azure acquisition	47
Figure 3.1- Standard deviation Bar Diagram AP-Axis	49
Figure 3.2- Standard deviation Bar Diagram ML-Axis Static	49
Figure 3.3- Standard deviation Bar Diagram UD-Axis	50
Figure 3.4- Standard deviation Bar Diagram AP-Axis	51
Figure 3.5- Standard deviation Bar Diagram ML-Axis	51
Figure 3.6- Standard deviation Bar Diagram UD-Axis	52
Figure 3.7- Angles representation seated dynamic task Intel D415-D435	54
Figure 3.8- Standard deviation Bar Diagram AP-Axis static standing task Intel D415-Orbbec artificial Light condition	55
Figure 3.9- Standard deviation Bar Diagram ML-Axis static standing task Intel D415-Orbbec artificial Light condition	56
Figure 3.10- Standard deviation Bar Diagram AP-Axis static standing task Intel D415-Orbbec artificial Light condition	56

Figure 3.11- Standard deviation Bar Diagram AP-Axis.....	59
Figure 3.12- Standard deviation Bar Diagram AP-Axis static standing task Azure-Orbbec artificial light condition	60
Figure 3.13- Standard deviation Bar Diagram AP-Axis static standing task	60
Figure 3.14- Standard deviation Bar Diagram AP-Axis static seated task Azure-Orbbec artificial light condition	61
Figure 3.15- Standard deviation Bar Diagram ML-Axis static seated task.....	62
Figure 3.16- Standard deviation Bar Diagram UD-Axis static seated task Azure-Orbbec artificial light condition	62
Figure 4.1- Bodies in the original reference system.....	65
Figure 4.2- Axonometric view of bodies in the common reference system	65
Figure 4.3- Frontal view of the bodies in the same reference system	66
Figure 4.4-a) CoP trend BTS-Orbbec AP-Axis. (b) CoP trend BTS-Orbbec ML-Axis (c) CoP trend BTS-Orbbec UD-Axis	67
Figure 4.5-(a) CoP swing BTS-Orbbec AP-Axis. (b) CoP swing BTS-Orbbec ML-Axis (c) CoP swing BTS-Orbbec UD-Axis	68
Figure 4.6-(a) Boxplot representation Orbbec. (b) Boxplot representation BTS.....	69
Figure 4.7-(a) Right elbows flexion angle BTS-Orbbec aligned. (b) Left elbows flexion angle BTS-Orbbec aligned	70
Figure 4.8-(a) Right Knee flexion angle BTS-Orbbec aligned. (b) Left Knee flexion angle BTS-Orbbec aligned	71
Figure 4.9-(a) Right Elbows flexion angular velocity BTS-Orbbec aligned. (b) Left Elbows flexion angular velocity BTS-Orbbec aligned	72
Figure 4.10- Bodies in the original reference systems	73
Figure 4.11- Axonometric view of the bodies in the common reference system.....	74
Figure 4.12- Frontal view of the bodies in the common reference system.....	74
Figure 4.13-(a) CoP trend BTS-Orbbec AP-Axis Seated task. (b) CoP trend BTS-Orbbec ML-Axis seated task(c) CoP trend BTS-Orbbec UD-Axis seated task.....	75
Figure 4.14-(a) CoP swing BTS-Orbbec AP-Axis seated task. (b) CoP swing BTS-Orbbec ML Axis seated task (c) CoP swing BTS-Orbbec UD-Axis seated task	76
Figure 4.15-(a) Boxplot representation Orbbec. (b) Boxplot representation BTS.	77
Figure 4.16-(a) Right elbows flexion angle increasing velocity BTS-Orbbec aligned. (b) Left elbows flexion angle increasing velocity BTS-Orbbec aligned.....	79
Figure 4.17-(a) Left knee flexion angle increasing velocity BTS-Orbbec aligned. (b) Right knee flexion angle increasing velocity BTS-Orbbec aligned	79
Figure 4.18-(a) Right Elbows flexion angular velocity BTS-Orbbec aligned. (b) Left Elbows flexion angular velocity BTS-Orbbec aligned	81
Figure 4.19-(a) Right Knee flexion angular velocity BTS-Orbbec aligned. (b) Left Knee flexion angular velocity BTS-Orbbec aligned	81
Figure 4.20-(a) Time-frequency mesh of the Orbbec recovered right elbow spectrum. -(b) Time-frequency mesh of the Orbbec recovered right elbow spectrum.	82
Figure 4.21-(a) Right Leg flexion BTS-Orbbec aligned. (b) Left Leg flexion BTS-Orbbec aligned.....	83
Figure 4.22-(a) Left leg flexion Orbbec recovered, with the peaks of the flexions. (b)Left leg flexions, BTS recovered with the peaks of the flexions.	84
Figure 4.23-(a) Right leg flexion Orbbec recovered, with the peaks of the flexions. (b)Right leg flexions, BTS recovered with the peaks of the flexions.	84
Figure 4.24-(a) Time-frequency contour of the Orbbec left leg spectrum. -(b) Time-frequency mesh of the Orbbec left leg spectrum. -(c) Time-frequency contour of the BTS left leg spectrum. -(d) Time-frequency mesh of the BTS left leg spectrum.....	86

Figure 4.25- (a)Time-frequency contour of the Orbbec left leg spectrum. -(b)Time-frequency mesh of the Orbbec recovered left leg spectrum. -(c)Time-frequency contour of the BTS recovered left leg spectrum. -(d)Time-frequency mesh of the BTS recovered left leg spectrum.	86
Figure 4.26- (a) Time-frequency contour of the Orbbec left leg spectrum. -(b) Time-frequency mesh of the Orbbec left leg spectrum. -(c) Time-frequency contour of the BTS left leg spectrum. -(d) Time-frequency mesh of the BTS recovered left leg spectrum	87
Figure 4.27- (a) Time-frequency contour of the Orbbec recovered right leg spectrum. -(b) Time-frequency mesh of the Orbbec recovered right leg spectrum. -(c) Time-frequency contour of the BTS recovered right leg spectrum. -(d) Time-frequency mesh of the BTS recovered right leg spectrum.	87
Figure 4.28- (a) Left Knee flexion angular velocity BTS-Orbbec aligned. (b) Right Knee flexion angular velocity BTS-Orbbec aligned task	88
Figure 4.29- Right elbows angle flexion sway damaged.....	88
Figure 4.30- Left elbows angle flexion sway damaged.....	89
Figure 4.31- (a)Depth image of Kinect Azure (b) IR image of Kinect Azure acquisition	89
Figure 4.32- Kinect Intensity sway	90
Figure 4.33- Kinect Measured Depth	91
Figure 4.34- Kinect Depth Wall Area.....	91

Introduction

Neurologic disorders are one of the most common diseases in the world, representing 3 percent of the total illness in the world [1]. They include all of the illnesses that stroke the central nervous system and the peripheral one. Between them, a big percent of the illnesses are neurodegenerative disorders, which are chronic diseases. They are commonly diagnosed through clinical manifestations of the illness [2] and less commonly with diagnostic biomarkers [3]. The most common diseases are Parkinson's Disease (PD), Alzheimer's Disease and Multiple Sclerosis. These diseases are very disabling with the advance of the illness due to the progressive loss of the neurons in different areas [4].

Between all the consequences of the disease progression, the most affecting on patient's quality life are the ones related with the mobility, like e.g. in the Parkinson's disease where the bradykinesia, that is, the condition of slowness in performing actions, make also the normal activities of the life much more complicated. [5]. It is not yet clear how big is the correlation between the advancement of the disease and the worsening of the mobility condition and a lot of factors can influence the patient's condition [6]. Another consequence it is the impairment of the vestibular system, the apparatus charged of the control of the own perception, that provokes the worsening of the posture [7]: due to this loss of stability it is also very diffuse the danger of falls in the elderly [8] that can induce other problems, individuating that class of people called frail elderly.

For this reason, focusing on the analysis of the mobility and the parameters correlated is fundamental to give answers about the progress of the illness and choose the best therapy to interface with. At this purpose, a large number of medical examinations are involved [9] and different medical scales have been developed and continually renewed, to allow the physician to give evaluations about the current conditions of the patient [10]. There are different approaches proposed that can include tests with biomedical instruments or simply based on the observations made by the physician in respect of certain tasks.

The high number of tests makes possible to classify the degree of severity of the disorder and therefore modify the therapy to reduce the visible effects of the neural damages [11]. Changing the therapy constantly allows making the effects of the illness less impairing improving the patient's quality of life [12].

The main problem of these approaches is that they often depend on the physician who conducts the tests, being him the only evaluator of the score. In this way, there is not only great inter-rater variability [13], but it is also really difficult to see little variations of the general conditions, that could suggest modifying the therapy earlier or to help to prevent accidents in the patients that could make worse the overall status.

Instead, collecting different parameters correlated to the tasks, giving in this way a quantitative assessment, would be helpful to make easier the work of the physician and to describe in a better way the condition of the disease [14][15].

Another problem is represented by the costs of public health deriving from the burden deriving from these diseases [16]. Making the evaluations more dependent on the analytic parameters and quite automatized with different systems, would make possible to produce a telemedicine system, which would permit physicians to follow the patient from home.

The motion capture is thus, highly analyzed in the medical context, to verify how its presence can give aid for the professionals and the patients before all.

Different works have been proposed in the context of evaluating low cost systems [17] in motion capture. In this context, the thesis has the aim of evaluating different RGB-D low-cost systems that can record the human movements, comparing them to the system recognized as the reference tool in the sector, that allow the analysis of all the parameters deriving from the acquisitions giving a powerful tool to the physician.

Then, technologies that are based on different physical phenomena are presented, focusing on their points of strength and points of weakness and how they are capable of providing more or less accurate results.

The thesis is, thus, divided into the following sections:
In the first chapter of the thesis all the most widespread neurodegenerative diseases are introduced, and it's explained how they are evaluated with. The most common tests are briefly exposed highlighting the most interesting kinematic parameters correlated with.

The second chapter presents the state of the art in motion capture and is deepened the different technologies currently available on the market, explaining their operating principles, focusing on their costs, and their main pros and cons. Subsequently, there is an explanation of how the technologies have been evaluated, to find the best set-up between the ones we had available. At the end of the chapter, the chosen set-up has been compared to the gold reference to verify the reliability of the system.

The third chapter is focused on the presentation of the optimal setup we have individuated, making clear the reasons that have convinced us to choose it.

The fourth chapter is focused on the presentation of the results obtained for the chosen setup, interfaced with the BTS Optitrack system. It has been evaluated the static task, to evaluate how the Center of Pressure (CoP) is computed and how his variation in the system reference axes is perceived furnishing statistical results about the task. They have been considered dynamic tasks in different positions, considering also one of the tasks involved in the diagnosis with the UPDRS scale, with the mean to consider how the systems can furnish the kinematic parameters like angles and velocity in the Coronal Plane, Sagittal Plane, and Transversal Plane.

The problematic deriving from the acquisitions are also discussed during the chapter. The last chapter is focused on the conclusions of the work, explicating how it will be followed up and the possible developments.

The fifth chapter gives the conclusions of the work, commenting on the results of the previous chapters, and the possible developments that the work could have.

1. Neurologic disorders

Neurologic disorders are referred to all the diseases of the nervous system. They can be caused by different factors and can be strokes or neurodegenerative disorders.

Generally, the cerebrovascular diseases commonly take to the strokes, in which the most common spread are ischemic stroke or ictus, cerebral embolism, and intracerebral hemorrhage. In the neurodegenerative disorders are included all the diseases of the central and nervous system that affect the neurons taking them to death.

They can be identified chronic disorders like Parkinson's Disease, Alzheimer's Disease, and Multiple sclerosis, which have different etiological causes and acute infections like neuroinfectious diseases, generally caused by external pathological agents.

During this chapter, it will be explicated the most widespread diseases, in a discursive manner treating: the diagnosis, etiology, prevalence in society, management of the illness and treatment.

1.1 Cerebrovascular diseases

They are referred to the neurologic deficits that are generally sudden. They can derive from different causes like **cerebral infarction**, caused by thromboembolism due to the parietal injury or **cerebral embolism** due to cardiac failures [\[18\]](#)

Depending on how they are treated and by their gravity they can affect the CNS in different ways. The temporary absence of nutrients provided by the blood can damage permanently or temporarily the nerves.

After the strokes, it's fundamental monitoring and following the patient with the rehabilitation.

The **Canadian Neurological scale** [\[19\]](#) is generally used to evaluate the conditions of the patient post-stroke. With this scale are evaluated the deficits in different functions among which the motor conditions. It's asked to perform different tasks with arms and legs evaluating how the patient gives the response to the tests.

So, also in this case provide automatized tools can be important for the patients that can recover their motor functions with the help of the physiotherapist but also in their autonomy.

1.2 Parkinson's disease

Parkinson's Disease (PD) is a neurodegenerative disorder that is mainly characterized by motor problems like freezing. It's a degeneration of the dopaminergic neurons involved in the

extrapyramidal motor system. Due to this, there is a decrease in dopamine that should be in balance with the acetylcholine [20].

This system is made by basal ganglia linked with the motor cortex, the thalamus, and the cerebellum. This network can modify the activity of the pyramidal beam and so on the spinal motor system. There are many triggering factors like the use of drugs interrupting the dopaminergic functions, or CO and heavy metals poisoning.

The clinic manifestations can occur between 40 and 70 years of age. The most commons are akinesia with freezing, rigidity, wrong posture, tremor in the rest condition, bradykinesia, deterioration of the writing, difficulty in standing up from a chair.

The patient has the compromising of the capacity in starting the movements, fulfilling precision movements. In the condition of rest, he has the so-called tremor at rest depending on his emotional condition that ends when he starts one intentional movement. The base therapy for the Parkinson is made by L-dopa that copes at the loss of dopamine that improves the kinetic condition of the patient.

It's important to set correctly the therapy to have better efficiency and decrease the collateral effects or the development of drug resistance. The state of the Parkinson is diagnosticated with the objective exams in which is essential to verify the tremor at rest and the rigidity.

Different tests have been proposed as the Webster rating scale [21] or the UPDRS [22] proposed by Movement Disorder society. These tests can furnish the level of progression of the illness and the response to the therapy.

The Webster rating scale parameters are resumed in **Table 1.1**.

Table 1.1-Webster Gravity Valuation of Parkinson's disease		
Webster gravity valuation of the Parkinson's disease		
I.	Hands bradykinesia	II. Rigidity
III.	Posture	IV. Commuter movements of the arms
V.	Gait	VI. Tremor
VII.	Facial mimic	VII. Seborrhea
IX.	Phonation	X. Self-Sufficiency

The UPDRS is divided into 4 parts: the first part focusing on the non-motor experience, the second one on the motor experience, the third part on the general valuation of the motor capability and the last one on the motor complication. Each proposed task has the instruction to be performed and can be addressed only to the patient, to the researcher or both. There are 5 grades of severity proposed by the scale, where 0 is the least serious level of the illness and 4 is the greatest one.

In this context we were interested in analyzing the most interesting tasks of the third chapter of the scale trying to give an important aid for the tests proposed, trying to adapt our system to them.

Furthermore, analyzing the tasks it's clear how they are pretty qualitative and little quantitative and depending on the subjectivity of the examiner. It would be innovative to enrich

the tasks with physical quantities extracted during the tasks. In order to do this, we analyzed how low-cost systems can provide these quantities to the physician.

The considered tasks are summarized in **Table 1.2**, **Table 1.3**, **Table 1.4**, **Table 1.5**, **Table 1.6** and **Table 1.7**.

Table 1.2-UPDRS Leg-agility

3.8	<i>LEG-AGILITY</i>
Instruction	The patient is positioned on a chair, lifting up one leg for time for 10 times as high and as fast as possible
Rating	0 Normal: performed correctly 1 Minimum: one or more interruptions, minimum slowdown, decrease of the amplitude finishing the test 2 Slight: 3 to 5 interruptions, slight slowdown, decrease of the amplitude in the middle of the test 3 Moderate: > than 5 interruptions, moderate slowdown, decrease of the amplitude at the start 4 Serious: impossibility to perform the task

Table 1.3-UPDRS Get-up from the chair

3.9	<i>GET-UP FROM THE CHAIR</i>
Instruction	The patient is positioned on a chair with armrests, with the arm crossed on the chest; it's asked to get-up with the arm crossed trying maximum three times, moving ahead on the chair if he didn't perform in a first way for maximum two times or helping himself with the armrests for maximum one time if he didn't perform the previous ones.
Valuation	0 Normal: ability to get-up with no problems. 1 Minimum: ability to get-up slowly with no armrests. 2 Slight: ability to get-up with the armrests. 3 Moderate: help with the armrests but with the trend to fall. 4 Serious: inability to get-up

Table 1.4-UPDRS Gait

3.10	<i>GAIT</i>
Instruction	The patient must walk for 10 meters then turn around and come back towards the examiner.
Valuation	0 Normal: performed correctly 1 Minimum: can walk with some problems 2 Slight: can walk but with substantial problems 3 Moderate: can't walk without help of a support 4 Serious: can't walk without help of a person

Table 1.5-UPDRS Freezing

3.11	<i>FREEZING</i>
Instruction	During the walk observation of episodes of freezing
Valuation	0 Normal: no freezing 1 Minimum: one episode of freezing during the start or crossing a door 2 Slight: more than one episode during the start or crossing a door 3 Moderate: one episode during the linear walk 4 Serious: more than one episode during the linear walk

Table 1.6-UPDRS Posture

3.12	<i>POSTURE</i>
Instruction	The posture of the patient when he's up, during the walk trying to correct it during the test.
Valuation	0 Normal: no problems. 1 Minimum: not perfect, but normal for the elder age. 2 Slight: flexion or pending on one side 3 Moderate: curve, not normal 4 Serious: flexion and evident pending on one side.

Table 1.7-UPDRS Bradykinesia

3.12	<i>BRADYKINESIA</i>	
Instruction	Considerations about the rapidity of general movements.	
Valuation	0	Normal: no problems.
	1	Minimum: global slowness
	2	Slight: slight slowness
	3	Moderate: moderate slowness
	4	Serious: serious slowness

1.3 Multiple sclerosis

Multiple sclerosis (MS) is characterized by the gradual loss of the neuron membrane, responsible for the isolation, the myelin. The demyelination occurs in different regions of the central nervous system focusing on the white matter. [23]

The main characteristic of the disease is recurrent episodes of neurological disorders with random intervals with the progressive recovery of the functions. From the point of view of the movements, the patient can suffer difficulty in the gait, in the coordination of the arms that are hard to move and diffuse tremor.

There is no specific treatment of the illness, but generally, it's aimed to mitigate the gravity of the acute attacks.

The exams of the MS are based principally on magnetic resonance imaging, but also foresee the analysis of the coordination, of the plantar response in the movements but there aren't specific tests to be performed. Different studies have focused on the utility of the Berg test [24] and the Timed Up and Go test [25], which are general tests for evaluating the mobility and predictors of Parkinson and Sclerotic patients at risk to fall.

The **Timed up and go test (TUG)** foresees the patient positioned in a sitting position on a chair with the armrests. It's required to stand up and go towards a marker positioned 3 meters from the chair. After reaching the objective the patient must come back and sit again. The time involved to perform the task is the parameter of the test and it's evaluated to give the condition of the patients. The normal values of the test divided by age are reported in **Table 1.8**.

Table 1.8-TUG Typical Results

<i>Age group</i>	<i>Time in seconds (95% Confidence Interval)</i>
60-69 years	8.1 (7.1-9.0)
70-79 years	9.2 (8.2-10.2)
80-99 years	11.3(10.0-12.7)

The **Berg** test has 5 levels of severity where the first level highlights the impossibility to perform the tasks without help and the last one is the total independence. The most interesting tasks in our thesis are resumed in **Table 1.9**.

Table 1.9-Berg Test

Berg Test	
Instructions	<ul style="list-style-type: none"> • Sitting position to standing position: the patient should try to stand up without using the hands for the support • Standing positions with no support: the patient should try to stand up for 2 minutes. • Standing position to sitting position: the patient should try to sit without using the hands for the support • Standing position with eyes closed: the patient should try to close the eyes and stay still for 10 s. • Standing position with feet together: the patient should try to stand up keeping the feet together. • Reaching forward with outstretched arm: the patient should try to take the arm in 90 degrees position and stretch the fingers the most he can. • Place foot alternatively on a step/stool: the patient should try to place the foot four times. • Standing position on one leg: the patient should try to stay still on one leg.

2.Methodologies

The process of capturing the movement is called motion capture or *Mocap* and it's possible to execute it with different systems. These instruments can be involved in a very wide field of applications as they can extrapolate a large number of parameters from a single acquisition.

The widespread systems can be an optical type or non-optical type. The first ones capture the scene and make possible to extrapolate the joints from the frames captured. The latter, instead, are based on different physical phenomena and they give back the parameters already measured.

In the first part of the chapter will be exposed to the state of the art of the different technologies currently used. Subsequently, the most used systems will be exposed explaining what they are based on, highlighting their pros and cons.

The most interesting parameters used to evaluate a system in motion capture depend on the application what they've been thought for, but generally, they can be expressed in term of:

- **Accuracy:** how the measurements are close to the real value of the object measured.
- **Jitter:** how the measurements are close to each other, in other terms how they are variable.
- **Drift:** the derivation of the measurements when the object measured is stationary.
- **Lag:** time that elapses between the measurements and the result provided.
- **Update rate:** how often the system updates the measurement.
- **Interference and noise:** how much the environment intrudes in the measurements and how the system is sensitive to it.
- **Price.**
- **Encumbrance**

Lastly, it will be presented the system we had available and will be explicated the methodologies used in order to evaluate our systems.

2.1 Non-optical systems

The non-optical systems are used to evaluate directly the kinematic parameters avoiding the pass between the capture of the image and their extrapolation from it. There are mainly three types of sensors utilized in motion capture: electromagnetic sensors, inertial sensors, and electromechanical sensors.

2.1.1 Electromagnetic sensors

These sensors are based on the magnetic field generated by the current: the emitter is made by three orthonormal coils run by a current, that generate the orthogonal magnetic fields according to the Ampère-Laplace Law (**Equation 2.1**)

Due to the law, it's computed the magnetic field produced in a close circuit run by a current.

$$\mathbf{B} = \frac{\mu_0 i}{4\pi} \oint \frac{d\mathbf{s} \times \mathbf{u}_r}{r^2} \quad (2.1)$$

According to **Equation 2.1**, the magnetic field is orthogonal to the axis of the circuit and its value it's inversely proportional to the distance from the circuit. Using three orthonormal coils it's possible to obtain the magnetic fields on three axes orthogonal between them that individuate a 3D system of coordinate.

The sensor instead has three orthogonal coils that measure the intensity of the three fields generated giving back the positions and the orientations from the emitter.

These systems have good reliability and their costs allow to build a system quite complete. The main problems derive from the sensibility of all of the ferromagnetic elements present in the acquisition room. Another problem can be represented by the reduced range of activity of the system, due to decreasing with the square of the distance.

2.1.2 Inertial sensors

The inertial sensors use the physical quantities as acceleration or angular velocity that accomplish physical law. Instead of the classical derivation in order to obtain the velocities and the acceleration they are based on the double integration starting from the accelerations to go back up until the positions.

According to what they are measuring they are divided in:

- **Accelerometers**

They are based on Newton's 2nd law, with which knowing the mass of the object and the force applied on it it's possible to find its acceleration [26]. In order to do this, it's possible to simplify the functioning of the accelerometer with a 2nd order system.

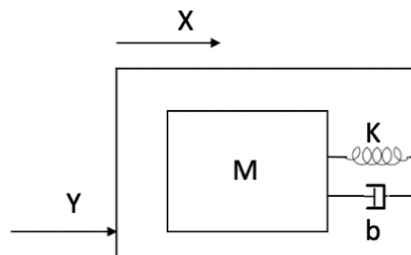


Figure 2.1- Scheme of an accelerometer

The system is governed by these two equations that describe the motion:

$$M \frac{d^2 x_m}{dt^2} = -b \frac{dx}{dt} - Kx \quad (2.2)$$

$$M \frac{d^2 x}{dt^2} + b \frac{dx}{dt} + Kx = -M \frac{d^2 y}{dt^2} \quad (2.3)$$

At regime it's the deformation of the spring it's proportional to the acceleration. The elongation of the spring it's transformed then by the sensor in a quantity with which to obtain the acceleration of the system. According to the transduction are defined different types of accelerometers as piezoresistive, capacitive or ferromagnetic.

One of the most used transductions from acceleration to voltage can be given by the Wheatstone bridge. When there is no acceleration the four resistances have the same value and the bridge is balanced. When an acceleration occurs, the resistance between R_a and R_b changes and in the middle of the bridge it's generated an unbalance tension given as output. Measuring it, it's possible to know the acceleration that occurred in the bridge.

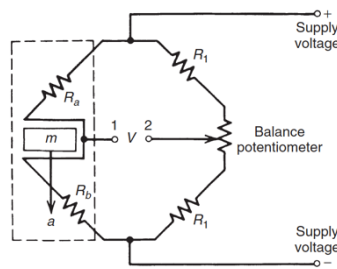


Figure 2.2-Accelerometer electrical scheme

The problems of the accelerometers derive from the offset of the sensors that when they can take to saturation of the system if not correctly conditioned and provide wrong measures. Furthermore, they are relatives to the limb segment they are connected with and provide a complete measurement that can be expensive and with a lot of encumbrances.

- **Gyroscopes**

Nowadays the most common types are the MEMS gyroscopes, that is to say, microelectromechanical systems [27].

They are able to compute the angular velocity in the axis in which it's used independently by a fixed reference system. Are used the systems of 2nd order with the springs positioned in the mass of the gyroscopes in order to produce tensions or other electric quantities from the movements.

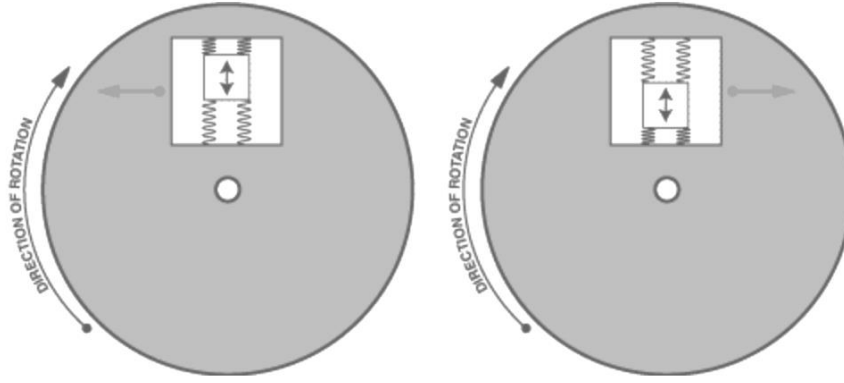


Figure 2.3-Gyroscopes scheme

Thus, the final output of the gyroscopes it's the angular velocity that can be integrated in order to build the angular positions.

$$\dot{\theta}(t) = \frac{d\theta}{dt} \quad (2.4)$$

$$\theta(t) = \int_0^T \dot{\theta} dt \quad (2.5)$$

Being based on a discrete-time acquisition the operations of integration become a series.

$$\theta(t) = \sum_0^t \dot{\theta}(t)T \quad (2.6)$$

Where T is the interval time.

The main problems of the gyroscopes are introduced by the drift because they are based on the temporal interval and when the changes are too fast the systems don't see the variations.

2.2 Optical systems

The optical systems applied to the motion capture are vision-based systems that acquire the scene and analyze it to get the information. They can be marker-based or completely marker-free. The markers are objects placed in sites of interest in order to be recorded and analyzed after the acquisition. In human motion capture, there is a big variety of points that can be interesting to analyze so it's possible to change what is recorded depending on what we are interested in. Below are introduced two types of systems more commonly used.

2.2.1 Marker-based optical systems

The marker-based systems are based on the principles of the optoelectronics provide the reconstruction of the points in 3D coordinates of reality in 2D coordinates of the video captured by the sensors of the cameras. The points of interest are highlighted with the markers, objects positioned in specific points of the body. The system is based on stereophotogrammetry, that is

to say, the reconstruction of a 3D object framing with two or more cameras in a fixed position between them. In order to map a real object in the coordinate space of the image, it's necessary a part of the calibration of the system.

It's necessary to find the rotation matrix that it's able to transfer the 3D coordinates $[X, Y, Z]$ in the space 2D $[x, y]$ of the camera. Commonly the method more used is the Direct Linear Transformation [28] that was introduced by Abdel-Aziz and Karara, in 1971.

There are specific assumptions to do: it's used the hypothesis of the camera pin-hole, that is described by an optical center K linked with the object in the space of 3D coordinates and intersect the 2D plane of the image and the hypothesis of collinearity of the points K, J and O. It's necessary to define the different points with their position:

- The object in the 3D coordinates space identified with the 3-axis reference system (XYZ) and has the coordinates $[X_1, Y_1, Z_1]$;
- The plane of the camera has identified with the 2-axis reference system of the image (x, y) ;
- The center of the pin-hole camera K that has in the 3D system the coordinates $[X_2, Y_2, Z_2]$

It's necessary to track the line joining the point K and the object O in the space individuating the point J in the 2D system of the camera with the coordinates $[x_1, y_1]$ individuating in **Equation 2.7**

$$\overline{OK} = [X_1 - X_2, Y_1 - Y_2, Z_1 - Z_2] \quad (2.7)$$

It's now necessary to transform the 2D system of the image plane in a 3D system, so the third axis is identified, and the system goes in the (x, y, z) reference system.

The orthogonal line joining the center K with the image plane is then drawn, and it's identified the point U with coordinates $[x_2, y_2, 0]$; while the point J becomes $[x_1, y_1, 0]$. In this way the point K can be identified also in the image plane with the coordinates: $[x_3, y_3, d]$, where d is the distance computed from the center K to the image plane. It's now drawn the vector B joining the point K with the point I identified in **Equation 2.8**.

$$\overline{JK} = [x_1 - x_3, y_1 - y_3, -d] \quad (2.8)$$

The hypothesis of collinearity is now fundamental to describe the equation linking vector B with vector A:

$$\overline{JK} = c \overline{OK} \quad (2.9)$$

Where c is a scalar.

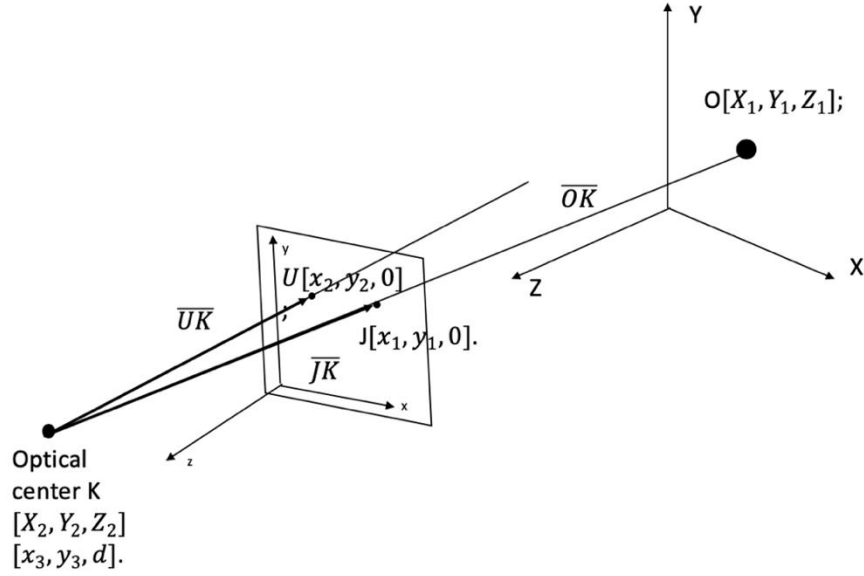


Figure 2.4- DLT scheme

It's now necessary to describe the vector \overline{OK} in the reference system of the image plane so it can be used the matrix of transformation that allow to pass from one system to another as in **Equation 2.10**.

$$M_{2D/3D} = \begin{bmatrix} r_{11} & r_{12} & r_{13} \\ r_{21} & r_{22} & r_{23} \\ r_{31} & r_{32} & r_{33} \end{bmatrix} \quad (2.10)$$

And multiply the vector \overline{OK} it's obtained **Equation 2.11**.

$$\overline{OK}^{(2D)} = M_{2D/3D} \overline{OK}^{(3D)} = \begin{bmatrix} r_{11} & r_{12} & r_{13} \\ r_{21} & r_{22} & r_{23} \\ r_{31} & r_{32} & r_{33} \end{bmatrix} \overline{OK}^{(3D)} \quad (2.11)$$

With $\overline{OK}^{(2D)}$ is the vector in the image plane and $\overline{OK}^{(3D)}$ is the vector in the object plane. Taking **Equation 2.10** and applying **Equation 2.11** it's obtained **Equation 2.12**.

$$\begin{bmatrix} x_1 - x_3 \\ y_1 - y_3 \\ -d \end{bmatrix} = c \begin{bmatrix} r_{11} & r_{12} & r_{13} \\ r_{21} & r_{22} & r_{23} \\ r_{31} & r_{32} & r_{33} \end{bmatrix} \begin{bmatrix} X_1 - X_2 \\ Y_1 - Y_2 \\ Z_1 - Z_2 \end{bmatrix} \quad (2.12)$$

Resolving in order to find c it's found **Equation 2.13**.

$$c = \frac{-d}{r_{31}(X_1 - X_2) + r_{32}(Y_1 - Y_2) + r_{33}(Z_1 - Z_2)} \quad (2.13)$$

From which it's possible obtain **Equation 2.14** and **Equation 2.15**.

$$x_1 - x_3 = -d \frac{r_{11}(X_1 - X_2) + r_{12}(Y_1 - Y_2) + r_{13}(Z_1 - Z_2)}{r_{31}(X_1 - X_2) + r_{32}(Y_1 - Y_2) + r_{33}(Z_1 - Z_2)} \quad (2.14)$$

$$y_1 - y_3 = -d \frac{r_{21}(X_1 - X_2) + r_{22}(Y_1 - Y_2) + r_{23}(Z_1 - Z_2)}{r_{31}(X_1 - X_2) + r_{32}(Y_1 - Y_2) + r_{33}(Z_1 - Z_2)} \quad (2.15)$$

And we can reorganize in order to isolate x_1 and y_1 obtaining **Equation 2.16**.

$$\begin{cases} x_1 = \frac{L_1 X_1 + L_2 Y_2 + L_3 Z_1 + L_4}{L_9 X_1 + L_{10} Y_1 + L_{11} Z_1 + 1} \\ y_1 = \frac{L_5 X_1 + L_6 Y_2 + L_7 Z_1 + L_8}{L_9 X_1 + L_{10} Y_1 + L_{11} Z_1 + 1} \end{cases} \quad (2.16)$$

With the L_j are indicated the grouping in **Equation 2.17**.

$$\left\{ \begin{array}{l} L_1 = \frac{x_3 r_{31} - dr_{11}}{D} \\ L_2 = \frac{x_3 r_{32} - dr_{12}}{D} \\ L_3 = \frac{x_3 r_{33} - dr_{13}}{D} \\ L_4 = \frac{(dr_{11} - x_3 r_{31})X_2 + (dr_{12} - x_3 r_{32})Y_2 + (dr_{13} - x_3 r_{33})Z_2}{D} \\ L_5 = \frac{y_3 r_{31} - dr_{21}}{D} \\ L_6 = \frac{y_3 r_{32} - dr_{22}}{D} \\ L_7 = \frac{x_3 r_{33} - dr_{23}}{D} \\ L_8 = \frac{(dr_{21} - x_3 r_{31})X_2 + (dr_{22} - x_3 r_{32})Y_2 + (dr_{23} - x_3 r_{33})Z_2}{D} \\ L_9 = \frac{r_{31}}{D} \\ L_{10} = \frac{r_{32}}{D} \\ L_{11} = \frac{r_{33}}{D} \\ D = -(X_2 r_{31} + Y_2 r_{32} + Z_2 r_{33}) \end{array} \right. \quad (2.17)$$

Rearranging it's possible obtain the final form of the equations in **Equation 2.18**.

$$\begin{cases} x_1 = X_1 L_1 + Y_1 L_2 + Z_1 L_3 + L_4 - x_1 X_1 L_9 - x_1 Y_1 L_{10} - x_1 Z_1 L_{11} \\ y_1 = X_1 L_5 + Y_1 L_6 + Z_1 L_7 + L_8 - y_1 X_1 L_9 - y_1 Y_1 L_{10} - y_1 Z_1 L_{11} \end{cases} \quad (2.18)$$

With the two equations in **Equation 2.18** it's possible to transform the image plane in 2D in the object plane 3D, using basically points of control whose coordinates are known in both the coordinates. Being eleven unknown parameters it's necessary to have at least 6 points of control that give twelve equations.

Actually, the problem is more complex having more parameters to be considered as the distortions included by the lens of the cameras so the minimum points of control should be at least 8 in order to fix these problems.

This process is developed in a laboratory where, all the cameras have a fixed position in the room and between them. Then different points are positioned and captured in order to find the parameters that resolve **Equation 2.18**.

After this first phase is concluded it's possible to effectuate the acquisition, so the markers can be positioned on the body of the subject.

Two types of markers can be used: active markers that are self-illuminated or passive markers that reflect the light coming from the cameras. Choosing the first ones gives more safety in terms of light interferences and they are easier to be labeled in the processing while the last ones reflect simply the light coming from the cameras and can be easily disturbed by other light sources. By the way, it could be harder to provide active markers being often wired and bulky.

Regardless of which type of marker is used, there are common problems to both the system: the occlusion of the markers and the swap of the markers.

The first problem is individuated when during a movement one marker is covered by others and result invisible to the different cameras making impossible his labeling. The swap instead it's problematic when two or more markers are very near and during the movement can be crossed and there is no certainty about the labels (**Figure 2.5**)

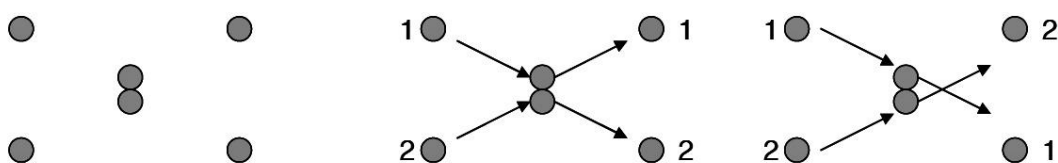


Figure 2.5- Marker Occlusion

The positioning of the markers is another fundamental step to have accurate measurements. It's necessary to individuate all the body segments giving information about the 3-axis so at least 3 markers for body segments.

In order to provide reliable data was developed different protocols during the years. The protocols are defined in order to guarantee the maximum visibility of each marker for the cameras and try to give the minimum number of markers strictly necessary.

The first protocol developed was the Davis-Helen Hayes one [29], where are defined as the markers to be positioned in order to obtain the joint axis. After one first part of calibration where the subject stays still in order to find the rotation centers of the joints.

In **Table 2.1** and in **Figure 2.6** are explained the markers positioned following the protocol.

Table 2.1-Davis protocol position markers

<i>Bone structure</i>	<i>Description</i>	<i>Acronym</i>
Torso	Right sternoclavicular joint	RS
	Left sternoclavicular joint	LS
	Spinous process C6	N
Hip Bone	Upper right iliac spine	R
	Upper left iliac spine	B
	Sacroiliac	H
Femur	Great Trochanter	RH
	Femur	RF
	Femoral epicondyle	RK
Shank	Fibula head	RP
	Tibia	RB
	Lateral malleolus	RA
Foot	Second metatarsal head	RT
	Heel	RQ

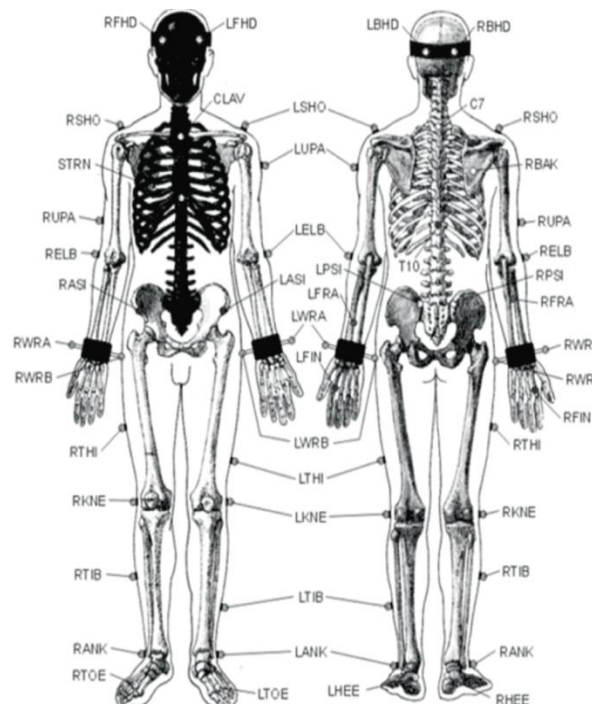


Figure 2.6-Davis protocol markers

This approach didn't consider the motion artifacts that is to say, the markers that changed positions during the movement due to the skin sliding. Then, it was used until the protocol C.A.S.T. was defined, solving the problems deriving from the motion artifacts [29].

This protocol has an anatomical calibration phase where different groups of markers are positioned in areas of the body where the sliding is not problematic. Sequentially it's defined the technical system, each of the anatomical joints is tracked in this reference system and the anatomical markers are removed. In this way, it's guaranteed that each point can be reconstructed from the technical system when it's requested. The positions of the markers are reported in **Table 2.2**.

Table 2.2- Cast protocol markers

<i>Bone structure</i>	<i>Description</i>	<i>Acronym</i>
Pelvis	Anterior superior iliac spine	ASIS
	Posterior superior iliac spine	PSIS
	Center of acetabulum	AC
Femur	Center of femoral head	FH
	Great Trochanter	GT
	Lateral epicondyle	LE
	Medial epicondyle	ME
	Antero-lateral apex of the patellar surface	LP
	Antero-medial apex of the patellar surface	MP
	Lateral Condyle	LC
	Medial Condyle	MC
Shank	Eminence intercondylar	IE
	Prominence of tibial tuberosity	TT
	Apex of perone head	HF
	Distal apex of medial malleolus	MM
	Lateral apex of medial malleolus	LM
	Medial point of tibial surface	MMP
	Lateral point of tibial surface	MLP
Foot	Heel	CA
	Dorsal of the first metatarsal head	FM
	Dorsal of the second metatarsal head	SM
	Dorsal of the fifth metatarsal head	VM

The points of forces of the optoelectronic products are the capability to have great accuracy due to the complex phase of calibration and the continuous monitoring of the points by software dedicated with a reduced drift and lag.

In terms of update rate, it is indispensable to respect the Nyquist theorem that limits the range of movements observable: more rapid are the movements analyzed, the largest need to be the

update rate. In the optoelectronic system, the update range can reach also 240 fps that guarantee the majority of movement can be captured.

How specified above, the system is though really sensible to the interference and the noise coming from the environment as well as coming from the marker used.

The last two evaluation parameters make impossible the use outside of the laboratory: the protocols explained above, foresees the positioning of a really large number of markers positioned with the aid of protectionists; while the price of these systems that is variable between 12.500 €-150.000 €. Nowadays the optoelectronic systems are the gold standard in the sector of the motion capture and in the thesis was used to validate the low-cost system.

2.2.2 Marker-free optical systems

The complexity of the set-up of the marker-based system made interesting the developments of the system that were completely free of markers.

In that direction, there was the advancement of other optical technologies as the RGB-D cameras.

The acronym RGB-D is referred to as the type of cameras which can provide the RGB information about the colors of the image acquired and the depth information with the technique of the time of flight.

The time of flight is consisting by a pulsed light in the infrared field, with a specific frequency, coming from the camera that reflects on the obstacle in the Field of view (*FoV*) of the camera. The phase difference between the emitted and the received light is computed and, knowing the emission frequency, it's possible to obtain the distance of the object from the camera [30].

$$d_{c-t} = \frac{\Delta\varphi}{4\pi f_{ir}} \quad (2.19)$$

Where:

d_{c-t} is the distance between the camera and the target.

$\Delta\varphi$ is the phase difference between emitted and received encoded rays.

$4\pi f_{ir}$ is the time relative to the emission frequency of the IR rays.

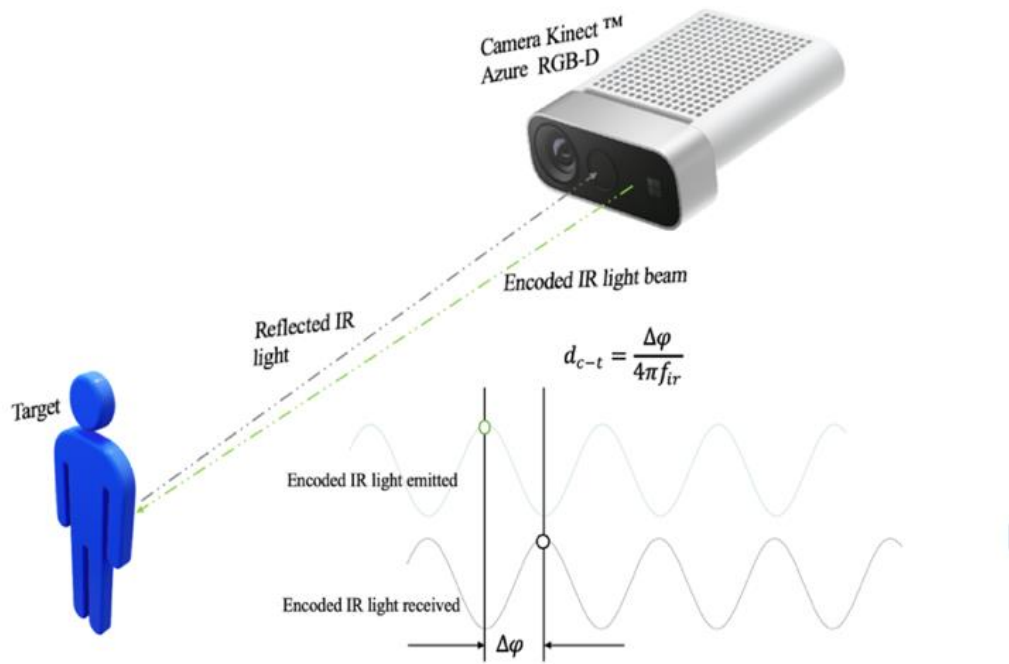


Figure 2.7-Time of flight camera

According to the different times of comeback of the ray, it's produced, during an acquisition, a depth map that can be used for different purposes. The depth map produced have different tones in greyscale that are relatives to the distance of the object from the camera (**Figure 2.8**)



Figure 2.8-Depth image produced

Due to the functioning of the system, it can be used to capture movements without encumbrance for the user that it's requested only to stay in the field of the camera.

Then, different tools can process the data coming from the depth map of the camera, joint with the RGB information and the intrinsic calibration, in order to extract the point of interest. In the following chapters are explicated the software used to elaborate the data and the types of joints extracted.

After this introduction of the RGB-D cameras will be elucidated the camera we had available, the software used, and the experiments carried on. Furthermore, during the various experiments, the main advantages of using the RGB-D camera and all of the problems that arose during them will be highlighted.

Finally, it will be investigated the possibility of using these powerful instruments to make easier the acquisition in a home-based system, validating first the results provide with the gold standard provided by the optoelectronic system and after investigating the utility of the data furnished.

2.3 Experimental setup

The chapter will be divided as follows: the cameras made available by CNR-IEIIT section of computer vision will be introduced, then, the software development kit (SDK) selected will be mentioned, explaining the data furnished by them, and will be explicated the methodologies used in order to find the best couple hardware-software chosen to be validated compared to the gold standard.

2.3.1 Equipment

The cameras provided by CNR-IEIIT are RGB-D cameras are:

- Intel® RealSense™ Depth Camera D415 [31]
- Intel® RealSense™ Depth Camera D435 [32]
- Orbbec Astra Pro [33]
- Microsoft Kinect Azure DK [34]

In **Table 2.3** the main features of the camera are summarized.

Table 2.3- Camera descriptions

	<i>D415</i>	<i>D435</i>	<i>Orbbec Astra Pro</i>	<i>Kinect Azure</i>
RGB Resolution	1920x1080	1920x1080	1280x720	3840x2160
Depth Resolution	1280x720	1280x720	640x480	1024x1024
Range	10 m	10 m	8 m	0.5 - 5.46 m
Framerate	30	30	30	30
FoV	65°±2° x 40°±1° x 72°±2°	87°±3° x 58°±1° x 95°±3°	60° x 49.5° x 73°	120°x120°

All of the systems utilized are considered low-cost in comparison to the cost of the gold standard they are validated with, varying between 300-400 €. This is fundamental to be able to think of these systems made available on a large scale.

The cameras need to be interfaced with the SDK in order to start the acquisition and more deeply to extract the joints of interest of the experiment. The software chosen for this purpose are NuiTrack SDK [35] and the one's own of the Azure Kinect, which provides a powerful tool, with the purchase of the camera.

This software, editable in C++, allows us to intercept the IR and RGB streams of the camera and to elaborate them in order to find the joints relatives to it.

The first SDK analyzed is NuiTrack. It's a middleware developed by 3DiVi Inc. to recognize gestures and track the skeletons with depth cameras. It's possible to execute it on OS like Windows, Android, and Linux. This tool when used to extract the skeleton can provide 19 joints summarized in **Figure 2.9**.

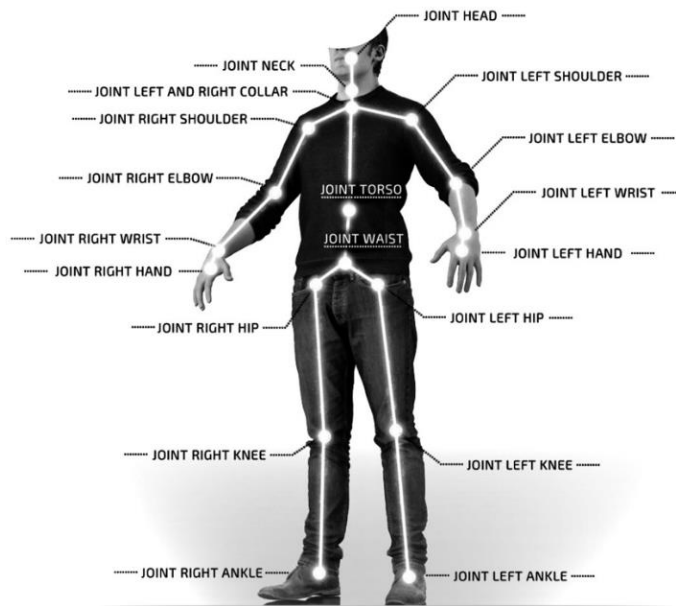


Figure 2.9-NuiTrack joints

With a changing on the C++ code, it has been possible to modify the NuiTrack source code in order to, besides to extract the joints, to extract the timestamp of the camera useful to monitoring the mean framerate and the RGB stream, useful to compare the video stream with the acquisition. The results of the acquisition are inserted in a *JSON* file that is subsequently imported in MATLAB. The second SDK used is the Azure Kinect SDK, provided by Microsoft and capable to extract at different levels of focus, the 3D joints of the human body. The joints of the entire human body are resumed in **Figure 2.10**.

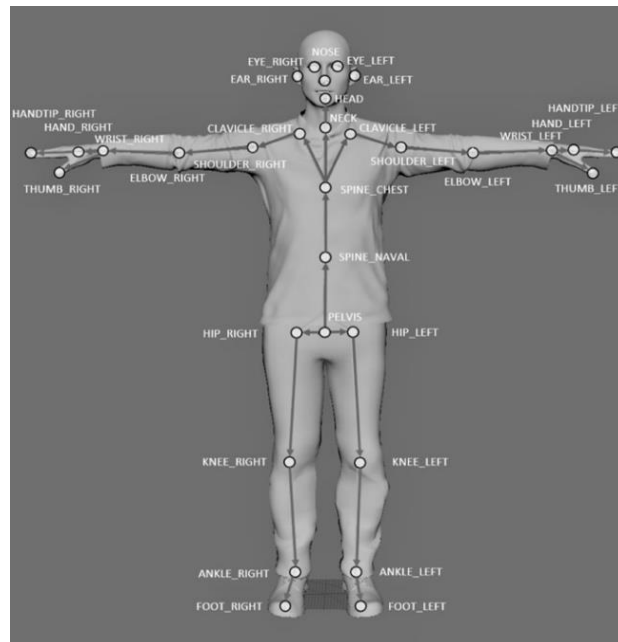


Figure 2.10-Kinect Azure Joints

The acquisition can be performed in two ways using this SDK: the online one, that is high requesting CPU and it makes visible the real-time mesh of the body as in **Figure 2.11**, with the tracking process, and the offline one that records the *MKV* file, containing the RGB channel and the IR channel, and that it needs to be passed to offline processor in order to extract the joints in **Figure 2.10** loading less the CPU.

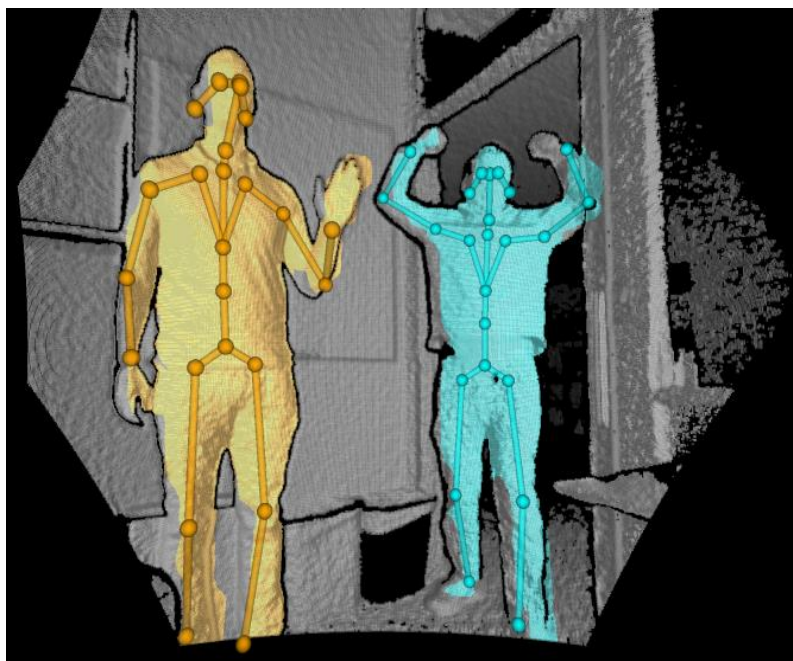


Figure 2.11-Kinect Azure Mesh

2.4 Data Handling

All of the programs utilized give as output a *JSON* file. The outputs coming from the three different approaches is slightly different from one to another, so three different personalized MATLAB codes have been programmed.

The typical structure of the NuiTrack JSON file provides as many structures as the frames captured, and it contains inside, the parameters of the acquisition, as the center of mass computed online, the identifier of the body tracked, the timestamp coming from the camera clock, all of the joints and their complete tracking as skeleton.

The Center of Pressure is computed in two ways: the mean arithmetic, and the weighted sum. The list of weight, used for the weighted sum [36], is resumed in the table of **Figure 2.12**.

Segment	Definition	Segment Weight/Total Body Weight	Center of Mass/ Segment Length		Radius of Gyration/ Segment Length			Density
			Proximal	Distal	C of G	Proximal	Distal	
Hand	Wrist axis/knuckle II middle finger	0.006 M	0.506	0.494 P	0.297	0.587	0.577 M	1.16
Forearm	Elbow axis/ulnar styloid	0.016 M	0.430	0.570 P	0.303	0.526	0.647 M	1.13
Upper arm	Glenohumeral axis/elbow axis	0.028 M	0.436	0.564 P	0.322	0.542	0.645 M	1.07
Forearm and hand	Elbow axis/ulnar styloid	0.022 M	0.682	0.318 P	0.468	0.827	0.565 P	1.14
Total arm	Glenohumeral joint/ulnar styloid	0.050 M	0.530	0.470 P	0.368	0.645	0.596 P	1.11
Foot	Lateral malleolus/head metatarsal II	0.0145 M	0.50	0.50 P	0.475	0.690	0.690 P	1.10
Leg	Femoral condyles/medial malleolus	0.0465 M	0.433	0.567 P	0.302	0.528	0.643 M	1.09
Thigh	Greater trochanter/femoral condyles	0.100 M	0.433	0.567 P	0.323	0.540	0.653 M	1.05
Foot and leg	Femoral condyles/medial malleolus	0.061 M	0.606	0.394 P	0.416	0.735	0.572 P	1.09
Total leg	Greater trochanter/medial malleolus	0.161 M	0.447	0.553 P	0.326	0.560	0.650 P	1.06
Head and neck	C7-T1 and 1st rib/ear canal	0.081 M	1.000	— PC	0.495	0.116	— PC	1.11
Shoulder mass	Sternoclavicular joint/glenohumeral axis	—	0.712	0.288	—	—	—	1.04
Thorax	C7-T1/T12-L1 and diaphragm*	0.216 PC	0.82	0.18	—	—	—	0.92
Abdomen	T12-L1/L4-L5*	0.139 LC	0.44	0.56	—	—	—	—
Pelvis	L4-L5/greater trochanter*	0.142 LC	0.105	0.895	—	—	—	—
Thorax and abdomen	C7-T1/L4-L5*	0.355 LC	0.63	0.37	—	—	—	—
Abdomen and pelvis	T12-L1/greater trochanter*	0.281 PC	0.27	0.73	—	—	—	1.01
Trunk	Greater trochanter/glenohumeral joint*	0.497 M	0.50	0.50	—	—	—	1.03
Trunk head neck	Greater trochanter/glenohumeral joint*	0.578 MC	0.66	0.34 P	0.503	0.830	0.607 M	—
Head, arms, and trunk (HAT)	Greater trochanter/glenohumeral joint*	0.678 MC	0.626	0.374 PC	0.496	0.798	0.621 PC	—
HAT	Greater trochanter/mid rib	0.678	1.142	—	0.903	1.456	—	—

Figure 2.12-Table of CoP weights [36]

The JSON is imported by an additive toolbox called *loadjson* [37]

It has been inserted control in the C++ code, imposing to discard automatically the corrupted frame where at least one of the joints was not individuated, making the import in MATLAB complete of the correct frames.

The reference system is individuated by three axes, the longitudinal one (**UD-Axis**), individuated by the Z-axis of the camera, the mediolateral one (**ML-Axis**), individuated by the Y-axis of the camera, and anteroposterior one (**AP-Axis**), individuated by the Z-Axis of the camera as in **Figure 2.13**.

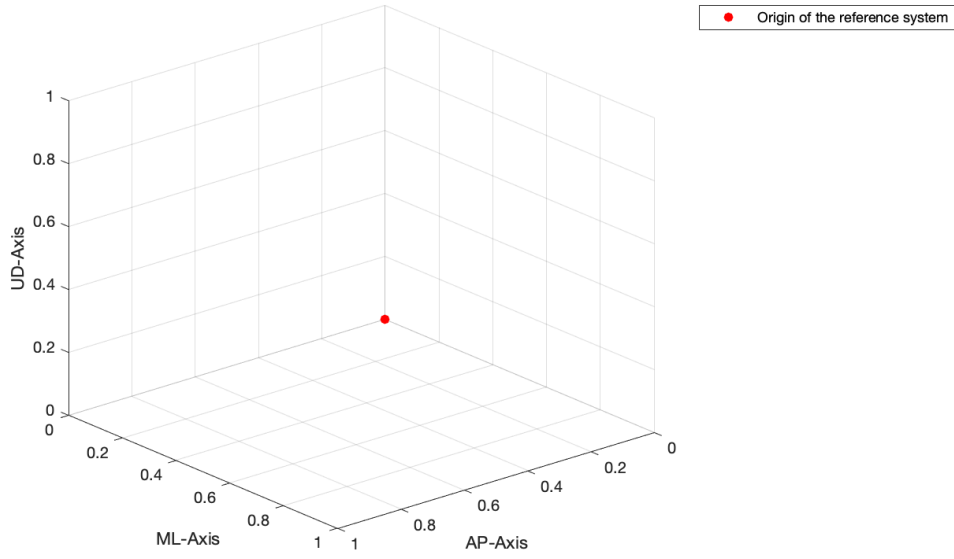


Figure 2.13-Reference system

Therefore, the most important parameters analyzed in the acquisition are introduced.

- **Framerate:** in the acquisition file it's saved the timestamp in μs for each frame. In the algorithm, it's computed the framerate in **Equation 2.20**.

$$FR_j = \frac{1}{(Ts_{i+1} - Ts_i) * 10^{-6}} \quad (2.20)$$

In this way, it's possible to find the relative framerates and compute also the mean framerate in **Equation 2.21**.

$$FR_m = \frac{\sum_{j=1}^N FR_j}{N} \quad (2.21)$$

It's important that the mean framerate stays at least at 30 fps in order to be sure to respect the Nyquist theorem for each movement considered. In **Figure 2.14**, it is plotted one example of a framerate recovered.

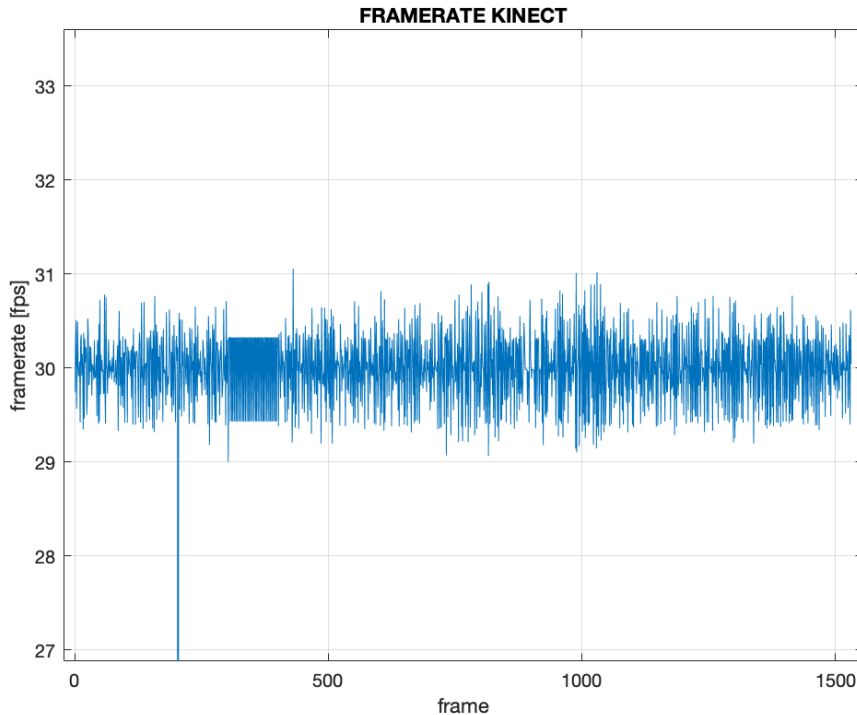


Figure 2.14-Framerate obtained from MATLAB

- **Confidence:** a threshold was set in order to eliminate the frame with a little confidence that could provide the wrong information. The values of confidence are different from SDK to another. The values provided by the SDK NuiTrack are between 0 and 1, so a threshold of 0.75 is set in order to delete the value less reliable. The values provided by Kinect Azure instead, are 0,1 and 2, so a threshold of 1 is set in this case.
- **Segment construction:** the joints are connected in order to rebuild all the skeleton and it's possible to see the final construction in **Figure 2.15**. It has been separated the entire body in four macrosegments, that is, one for the right lower limb, one for the left lower limb, one for the trunk with the head, and one for the upper limbs. From the body model, it is possible to observe immediately how the model provided by the Kinect Azure is much more complete, having the possibility of tracking the front and back of the body, while the Orbbec Astra model is limited to the front representation.

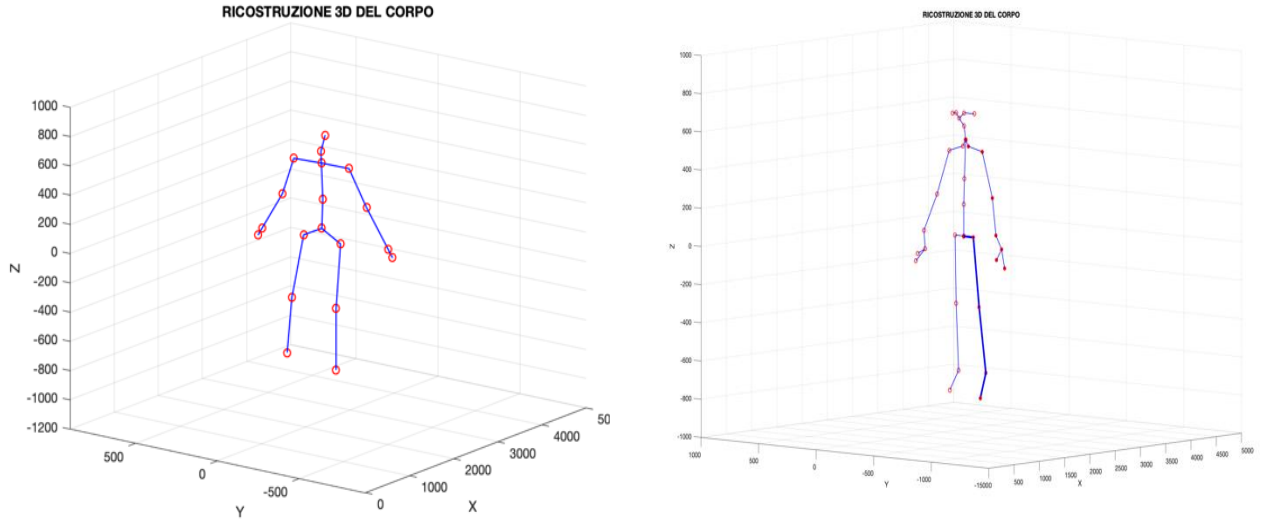


Figure 2.15-Skeleton recovered on MATLAB

- **Joint angles:** the angles are computed as the inverse of the inner product between the segments built. The global reference is given by the camera that has a triad XYZ build as in **Figure 2.13**. The angles are evaluated according to the development of the desired movement to be evaluated, so e.g. the angle seen in the sagittal plane, expressed in degrees, can be evaluated taking the AP-Axes and the UD-Axes components of the joints involved.

$$\theta_{x,z} = \cos^{-1} \frac{l_i(x,z) \cdot l_j(x,z)}{\|l_i(x,z)\| \|l_j(x,z)\|} \quad (2.22)$$

Where $l_i(x, z)$ and $l_j(x, z)$ are the i -th and j -th limb considered.

Especially, the limbs computed have been the upper and lower limbs, using for the different body models:

- The angle between the segment made by the wrist joint and elbow joint and the segment made by the shoulder joint and the elbow joint for the right and left arms, for all of the cameras.
- The angle between segment made by the hip joint and knee joint and the segment made by the knee joint and the ankle joint for the lower limbs in the dynamic standing task, for the Nuitrack cameras and the Kinect camera.
- The angle between segment made by the torso joint and hip joint and the segment made by the hip joint and the knee joint for the lower limbs in the dynamic seated task, for the Nuitrack cameras and the Kinect camera.
- The angle between segment made by the *asis* joint and knee joint and the segment made by the knee joint and the ankle joint for the lower limbs in the dynamic standing task, for the BTS camera.
- The angle between segment made by the *C7* joint and *asis* joint and the segment made by the *asis* joint and the knee joint for the lower limbs in the dynamic seated task, for the BTS camera.

- **Angle synchronization:** due to the possibility of checking in each frame the angle relative to every limb, we've used these parameters in order to make synchronization between the acquisition and the observation window desired. It's asked to flex the right arm so, matching the elbow angle formed by the right forearm and the right arm it's possible, with the MATLAB function *findpeaks* find the moment of maximum flexion in the frontal plane and to individuate there the beginning of the observation window (Figure 2.16). The same thing is made in order to close the observation.

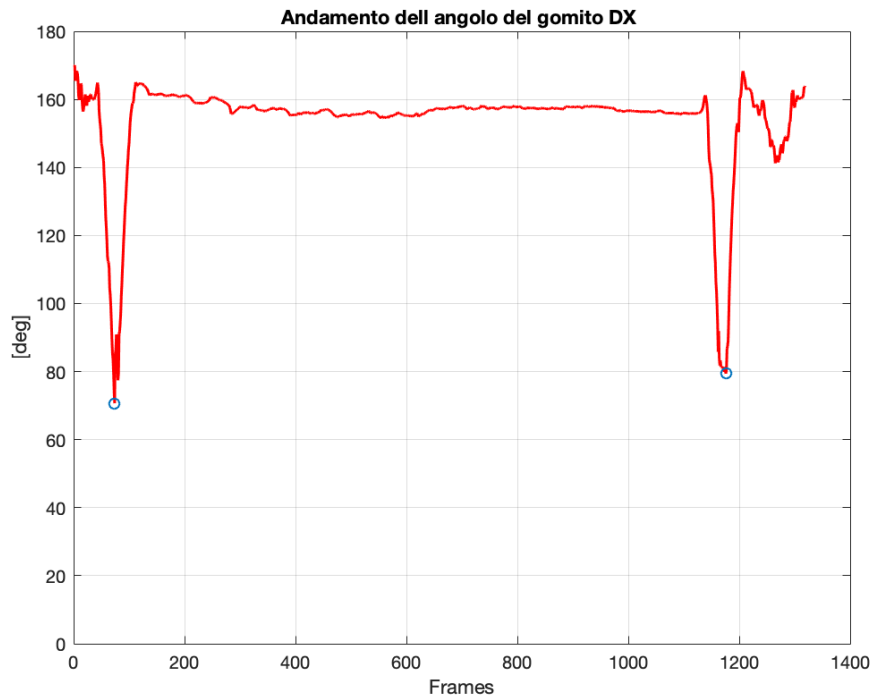


Figure 2.16-Synchronization with the right elbow

- **Parameters filtering** the acquisition of the parameters and their analysis is affected by high-frequency noise. In order to make smoother the signals, it was computed the parametric power spectral density with the Burg method in order to have a good spectral resolution. The parameters of the Burg estimation are computed using the variance until the 50th order, using values, less than the asymptotic variance increased by 5%, and taking the second value as the order. The number of values of the Fast Fourier Transform is 1024. In this way it has been obtained a better resolution of the spectrum, and, consequently it has been designed a Chebyshev low pass filter of order 1, with the cut-off frequency depending on the movement analyzed [38]. The MATLAB command *filtfilt* has been used to avoid the introduction of delays.

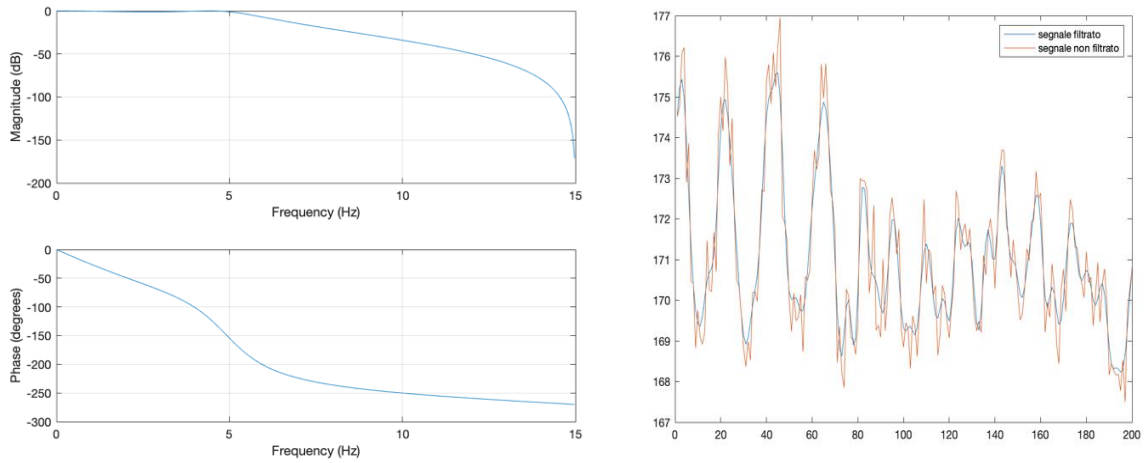


Figure 2.17-Chebyshev order 1 low pass filter and example of filtering performed

- **Velocity:** the velocities are computed deriving the angles found and the center of pressure. Having the timestamp for each frame they're computed in **Equation 2.23**.

$$\dot{\theta}_{x,z} = \frac{\theta_{i+1}(x,z) - \theta_i(x,z)}{t_{i+1} - t_i} \quad (2.23)$$

- **CoP variation:** it's plotted the variation of the center of Pression, respect to the first value, in order to have visual information about its moving on the three planes as in **Figure 2.18**.

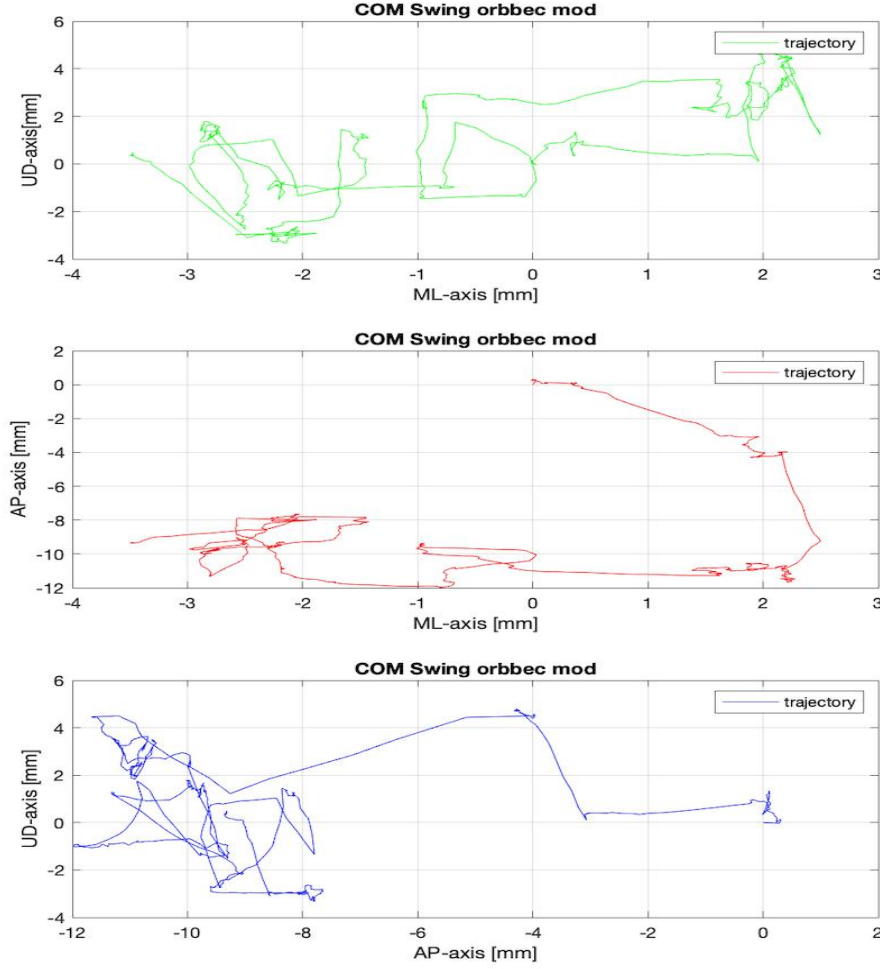


Figure 2.18-CoP sway extracted from one acquisition.

- **Standard deviation:** it's computed as the measurement of the deviations, in order to evaluate the variability around the mean value of the static position [39].

$$s_c = \sqrt{\frac{1}{n-1} \sum_{i=1}^n (x_i - \bar{x})^2} \quad (2.24)$$

- **Video reconstruction:** the last part of the algorithm records all the movement in an AVI file ready to be opened each time in order to analyze visually the movement.

2.5 Experiments conducted

In order to choose the best possible setup between we had available, we've based on the metrological accuracy of the cameras already tested by different works [42][43][44] to ensure that the camera had optimal performance, regardless this specific application, and then we made a set of test to verify the feasibility of the acquisitions with the setup available.

It has been thought to test two cameras the time, in order to decrease the encumbrance in the acquisition set and avoid the interference that all of the rays used by the camera could interfere with each other.

We tried to characterize also the best conditions the cameras and the SDK need to operate in.

Furthermore, we used a set of objects in order to simulate the home environment in which these systems could be used in the future.

Different clothes, physicality, and position have been used in order to highlight the possible problems deriving from the subject in front of the camera.

2.5.1 Preliminary tests

The cameras have been positioned in the same position (**Figure 2.19**) in order to have comparable information about the position and orientation of the joints, even if only absolute parameters are considered in the analysis.



Figure 2.19-Orbbec and Kinect Azure positioning

The list of tests conducted has been:

- **Static standing task for 30 seconds in artificial and natural light conditions:** the test aims to evaluate the standard deviations of all of the joints provided in all of the 3 axes, in order to evaluate the most critical ones in static condition. It's asked to stay completely still in front of the camera in the standard anatomical position for a duration of 30 seconds. The light coming from the led lamps before, and the natural light from the windows after, have been used to see in which way they conflict with the IR ray of the cameras. Furthermore, the number of frames not recorded are evaluated to see how the cameras struggle to acquire.
- **Dynamic standing for 30 seconds in artificial and natural light conditions:** the test aims to evaluate how the cameras capture the movements. After the synchronization, these movements are performed: one flexion of the right arm, one flexion of the left arm, one squat. The results are compared between them in order to compute the Pearson's correlation, and compared with the time recorded with a timer in order to compute the delay with the real occurrence of the movement. The considerations about the lights are the same ones as the static test.
- **Seated static task for 30 seconds in artificial and natural light conditions:** the interest is focused on the evaluation of how the presence of a disturbing element as a chair or the sitting position could influence the acquisition. The parameters considered are the same ones as the static test.
- **Seated dynamic task for 30 seconds in artificial and natural light conditions:** the same parameters of the dynamic test are evaluated seeing how the sitting position is influent on them.

After the best choice of the couple Nuitrack-Camera, we passed to evaluate the latter with the Azure Kinect with his own SDK with the same evaluation parameters. It's important to linger about the Azure Kinect that substituted the older Kinect V1 and V2 that, in the past, were the main low-cost systems, which most of the research works have been focused on. [40][41]

Finally, we chose to validate as systems the camera best performed with Nuitrack and the Azure Kinect with his SDK.

The main parameters evaluated from the tasks are the standard deviation for each joint in the three reference system axes comparing the performance between the camera individuating the most critical joints in the static task.

In the dynamic tasks have been evaluated the angles computed in terms of Pearson's correlation defined in **Equation 2.25**.

$$\rho_{xy} = \frac{\sigma_{xy}}{\sigma_x \sigma_y} \quad (2.25)$$

Where σ_x and σ_y are the standard deviations of X and Y and σ_{xy} is their covariance. It's included between $-1 \leq \rho_{xy} \leq 1$. All the values are computed how the mean between the upper and lower value in the 95% confidence of the distribution.

All the tasks have been repeated three times in order to have a better statistical value and to increase the probability to have at least one task correctly captured.

It has been used the cross-correlation as described in **Equation 2.26** after the resample of the signals provided by the BTS. The BTS worked at 100 fps but, for the movements we wanted to test, the 30 fps by default of our camera respected the Nyquist theorem avoiding the aliasing.

$$R_{xy}[n] = \sum_{m=-\infty}^{\infty} x^*[m] y[n + m] \quad (2.26)$$

With the MATLAB functions of resampling the signals have been so resampled at 30 fps in order to be comparable with the signals coming from our systems. Computing the maximum of the cross-correlation we found the delay between the two signals and we aligned the two signals.

After the alignment has been necessary to interpolate the signals in order to have the same length in the signals and compute the correlations of Pearson.

For the static tests, we have focused on the variation on the different axis could not realigning the reference systems of the two systems. In this way, we had information about the swing of the CoP, used in the analysis of the equilibrium.

2.5.2 Validation of the system

The validation of the system has been performed in the laboratory “*L. Divieti*” of the Polytechnique of Milan. The system used in the laboratory was the BTS-SMART DX [45] that is resumed in **Table 2.4**

Table 2.4-BTS SMART DX-400 Characteristics	
	<i>BTS SMART DX-400</i>
Sensor Resolution	1 MP
Cameras per workstation	16
Accuracy	<0.3 mm in 4x3x3
Framerate	100 -300 fps

Our systems have been positioned in front of the subject in order to capture the movement frontally while the BTS system needs to capture the movement at 360° to ensure the complete capture of the markers (**Figure 2.20**).



Figure 2.20-Positions of the camera in the Laboratory

The markers have been positioned on the subjects with the Davis protocol as in **Table 2.1**.

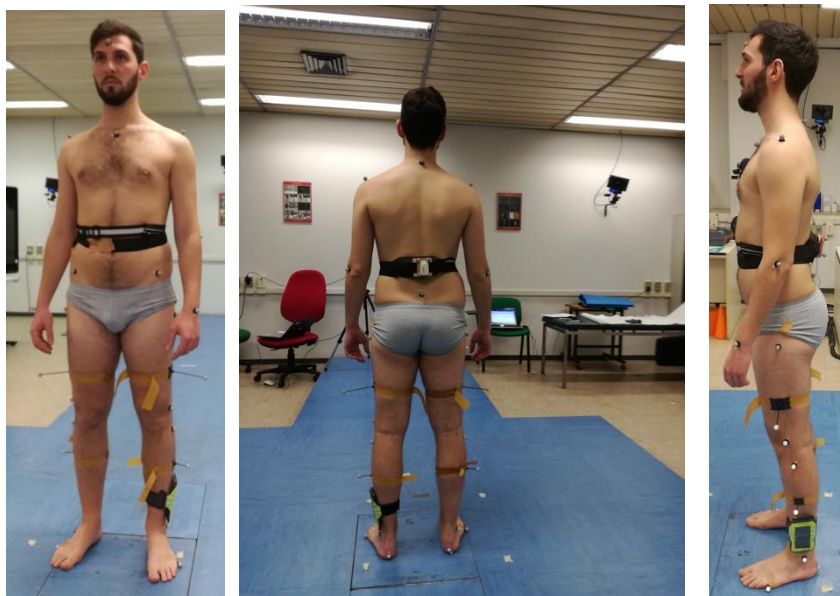


Figure 2.21-Markers positions

The BTS software for the manual labeling of the markers, showed in **Figure 2.23**, allows us to follow the motion and recognize all of the joints, saving them in an *EMT* file.

The joints extracted are then imported in a custom MATLAB script, finding the body model showed in **Figure 2.22**.

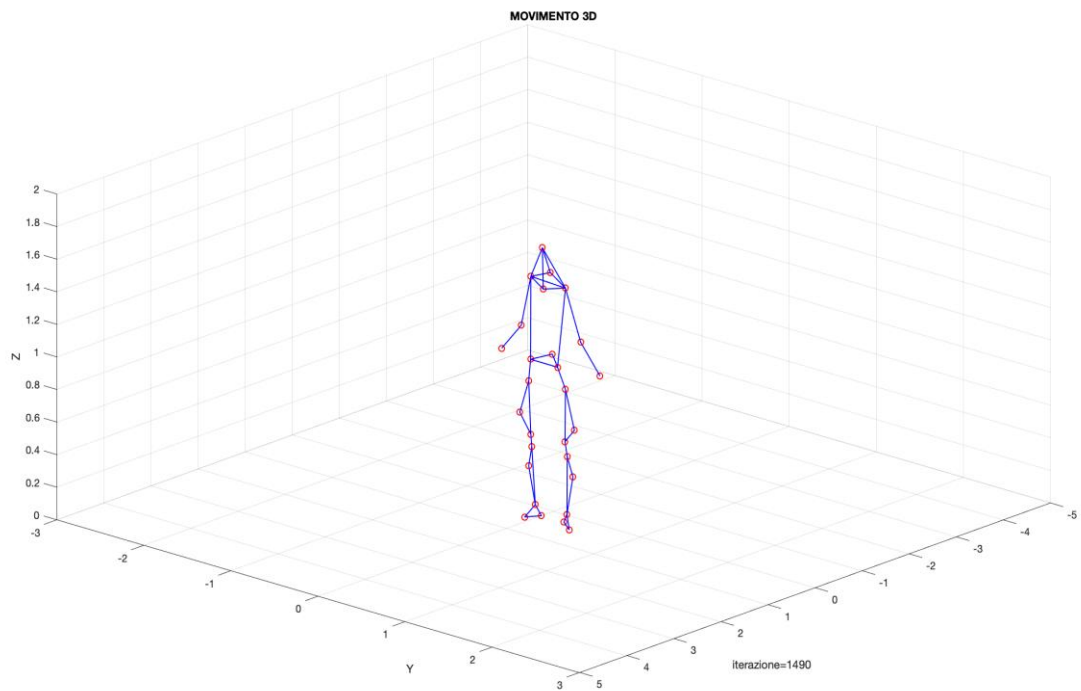


Figure 2.22-BTS skeleton recovered in MATLAB

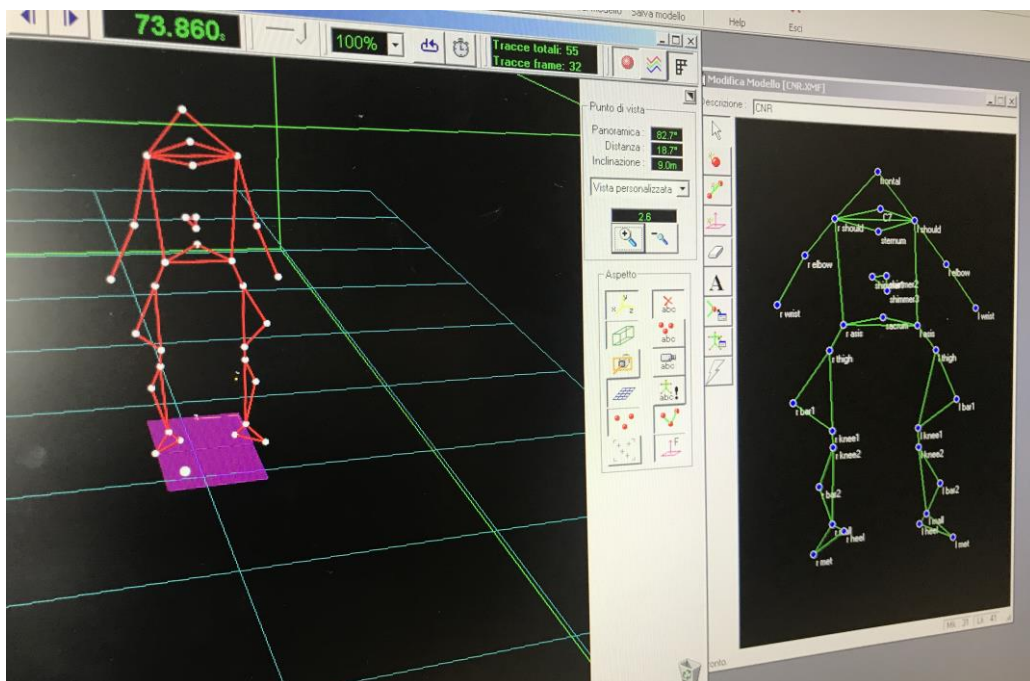


Figure 2.23-Joints labeling BTS

In order to have reliable results between the two cameras, we performed a recalibration phase between the two systems.

Each of the cameras has its own reference system, but we have chosen to use the same reference system, individuated in the origin of the MATLAB axis, overlapping the first head joint to it.

To perform this recalibration system, we have first centered in the MATLAB reference system origin the Head joints provided by the BTS system.

$$P_{i,O'}(j) = P_{i,m}(j) - P_{h,m}(1) \quad (2.27)$$

Where:

$P_{i,O'}(j)$ is the i-th point in j-th frame centered in the origin O' defined in the origin of the MATLAB reference system.

$P_{i,m}(j)$ is the i-th point in the j-th frame in the reference system M defined from the camera intrinsic reference system.

$P_{h,m}(1)$ is the head joint in the first frame in the reference system M defined from the camera intrinsic reference system.

In this way, it has been centered the head in the zero of the axes for both the Orbbec and BTS system.

Subsequently, due to the missing of a common reference system in which execute the analysis, two local reference systems have been individuated, with the origins in the medium point of the *Lasis* and *Rasis* for the BTS, and the right hip and left hip for the Orbbec system as expressed in **Figure 2.24**.

For the BTS local reference system, these steps have been followed in order to find the reference systems.

1. The medium point between *Lasis* and *Rasis* have been computed in **Equation 2.28**

$$\text{Medium} = \frac{\text{Lasis} + \text{Rasis}}{2} \quad (2.28)$$

The medium has been used as the origin of the local reference system.

2. The e_{yan} mediolateral unit vector is computed as the vector between the medium point and the *Rasis*, in **Equation 2.29**.

$$\overrightarrow{e_{yan}} = \frac{\text{Medium} - \text{Rasis}}{\|\text{Medium} - \text{Rasis}\|} \quad (2.29)$$

3. The e_{zan} upper down unit vector is computed in **Equation 2.30**.

$$\overrightarrow{e_{zan}} = \frac{\text{Medium} - \text{Sternum}}{\|\text{Medium} - \text{Sternum}\|} \quad (2.30)$$

We have verified that the angle between e_{zan} and e_{yan} was 90° with the dot product.

4. The e_{xan} anteroposterior unit vector is computed as the cross product of the e_{zan} and e_{yan} as in **Equation 2.31**.

$$\overrightarrow{e_{xan}} = \overrightarrow{e_{zan}} \times \overrightarrow{e_{yan}} \quad (2.31)$$

The e_{xan} is already a unit vector, being the two elements of the cross products two-unit vectors.

For the Orbbec local reference system, these steps have been followed in order to find the reference systems.

1. The medium point between *Lasis* and *Rasis* have been computed in **Equation 2.32**.

$$P_{Medium} = \frac{P_{Lhip} + P_{Rhip}}{2} \quad (2.32)$$

P_{Medium} has been used as the origin of the local reference system.

2. The e_{yan1} mediolateral unit vector is computed as the vector between the medium point and the Rasis, in **Equation 2.33**.

$$\overrightarrow{e_{yan1}} = \frac{P_{Medium} - P_{rhip}}{\|P_{Medium} - P_{rhip}\|} \quad (2.33)$$

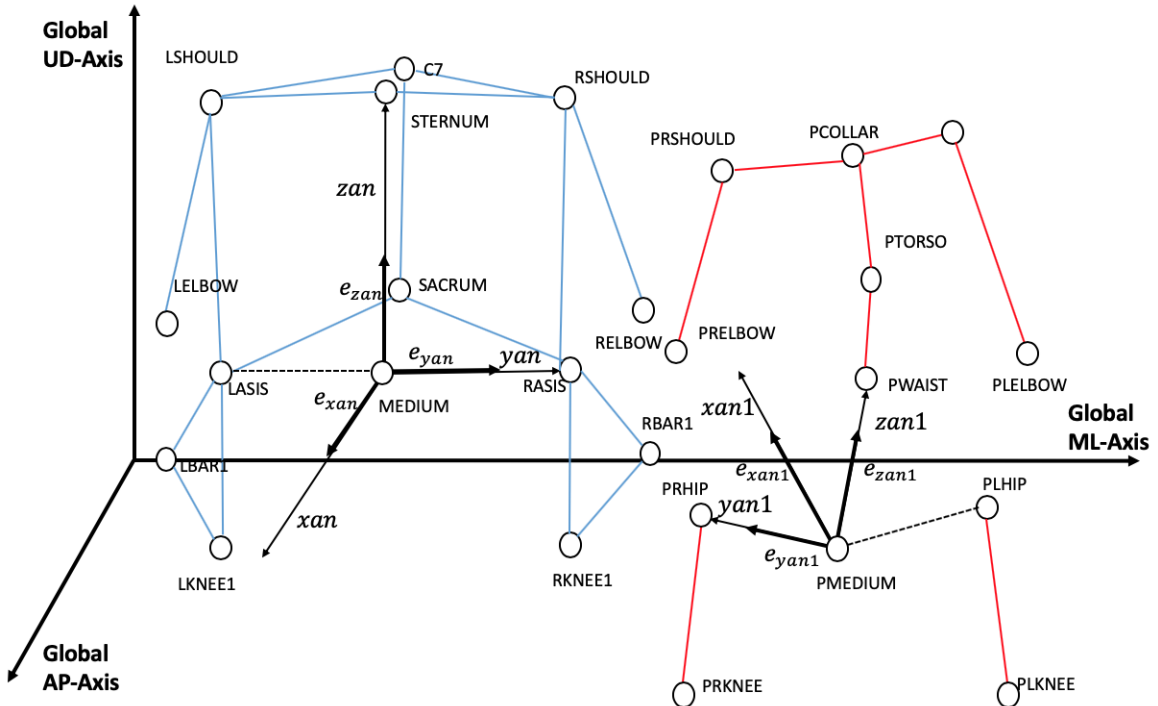


Figure 2.24-Local reference systems BTS-Orbbec

After the definition of the local reference systems, we passed to the phase of the alignment between the two reference systems. The axes have been projected in the 2D-planes in order to compute the angles of rotation. Especially we have computed first the angle of rotation around the UD-Axis represented by the angle γ_{12} as in **Equation 2.35**.

$$\gamma_{12} = \cos^{-1} \frac{\mathbf{e}_{yan}(x,y) \cdot \mathbf{e}_{yan1}(x,y)}{\|\mathbf{e}_{yan}(x,y)\| \|\mathbf{e}_{yan1}(x,y)\|} \quad (2.35)$$

And we applied the rotation matrix for the UD-axis rotation as in **Equation 2.36**.

$$R_{UD} = \begin{bmatrix} \cos\gamma_{12} & -\sin\gamma_{12} & 0 \\ \sin\gamma_{12} & \cos\gamma_{12} & 0 \\ 0 & 0 & 1 \end{bmatrix} \quad (2.36)$$

In this way, it has been aligned spatially the \mathbf{e}_{yan1} with the \mathbf{e}_{yan} of reference of the BTS system. Subsequently, it has been computed the \mathbf{e}_{zan1} upper down unit vector as in **Equation 2.37**.

$$\overrightarrow{e_{zan1}} = \frac{P_{Medium-PWaist}}{\|P_{Medium-PWaist}\|} \quad (2.37)$$

It has been computed the angle of rotation α_{12} around the AP-axis as in **Equation 2.38**.

$$\alpha_{12} = \cos^{-1} \frac{\mathbf{e}_{zan}(y,z) \cdot \mathbf{e}_{zan1}(y,z)}{\|\mathbf{e}_{zan}(y,z)\| \|\mathbf{e}_{zan1}(y,z)\|} \quad (2.38)$$

And then it has been applied the rotation matrix for the AP-axis rotation as in the **Equation 2.39**

$$R_{AP} = \begin{bmatrix} 1 & 0 & 0 \\ 0 & \cos\alpha_{12} & -\sin\alpha_{12} \\ 0 & \sin\alpha_{12} & \cos\alpha_{12} \end{bmatrix} \quad (2.39)$$

In this way, it has been aligned spatially the \mathbf{e}_{zan1} with the \mathbf{e}_{zan} of reference of the BTS system. Lastly, it has computed the last unit vector of the reference system \mathbf{e}_{xan1} as the cross product the \mathbf{e}_{zan1} and \mathbf{e}_{yan1} as in **Equation 2.40**.

$$\overrightarrow{e_{xan1}} = \overrightarrow{e_{zan1}} \times \overrightarrow{e_{yan1}} \quad (2.40)$$

It has been computed then the last rotation angle around the ML-Axis, the β_{12} angle.

$$\beta_{12} = \cos^{-1} \frac{e_{xan}(x,z) \cdot e_{xan1}(x,z)}{\|e_{yan}(x,z)\| \|e_{xan1}(x,z)\|} \quad (2.41)$$

And the rotation matrix relative to the ML-Axis has been applied.

$$R_{ML} = \begin{bmatrix} \cos\beta_{12} & 0 & \sin\beta_{12} \\ 0 & 1 & 0 \\ -\sin\beta_{12} & 0 & \cos\beta_{12} \end{bmatrix} \quad (2.42)$$

In **Figure 2.25** are represented the angles that have been computed, computing first the angle γ_{12} between the projections $e_{yan}[1,2]$ and $e_{yan1}[1,2]$ on the transversal plane e and realigning according to it. Subsequently the angle α_{12} between the projections $e_{zan}[1,2]$ and $e_{zan1}[1,2]$ on the coronal plane it's computed and realigned. After the realignment of the e_{yan1} and e_{zan1} , it has been computed the e_{xan1} axes with the cross product according to **Equation 2.30** and finally projected on the sagittal plane, computing the β_{12} angle of rotation.

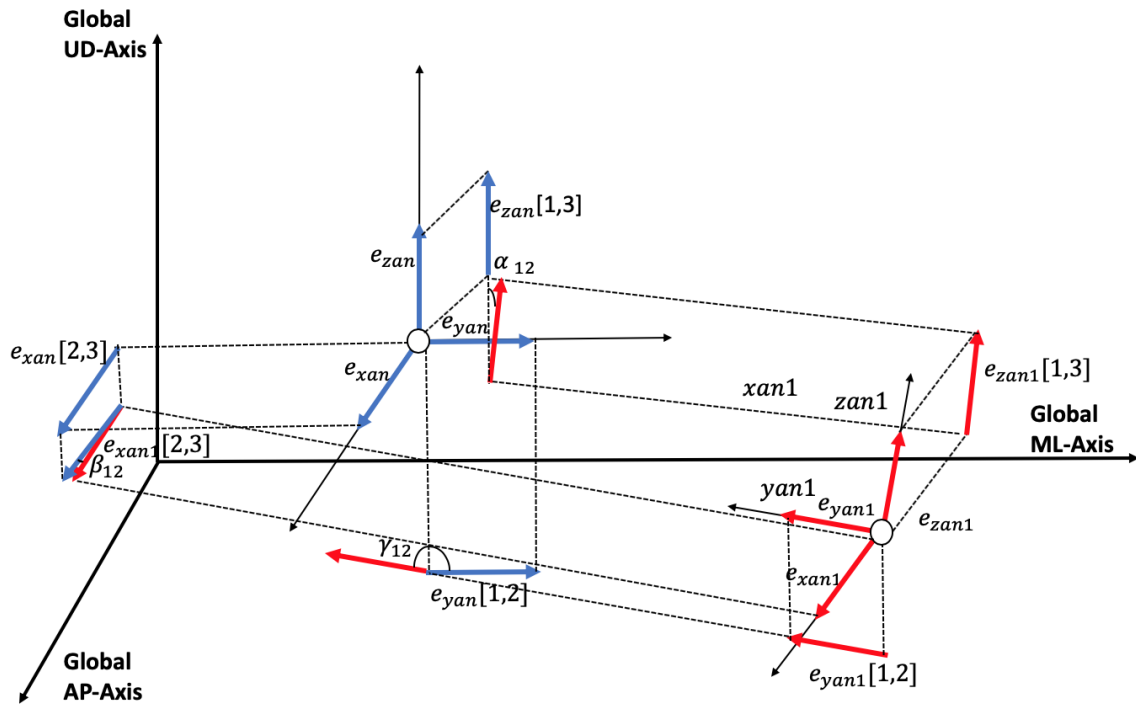


Figure 2.25-Projections of the local reference systems.

The final joints used for the analysis have been computed as in **Equation 2.43**.

$$Pi_{o'}(j) = (Pi_{i,o}(j) \cdot R_{UD}) \cdot R_{AP} \cdot R_{ML} \quad (2.43)$$

Thanks to this operation of realignment we have assured that the body models were in the same orientation in the space, making more reliable the analysis. By the way, we observed that most of the difference was in the orientation in the γ angle, relative to the AP-Axis rotation.

Indeed, from the first representations of the body together, it was possible to observe how basically they were simply specular. Coherently it has been found a mean γ_{12} angle of 177° , a mean β_{12} angle of 15° and a mean α_{12} angle of 3° .

After the phase of reposition, it has been thought of a list of tasks in order to validate the cameras in different conditions.

- **Static standing task for 30 seconds in artificial and light conditions:** the test aims to evaluate the standard deviations of all of the joints provided in all of the 3 axes compared with the information provided by the BTS. It's asked to stay completely still in front of the camera in the position of reference for 30 seconds. The observation window it's synchronized as mentioned above using as reference the right elbow movement of flexion.
It's computed the CoP according to the weights of **Figure 2.12**.
- **Standing dynamic task for 30 seconds in artificial conditions:** the test aims to evaluate how the cameras capture different simple movements compared to the BTS. After the synchronization movement, the movements performed are one flexion of the right arm, one flexion of the left arm, one squat. The results are compared between them in order to compute Pearson's correlation [49].
- **Seated static task for 30 seconds in artificial light conditions:** the interest is focused on evaluating how the presence of a chair or the sitting position can influence the acquisition. The parameters considered are the same ones as the first test.
- **Seated dynamic task for 30 seconds in artificial conditions:** the same parameters of the second test are evaluated seeing how the sitting position is influent on them.
- **Leg-agility:** it's asked to perform the task of the leg-agility as in **Table 1.2** in order to evaluate the behavior of the camera in a specific medical task.
- **Dynamic of the limbs:** it's asked to perform the rapid movements of the limbs, doing 10 flexion of the right and left arms, and 10 squats. This task is used to evaluate the behavior of the camera in movements at increasing velocity.

Have been computed then the CoP and are computed the trends of the CoP from the initial value in the observation interval.

$$\Delta CoP = CoP_j(i) - CoP_j \quad (2.44)$$

Where $CoP_w(i)$ is the i-th value of the CoP in the w-th axes.

The variations, instead, have been plotted in the three planes, in order to observe the sway for the Orbbec and the BTS CoP.

Are then computed the variation coefficients as defined in the equation, in order to refer the standard deviation with the mean value of the static position [47].

$$CV = \frac{s}{\bar{x}} \quad (2.44)$$

With s the standard deviation and \bar{x} the mean value.

Finally, the Boxplot of the three axes is plotted, individuating easily the number of outliers coming from the components of the CoP.

In it are represented the mean value of the distribution with the red line, the box of the min value and the max value, and the whiskers of the 25th percentile and the 75th percentile. In this way, it's easy to evaluate the outliers of the distributions.

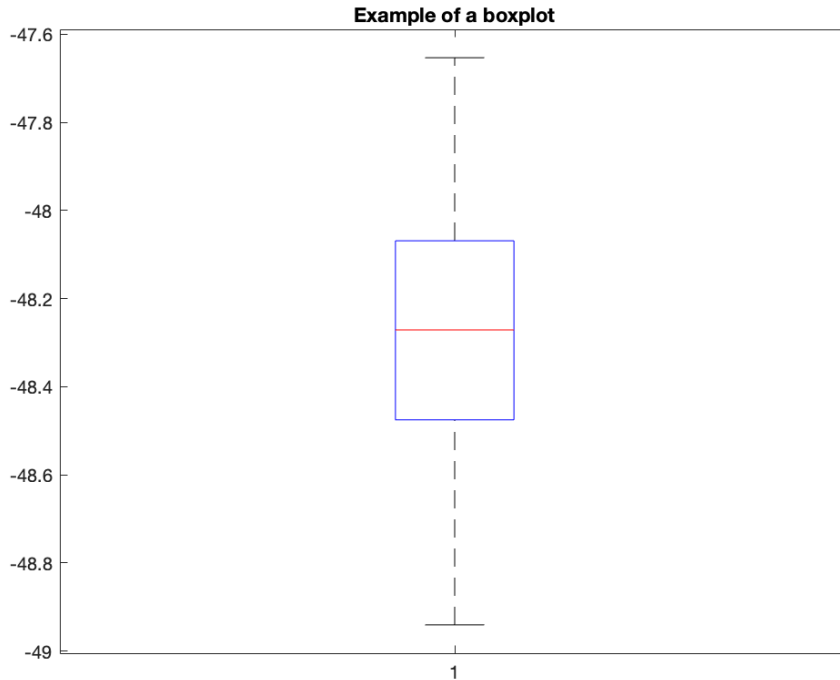


Figure 2.26-Example of Boxplot

2.6 Leg-agility Parameters

It has been chosen to focus on the leg-agility task extracted from the UPDRS scale because it was representative of how the systems could extract parameters from the clinical task. We followed the approach in literature used for the leg-agility analysis [48], in order to extract the time and frequency domain parameters.

After the phase of realigning between the leg signals coming from the two systems and their filtering, we computed the features of the tasks from both of them. In **Figure 2.27** are described the values taken into account by a single Leg-agility acquisition.

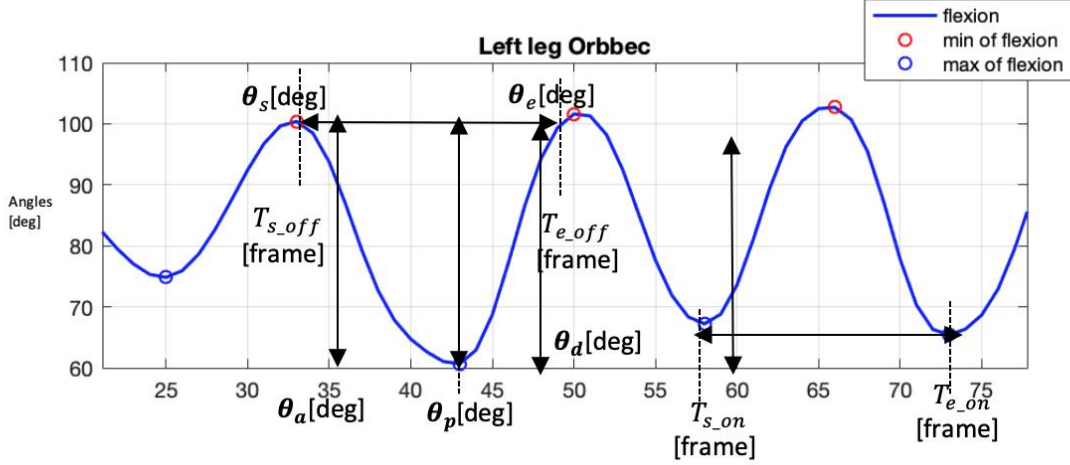


Figure 2.27-Leg agility task angle

- T_{s_off} is the time of the start of the movement of the flexion of the leg.
- T_{e_off} is the time of the ending of the movement of the leg flexion, taking again the position of rest.
- $\theta_s[\text{deg}]$ is the amplitude of the flexion measured as the difference from the i -th rest position and the i -th maximum peak.
- $\theta_a[\text{deg}]$ is the amplitude of the flexion measured as the difference from the i -th+1 rest position and the i -th+1 maximum peak.
- $\theta_p[\text{deg}]$ is the amplitude of the flexion measured as the mean of the $\theta_s(i)$ and $\theta_a(i)$
- T_{s_on} is the time of the i -th maximum of the leg-flexion.
- T_{e_on} is the time of the i -th+1 maximum of the leg flexion.

With the MATLAB function *findpeaks*, it has been found the peaks of the start of the movement with their relative time of occurrence and the peaks of the maximum flexion with their time.

After this phase, it has been computed the time parameters of the movement.

- $\omega(i)[\text{deg/s}]$ is the i -th velocity of the flexion computed with **Equation 2.45**.

$$\omega(i) = \frac{\theta_a(i) + \theta_s(i)}{T_{e_off} - T_{s_off}} \quad (2.45)$$

- The $P(i)$ [s] is the i -th rest parameter computed in **Equation 2.46**, that represents the time of rest position between two flexions.

$$P(i) = T_{e_off} - T_{s_off} \quad (2.46)$$

- The parameter $R(i)[s]$ is the i -th precision parameter computed in **Equation 2.47**, that represents the precision between two flexion.

$$R(i) = T_{e_on} - T_{s_on} \quad (2.47)$$

- The i-th difference between the angle flexion of the right leg and left leg $D\theta_{L_R}(i)$ [%] defined in **Equation 2.48**.

$$D\theta_{L_R}(i) = \frac{\theta_{mR}(i) - \theta_{mL}(i)}{\theta_{mR}(i)} \cdot 100 \quad (2.48)$$

- The i-th difference between the velocity of flexion of the right leg and left leg $D\omega_{L_R}(i)$ [%] defined in **Equation 2.49**.

$$D\omega_{L_R}(i) = \frac{\omega_{mR}(i) - \omega_{mL}(i)}{\omega_{mR}(i)} \cdot 100 \quad (2.49)$$

The parameters for the ten flexions required during the task have been computed and have been analyzed the mean values for each task. The tasks have been repeated three times in order to extract the variation between the different repetitions.

- θ_m is the mean amplitude computed in the ten repetitions in **Equation 2.50**.

$$\theta_m = \frac{\sum_{i=1}^{10} \theta_p(i)}{10} \quad (2.50)$$

- ω_m is the mean velocity computed in the ten repetitions in **Equation 2.51**.

$$\omega_m = \frac{\sum_{i=1}^{10} \omega(i)}{10} \quad (2.51)$$

- P_m is the mean Rest parameter computed in the ten repetitions in **Equation 2.52**.

$$P_m = \frac{\sum_{i=1}^{10} P(i)}{10} \quad (2.52)$$

- R_m is the mean Precision parameter computed in the ten repetitions in **Equation 2.53**.

$$R_m = \frac{\sum_{i=1}^{10} R(i)}{10} \quad (2.53)$$

- $D\theta_{L_R_m}$ is the mean difference of the angle parameter computed in the ten repetitions in **Equation 2.54**.

$$D\theta_{L_R_m} = \frac{\sum_{i=1}^{10} D\theta_{L_R}(i)}{10} \quad (2.54)$$

- $D\omega_{L_R_m}$ is the mean difference of the angular velocity parameter computed in the ten repetitions in **Equation 2.55**.

$$D\omega R_L_m = \frac{\sum_{i=1}^{10} D\omega R_L(i)}{10} \quad (2.55)$$

Furthermore, the standard deviations of the Precision parameter and the Rest parameter have been computed.

The frequency parameters have been evaluated, computing the peak in the Power spectral density. Due to the reduced length of the signals, it has been chosen to perform a parametric estimation of PSD with the Burg method [50], as showed in the **Figure 2.28**.

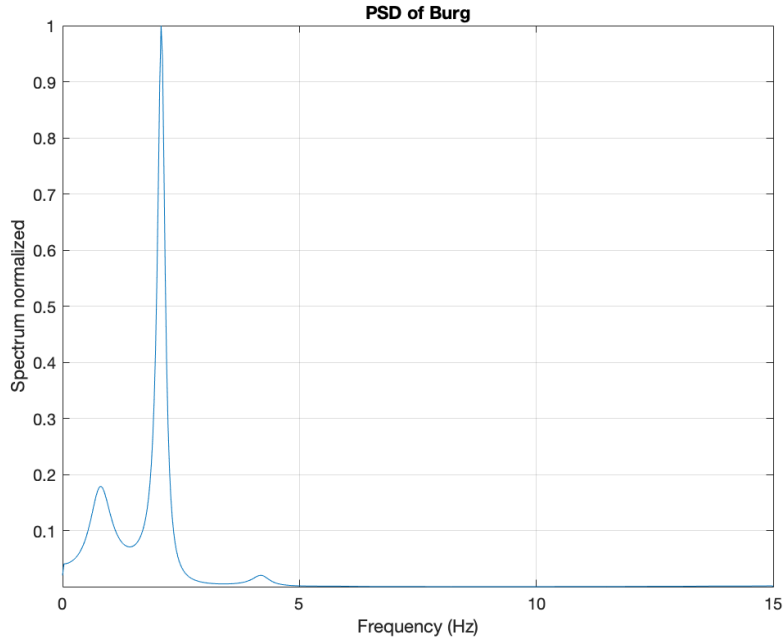


Figure 2.28-Burg Parametric PSD

Furthermore, it has been computed the short time Fourier transform (*STFT*) [52] in **Equation 2.56**, in order to see the variation of the spectrum during the tasks, realizing the *contour* and the *mesh* in order to have a representation of the spectrum as in **Figure 2.29**.

$$STFT_x^Y = \int_{-\infty}^{+\infty} x(\tau) \gamma(\tau - t) e^{-j2\pi f \tau} d\tau \quad (2.56)$$

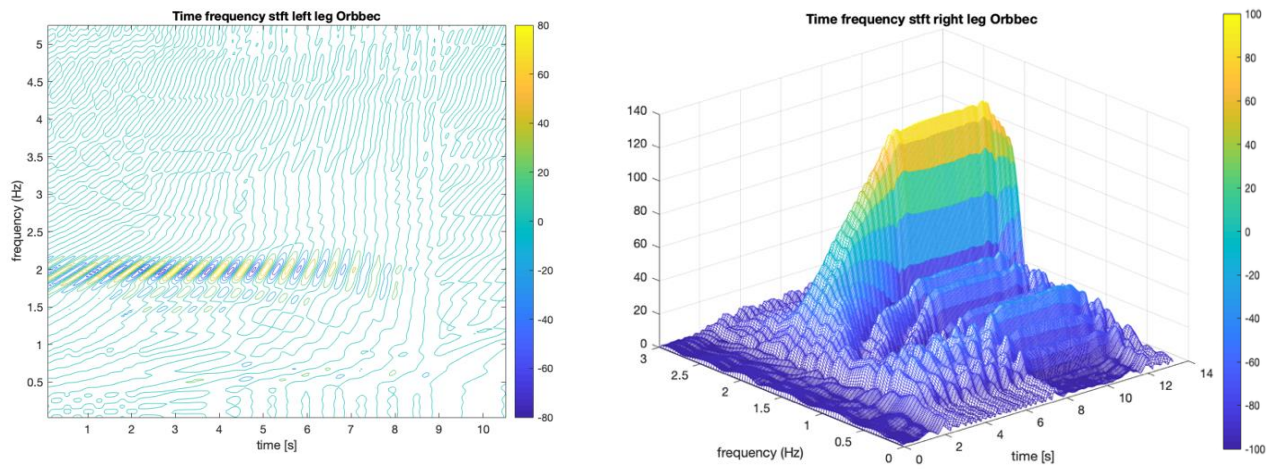


Figure 2.29-(a)Contour of the STFT (b)Mesh of the STFT

2.7 Kinect Azure Insight

Due to the problem deriving from the synchronous acquisition with the Kinect Azure and the BTS system we deepened these problems using the possibility of extraction of the IR channel and the Depth channel as showed in **Figure 2.30**, images represented with a MATLAB code that show them in a colormap *Summer*.

The depth and IR images are extracted by the MKV file produced by the Kinect azure with the software *ffmpeg* [51].

Three squares in the wall have been individuated in order to follow the intensity of the lights in that area of measurement, and three points that are representing the BTS cameras present in the scene. These points have been followed in the analysis in order to analyze how the intensity in the depth and IR scenes have swung.

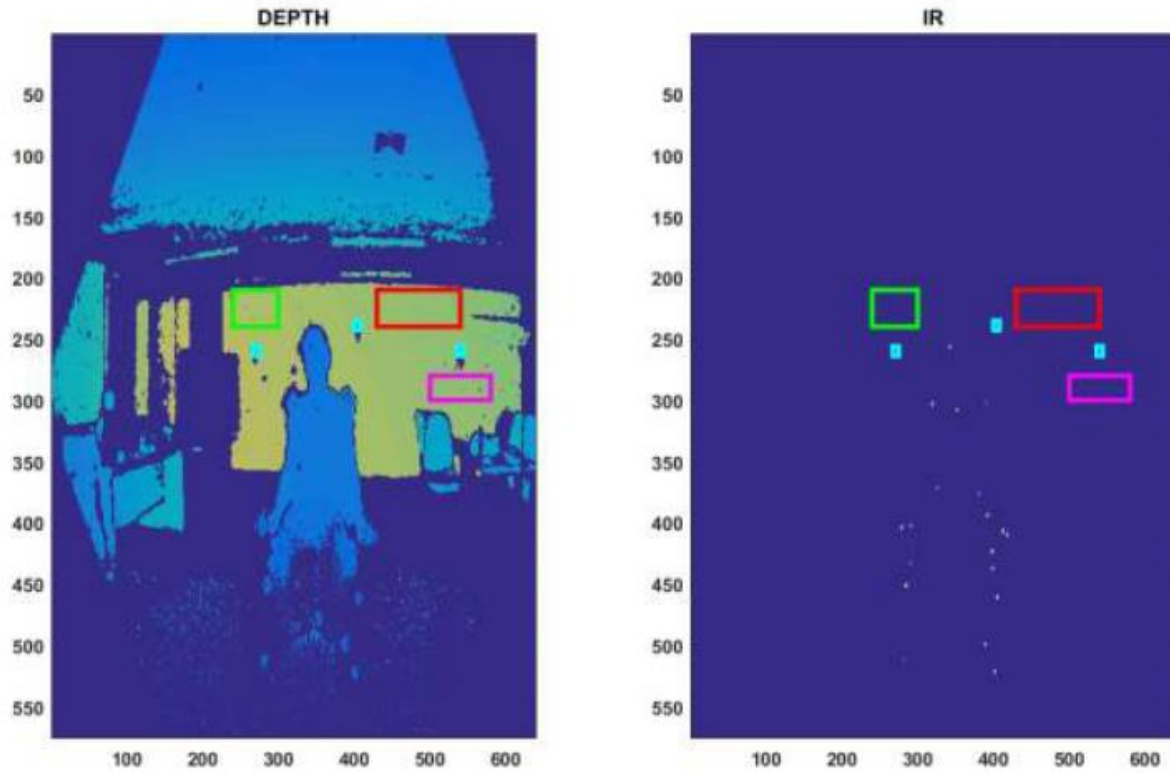


Figure 2.30-(a)Depth image of Kinect Azure (b) IR image of Kinect Azure acquisition

The images are extracted by the test of the LEG-AGILITY conducted to validate the camera, in order to find enough BTS camera in the scene viewed by the Kinect Azure.

3. Preliminary Results

In this chapter, they will be exposed all the preliminary results conducted in order to choose the best setup to validate with the BTS system. The structure of the chapter will follow the scheme of chapter [2.5.1](#). The intel cameras have been analyzed firstly, then it has been evaluated the Orbbec Astra Pro camera and the Kinect Azure camera.

3.1 Intel D415-D435

The subchapter gives the results for the tests conducted on the cameras highlighting the most interesting observation from the graphs. All of the subparagraphs are dedicated to the cameras compared, with the proves carried out.

3.1.1 Static standing task in artificial light conditions

The first test was carried out in the condition of artificial lights, with the cameras at different distances due to their FoV, as reported in **Table 3.1**.

Table 3.1-Static standing results Intel D415-D435 artificial light condition

<i>CAMERA</i>	<i>MEAN FRAMERATE [fps]</i>	<i>LOST FRAMES</i>	<i>REPEATED FRAMES</i>	<i>MEASURED DISTANCE</i>
D415	29.9826	22	32	2400 [mm]
D435	29.8904	25	28	2000 [mm]

From **Table 3.1** it emerges that the mean framerate it's stable for both the camera and the results of lost frames is acceptable being less than one second of acquisition.

The standard deviation, expressed in terms of millimeters, gives back as result the difficulty found by the Intel D435 in tracking the lower limbs, visible both in the bad results for both the ankles and knees. This trend can be seen in all the 3D axes of the reference system, with the greatest peaks on the AP-axes (**Figure 3.1**). The other joints have obtained values high comparable, showing no difference between the cameras.

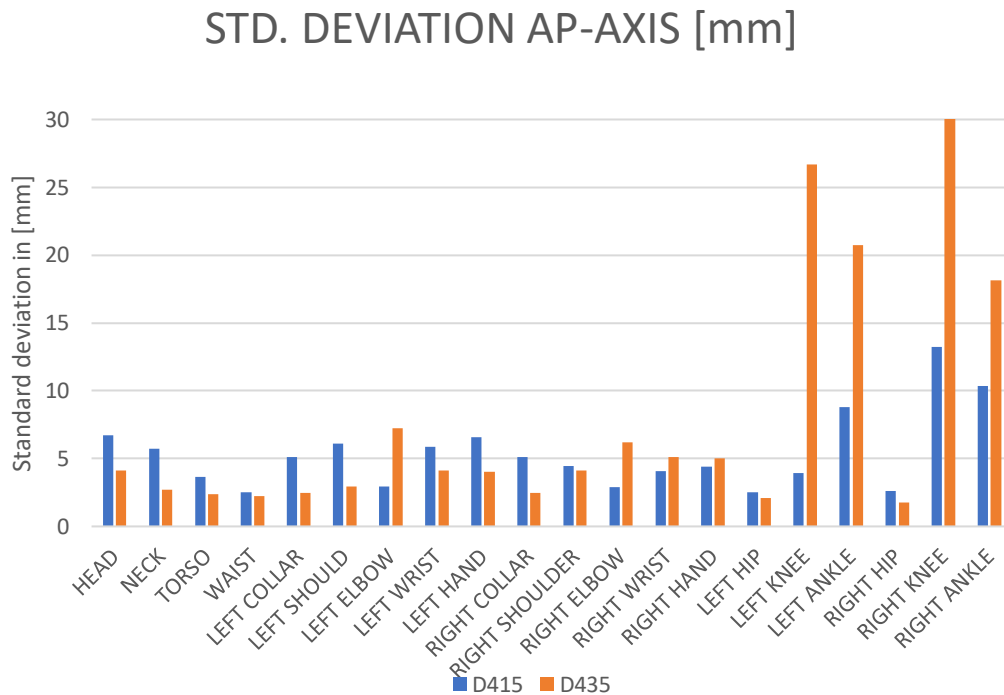


Figure 3.1- Standard deviation Bar Diagram AP-Axis
Static standing task D415-D435

In **Figure 3.2** the Intel D435 shows its problems in the acquisition of the lower limbs in the ML-Axis, having the right knee and the left knee the highest standard deviation. This result shows how the problem doesn't derive by interference on a single side, as it could be thought, assuming the presence of an interference object, but it's visible in both of them.

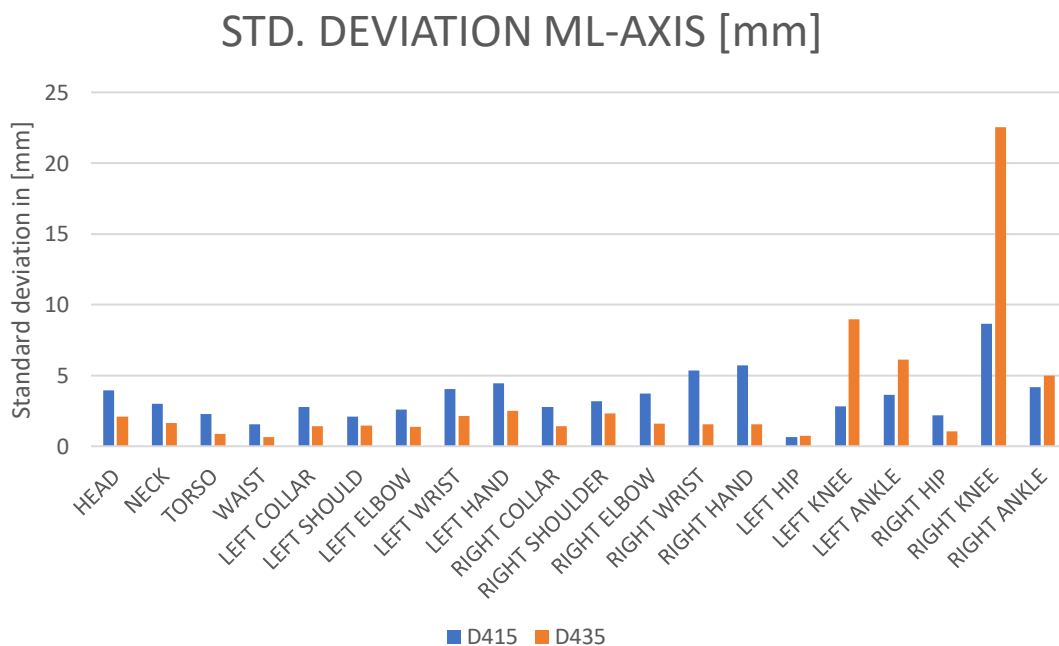


Figure 3.2-Standard deviation Bar Diagram ML-Axis Static
standing task D415-D435

In **Figure 3.3** it's observable how the joints of the limbs are now critical in the UD-axis for both the cameras. The computation of the CoP it's highly influenced by the lower limbs so, for the considerations about the sway of the CoP, these results would be not highly reliable.

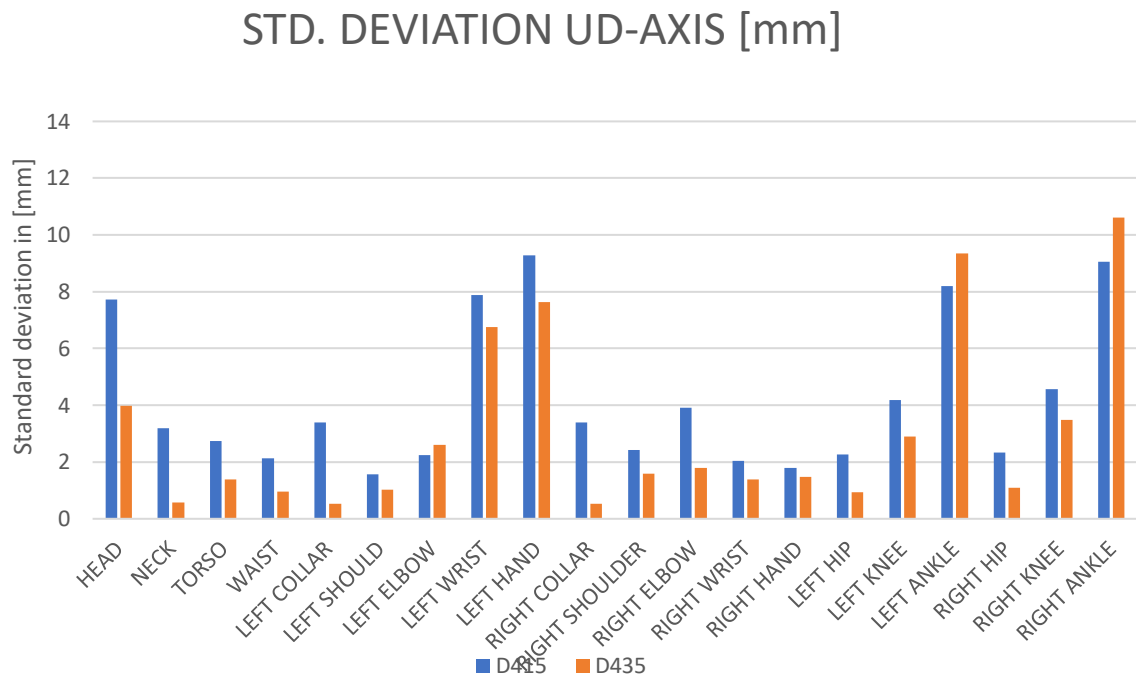


Figure 3.3-Standard deviation Bar Diagram UD-Axis
Static standing task D415-D435

3.1.2 Static standing task in natural light conditions

The task has been carried out in natural light conditions, turning off the lights of the laboratory. In **Table 3.2** the characteristic of the tasks and the performance of the cameras are summarized .

Table 3.2-Static standing results Intel D415-D435 Natural light condition

<i>CAMERA</i>	<i>MEAN FRAMERATE [fps]</i>	<i>LOST FRAMES</i>	<i>REPEATED FRAMES</i>	<i>MEASURED DISTANCE</i>
D415	29.9607	15	27	2400 [mm]
D435	29.9584	0	46	2000 [mm]

In **Figure 3.4** it's possible to observe that using only the natural light the performances of both the cameras improve lightly, underlying a possible optimal setup for these two systems. In this way, the two cameras provide basically the same quality of results.

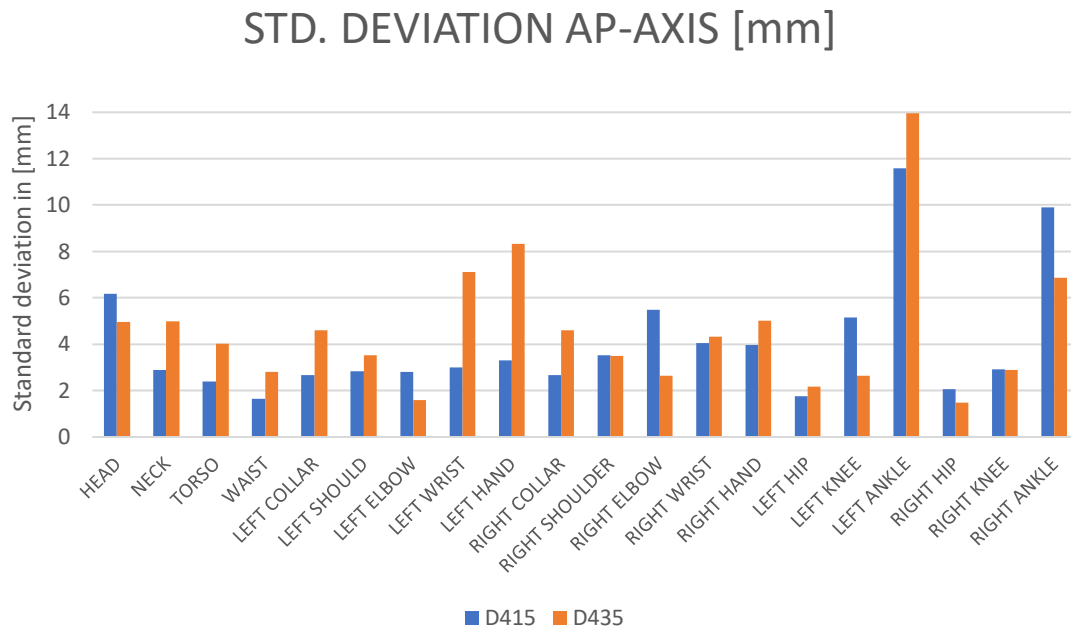


Figure 3.4-Standard deviation Bar Diagram AP-Axis
Static standing task D415-D435 Natural lights

Compared with the results in **Figure 3.5** in the three axes the performances are improved passing from a maximum standard deviation of 20 mm to one of 5 mm, individuating a better condition of work for the two Intel Cameras.

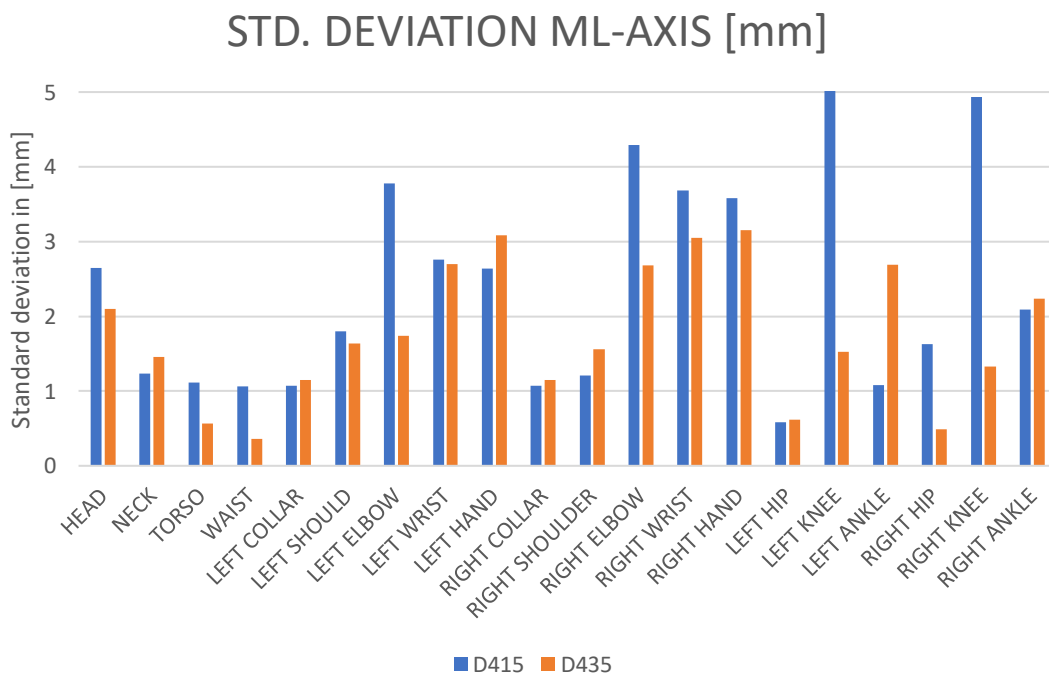


Figure 3.5-Standard deviation Bar Diagram ML-Axis
Static standing task D415-D435 with Natural light.

In the UD-axis in **Figure 3.6** even if the highest deviations are again figured by the joints, it can be seen a good improvement compared to the artificial lights' conditions results.

In this case, the waist, that previously hasn't been a critical joint, has one of the worst results for the D415. This is representative of how, even if the conditions are changed, the acquisitions are still too much variable.

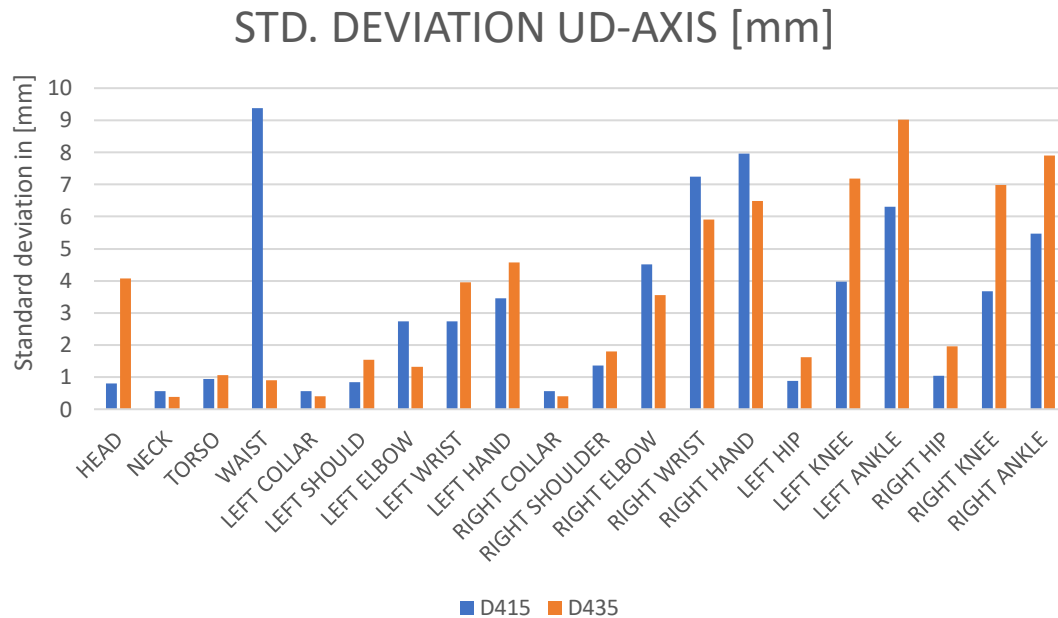


Figure 3.6-Standard deviation Bar Diagram UD-Axis
Static standing task D415-D435 with Natural light.

3.1.3 Standing dynamic Task in artificial light conditions

The task was executed with the lights in the laboratory turned on, and in **Table 3.3** it's possible to extract that the intel D435 in this task has lost 93 frames, that is 3 seconds of acquisition, while the Intel D415 has a good performance repeating only 28 frames losing no frames.

Table 3.3- Standing dynamic task results Intel D415-D435 artificial light condition				
<i>CAMERA</i>	<i>MEAN FRAMERATE [fps]</i>	<i>LOST FRAMES</i>	<i>REPEATED FRAMES</i>	<i>MEASURED DISTANCE</i>
D415	30.0060	0	28	2400 [mm]
D435	29.8220	93	46	2000 [mm]

Besides being comparable visually in **Table 3.4** , Pearson's correlation is computed, finding a high correlating coefficient that reaches 0.99.

Table 3.4-Pearson's correlation coefficient standing dynamic task Intel D415-D435 artificial light condition

Parameter	Pearson's Correlation Coefficient r^a	
	Mean \pm Std. Dev.	p-value
Left Elbow Flexion	0.99 \pm 0.03	<0.05
Right Elbow Flexion	0.98 \pm 0.04	<0.05
Left Knee Flexion	0.98 \pm 0.01	<0.05
Right Knee Flexion	0.97 \pm 0.01	<0.05

3.1.4 Seated dynamic task in artificial light conditions

The task was executed with the lights in the laboratory turned on, and in the **Table 3.5** are resumed the performances, concluding that the Intel D435, in this case, has lost 174 frames, about 6 seconds of acquisition, while the Intel D415 has again a better behavior, losing less captures and repeating a smaller number of frames.

Table 3.5-Seated dynamic task results Intel D415-D435 artificial light condition

<i>CAMERA</i>	<i>MEAN FRAMERATE [fps]</i>	<i>LOST FRAMES</i>	<i>REPEATED FRAMES</i>	<i>MEASURED DISTANCE</i>
D415	29.9793	19	29	2400 [mm]
D435	29.6723	174	34	2000 [mm]

In **Figure 3.7** it's possible to observe how the left elbows movement was completely lost, probably due to the high number of frames missed during the acquisition, result highlighted also in **Table 3.6** where the coefficient relative to the right elbow flexion has obtained a value of 0.5026 \pm 0.0724.

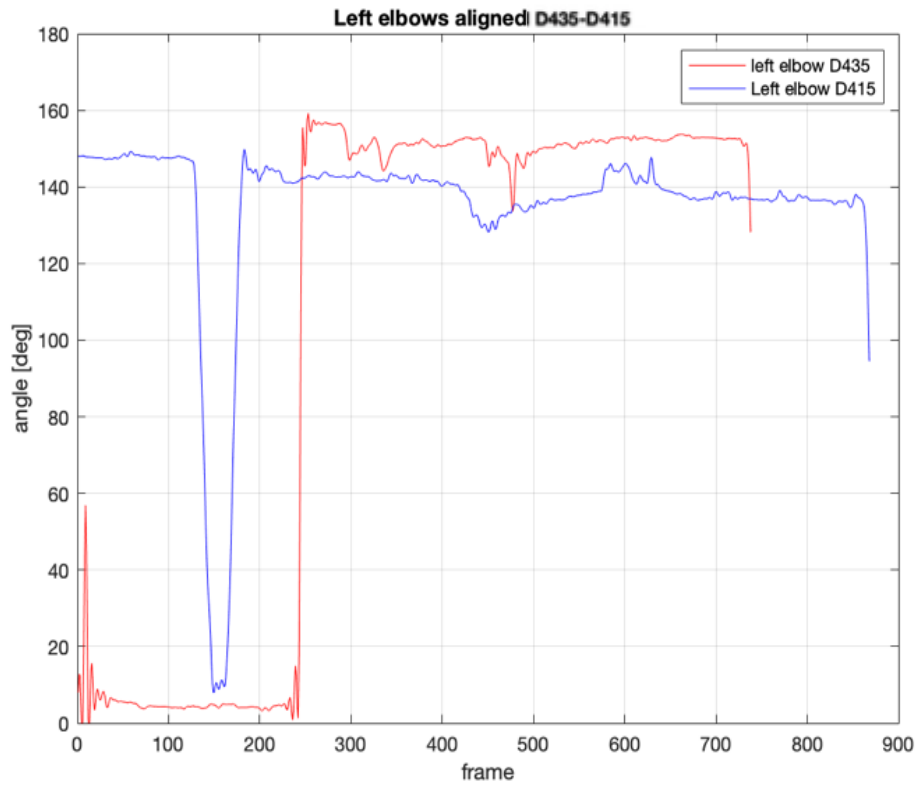


Figure 3.7-Angles representation seated dynamic task Intel D415-D435 artificial light condition

Table 3.6-Pearson's correlation coefficient seated dynamic task Intel D415-D435 artificial light condition

Parameter	Pearson's Correlation Coefficient r^a	
	Mean \pm Std.Dev.	p-value
Right Elbow Flexion	0.1135 \pm 0.0957	0.0011
Left Elbow Flexion	0.9851 \pm 0.0028	<0.05
Left Knee Flexion	0.8431 \pm 0.0280	<<0.05
Right Knee Flexion	0.5026 \pm 0.0724	<<0.05

r^a significance level $p < 0.05$

Considered all of these previous tasks, and the results obtained, highlighting a difficult use of the Intel D435, and the difficult of guarantee a correct functioning, it has been chosen to use the Intel D415 in order to be compared with the Orbbec Astra Pro.

3.2 Intel D415-Orbbec Astra Pro

The same tasks of [chapter 3.1](#) are repeated in the evaluation of the Intel D415 with the Orbbec Astra Pro.

3.2.1 Static standing task in artificial light conditions

In **Table 3.7**, the results of the two cameras placed side by side are summarized. It emerges that the D415, that previously had better behavior in the analysis of [chapter 3.1](#), has a low result, reaching an elevated number of missing frames.

Table 3.7- Standing static task results Intel D415-Orbbec artificial light condition

<i>CAMERA</i>	<i>MEAN FRAMERATE [fps]</i>	<i>LOST FRAMES</i>	<i>REPEATED FRAMES</i>	<i>MEASURED DISTANCE</i>
ORBBEC	29.9849	0	0	2500 [mm]
D415	29.9779	179	40	2700 [mm]

In **Figure 3.8**, **3.9** and **3.10** it's possible to observe how the Orbbec can have a good performance in terms of Standard deviations and number of lost frames.

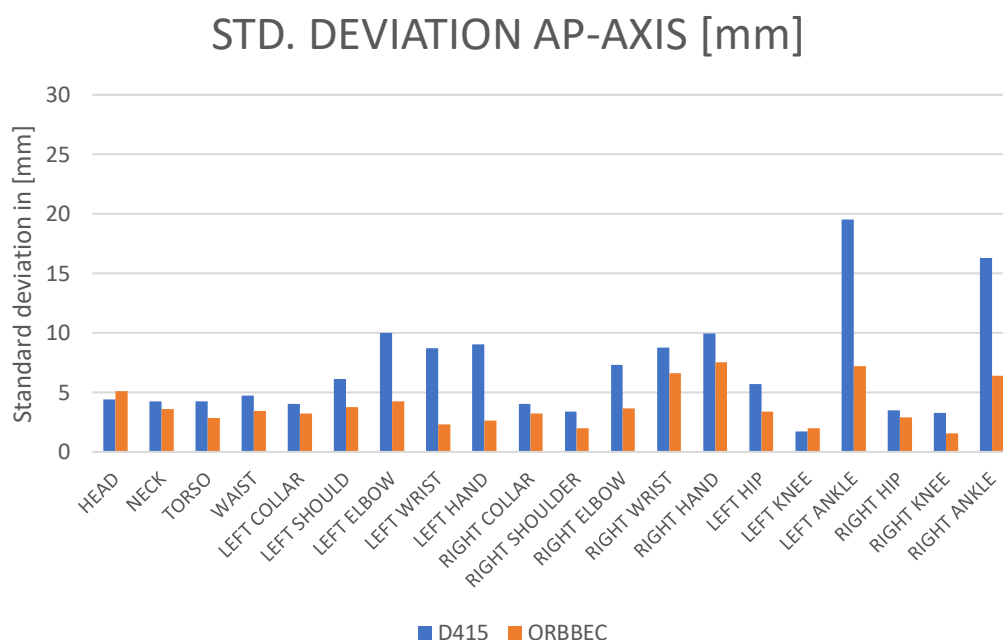


Figure 3.8-Standard deviation Bar Diagram AP-Axis static standing task Intel D415-Orbbec artificial Light condition

In the ML-Axis the left ankle of the Intel D415 results to have a standard deviation of 25 mm, which is much more than all the standard deviations of the other joints and the performances of the Orbbec Astra Pro.

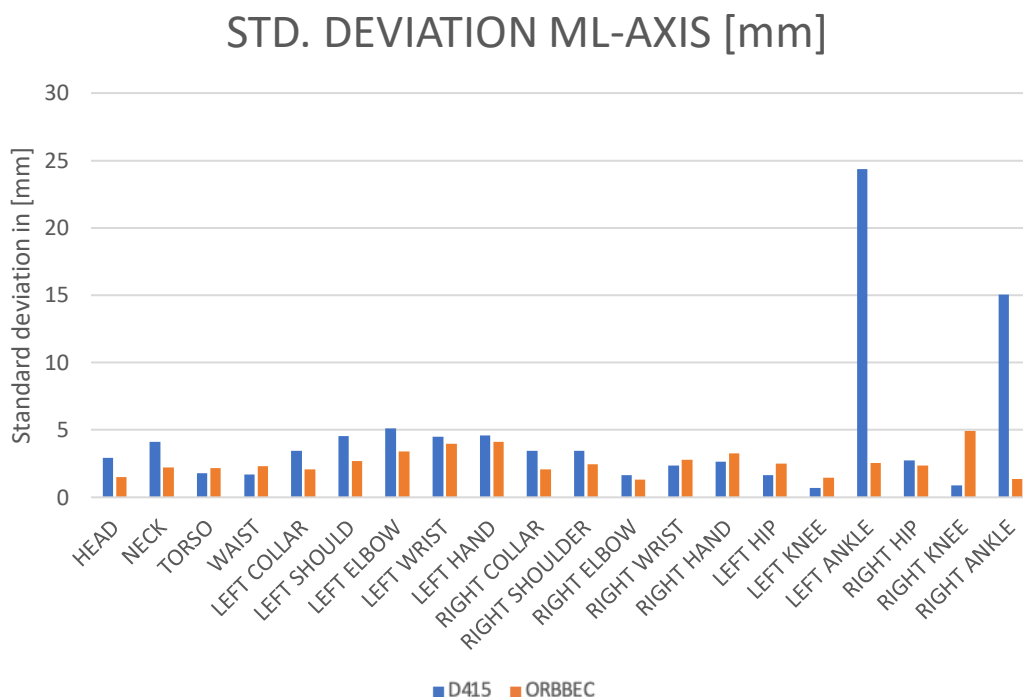


Figure 3.9-Standard deviation Bar Diagram ML-Axis static standing task Intel D415-Orbbec artificial Light condition

In the UD-axis, as described in **Figure 3.10**, the critical joints are basically the same and keep being the ones referred to the limbs, that are the hardest to be segmented during the elaboration. The joints of the hands have been analyzed, but operatively they are hard to use being in commerce a specific SDK that uses different points for the tracking of the hand.

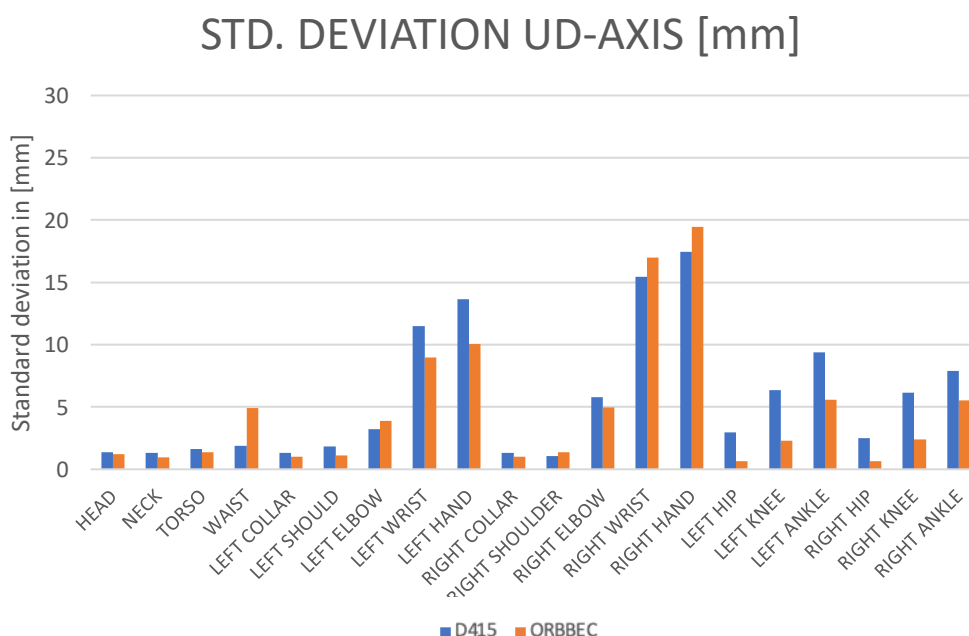


Figure 3.10-Standard deviation Bar Diagram AP-Axis static standing task Intel D415-Orbbec artificial Light condition

3.2.2 Static standing task in natural light conditions

Trying to acquire with natural lights we observed a brusque decrease of the framerate of the Orbbec as described in **Table 3.8**

Table 3.8- Standing static task results Intel D415-Orbbec Natural light condition

<i>CAMERA</i>	<i>MEAN FRAMERATE [fps]</i>	<i>LOST FRAMES</i>	<i>REPEATED FRAMES</i>	<i>MEASURED DISTANCE</i>
ORBBEC	7.5326	0	5	2500 [mm]
D415	30.0129	0	32	2700 [mm]

All the previous tests showed that the Orbbec interfaced with NuiTrack could keep the mean framerate of 30 fps while in this light condition the mean framerate went down until 7.5326 fps. Furthermore, we didn't observe this behavior with the PC of the laboratory with the GPU Nvidia XForce, but only when we used the camera with the Laptop.

Searching in the literature, the problem was not reported either in the Orbbec requirements, neither in the articles.

This behavior could derive from the settings of the camera, that, when it's not interfaced with a performant CPU decreases by default the framerate in order to don't stress too much the processor.

We tried to modify this setting on the NuiTrack configuration file, but it's commanded by the intrinsic settings of the camera.

According to these results, we chose to avoid any use of the Orbbec Astra Pro in natural light conditions or in low light conditions, considering the performances of the framerate proposed not satisfying to do analysis and considerations compared to other cameras.

3.2.3 Standing dynamic task

In **Table 3.9**, the parameters of the task, that are overall similar between the two cameras are summarized.

Table 3.9- Standing static task results Intel D415-Orbbec artificial light condition

<i>CAMERA</i>	<i>MEAN FRAMERATE [fps]</i>	<i>LOST FRAMES</i>	<i>REPEATED FRAMES</i>	<i>MEASURED DISTANCE</i>
ORBBEC	29.9604	44	0	2500 [mm]
D415	29.8781	33	28	2700 [mm]

The performances in the dynamic tasks result to be highly correlated with the same acquisition of the movements in terms of angular variation in the frontal and sagittal plane for the elbows and the knees respectively. Pearson's coefficients are summarized in **Table 3.10** and they show the high correlations that reach 0.9935 ± 0.0016 as the highest results.

Table 3.10-Pearson's correlation coefficient standing dynamic task Intel D415-Orbbec artificial light condition

<i>Parameter</i>	<i>Pearson's Correlation Coefficient r^a</i>	
	Mean \pm Std. Dev.	p-value
Right Elbow Flexion	0.9696 \pm 0.0076	<<0.05
Left Elbow Flexion	0.9402 \pm 0.0148	<<0.05
Left Knee Flexion	0.9955 \pm 0.0012	<<0.05
Right Knee Flexion	0.9935 \pm 0.0016	<<0.05
r^a significance level $p<0.05$		

3.2.4 Seated dynamic task

In **Table 3.11**, the outcomes of the task are summarized, underlining a good performance for both the camera, with some slight issues for Intel.

Table 3.11-Seated static task results Intel D415-Orbbec artificial light condition

<i>CAMERA</i>	<i>MEAN FRAMERATE [fps]</i>	<i>LOST FRAMES</i>	<i>REPEATED FRAMES</i>	<i>MEASURED DISTANCE</i>
ORBEC	29.9474	19	0	2500 [mm]
D415	29.9585	37	27	2700 [mm]

The elbow flexions are highly correlated, data confirmed by the table of Pearson's coefficient in **Table 3.12**.

Regarding the knee flexions, we observed a different correlation that goes down until 0.5815 \pm 0.0746 due to the reduced angular variation visible by the Intel D415, which keeps being highly variable during different acquisitions.

Table 3.12-Pearson's correlation coefficient seated dynamic task Intel D415-Orbbec artificial light condition

<i>Parameter</i>	<i>Pearson's Correlation Coefficient r^a</i>	
	Mean \pm Std. Dev.	p-value
Right Elbow Flexion	0.9624 \pm 0.0082	<0.05
Left Elbow Flexion	0.9915 \pm 0.0019	<0.05
Left Knee Flexion	0.5815 \pm 0.0746	<<0.05
Right Knee Flexion	0.6959 \pm 0.0578	<<0.05
r^a significance level $p<0.05$		

Looking at the previous results exposed, considered the more robust performances and the facility of the setup, it has been chosen to interface the SDK Nitrack with the Orbbec Astra Pro, despite the limitation of use in low-light conditions due to the low framerate. It's assumed, indeed, that the acquisitions, even if conducted in a domestic environment, will be furnished of a good brightness.

Subsequently, it has been used the same approach in order to evaluate the behavior of the Kinect Azure with his SDK, with Orbbec Astra Pro and NuiTrack SDK.

3.3 Orbbec Astra Pro-Azure Kinect

During the setting of the cameras, we observed that only a computer with a powerful GPU (Nvidia Graphics Processing Unity) could sustain the specific requirements of the Kinect in order to represent the real-time mesh of the body and at the same time elaborate the images with the convolutional networks in order to find the joints.

Thinking of that these applications how meant to be low-cost, the presence of a GPU could be not ensured. To cope with this problem, we used the Offline processor provided by Microsoft, in order to find the joints of the tasks removing the real time-mesh executed by the SDK.

3.3.1 Orbbec Astra Pro-Azure Kinect Static Standing task

In **Figure 3.11** are presented all the standard deviations of the common points of the Kinect Azure and Orbbec Astra Pro in the three axes. It's possible to observe that in the AP-Axis the performances are similar to the left and right hands as more critical joints.

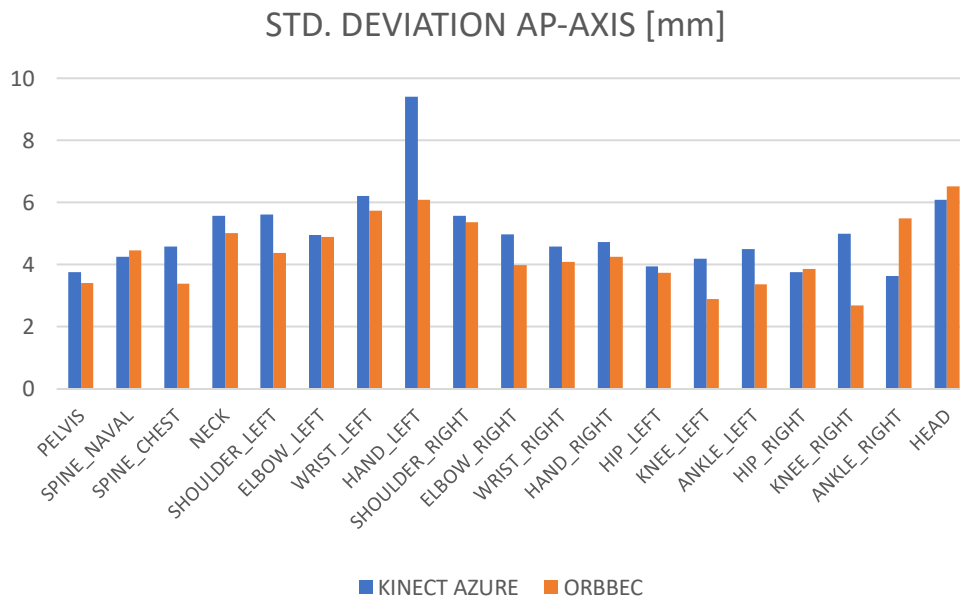


Figure 3.11-Standard deviation Bar Diagram AP-Axis static standing task Azure-Orbbec

In the ML-Axis, as described in **Figure 3.12**, it can be observed the same critical joints, putting an accent on the Left-Hand joint that has the double of the other standard deviation, with a value of about 10 mm.

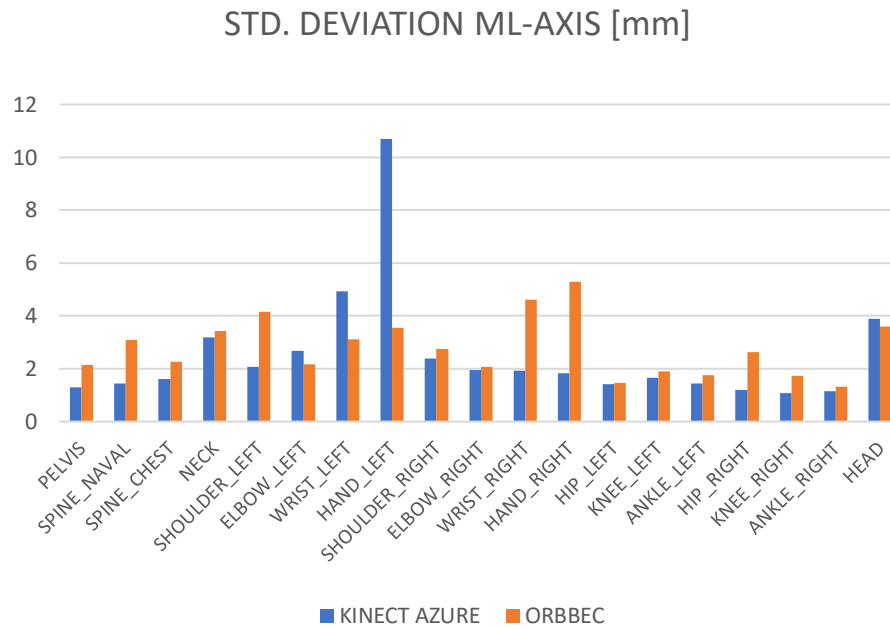


Figure 3.12-Standard deviation Bar Diagram AP-Axis static standing task Azure-Orbbec artificial light condition

In the UD-Axis (**Figure 3.13**), the Kinect Azure has difficulties in the tracking of the left upper limb in totality, starting from the shoulder. This behavior, never founded before, could be reconducted to the presence of an interference element in the scene at the height of the left arm. The same problems of the lower limbs are again evidenced in the Orbbec Astra Pro, where the Kinect joints are instead tracked with no particular problem. Generally, the Kinect Azure has a better way to track the lower limbs, having the possibility of finding the entire body, segmenting the floor, achieving to anchor exactly the tracking of the feet.

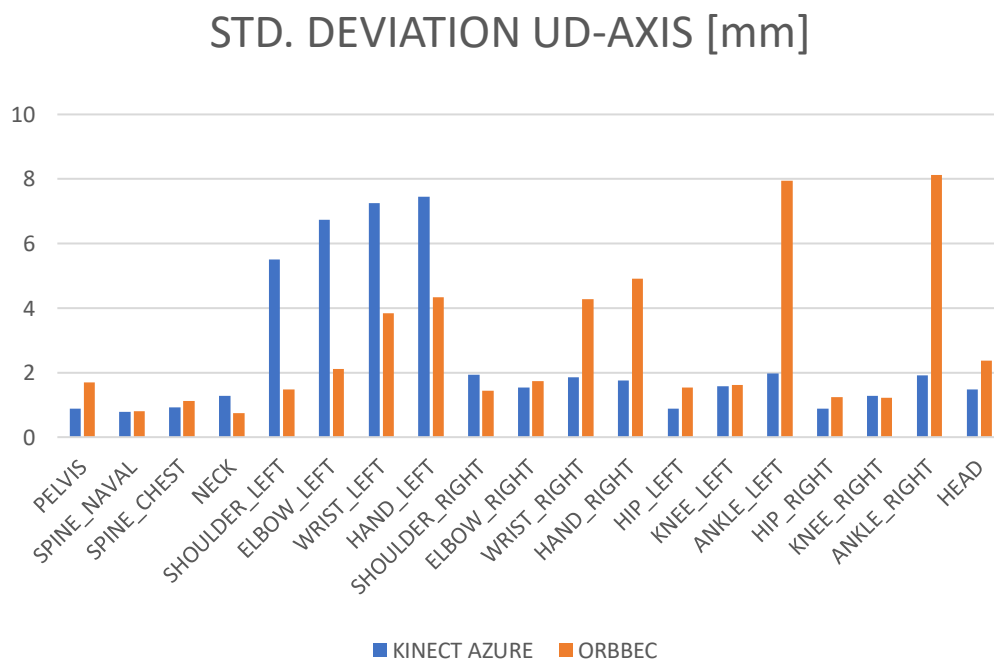


Figure 3.13-Standard deviation Bar Diagram AP-Axis static standing task

3.3.2 Orbbec Astra Pro-Azure Kinect Standing dynamic task

In the dynamic task, the angular variation resulted to be high correlated with no evidence of particular problems between the two acquisitions, as visible in **Table 3.13**, where are shown Pearson's correlation coefficients, descriptive of a high correlation with a mean value of 0.98.

Table 3.13-Pearson's correlation coefficient standing dynamic task Azure-Orbbec artificial light condition

Parameter	Pearson's Correlation Coefficient r^a	
	Mean \pm Std. Dev.	p-value
Right Elbow Flexion	0.9956 \pm 0.0007	<0.05
Left Elbow Flexion	0.9864 \pm 0.0021	<0.05
Left Knee Flexion	0.9903 \pm 0.0015	<<0.05
Right Knee Flexion	0.9887 \pm 0.0018	<<0.05

3.3.3 Orbbec Astra Pro-Azure Kinect seated static task

In **Figure 3.14**, the Orbbec showed the same problems highlighted in [Chapter 3.1.2](#), that is, having no fixed point of the feet to the ground, has in the joints of the lower limbs the highest variable joints.

Regarding the Azure, the segmentation that is generated from the ground gives as often great aid in the identification of the joints, underlining the results in the lower deviation in spite of the Orbbec Joints.

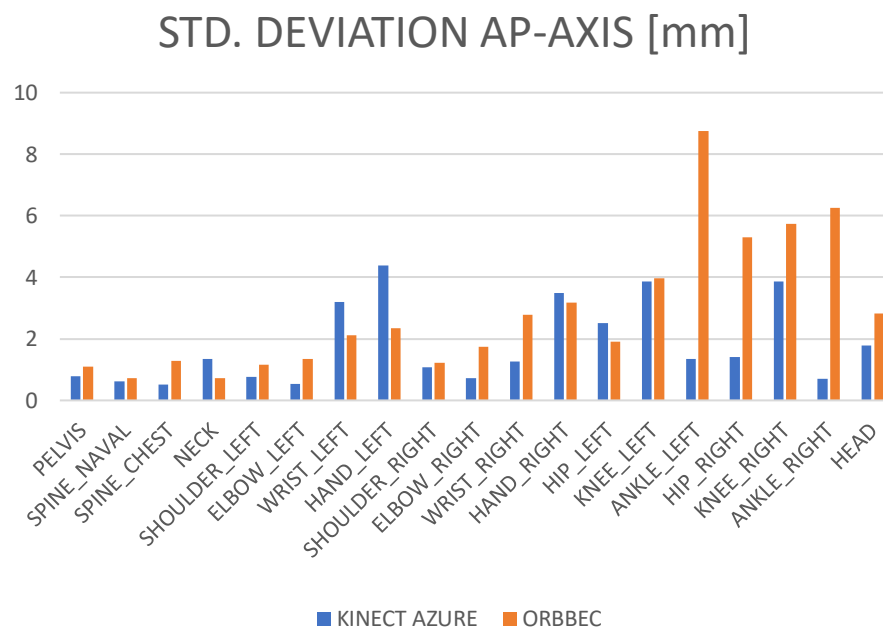


Figure 3.14-Standard deviation Bar Diagram AP-Axis static seated task Azure-Orbbec artificial light condition

The considerations about the Lower limbs are the same explicated previously, although in **Figure 3.15** the deviation is much more contained, reaching the maximum value for the right and left hip.

This behavior is explicable with the seated pose used in the task, where the body in the frontal plane gives occlusion of the hips that are harder to be individuated and followed.

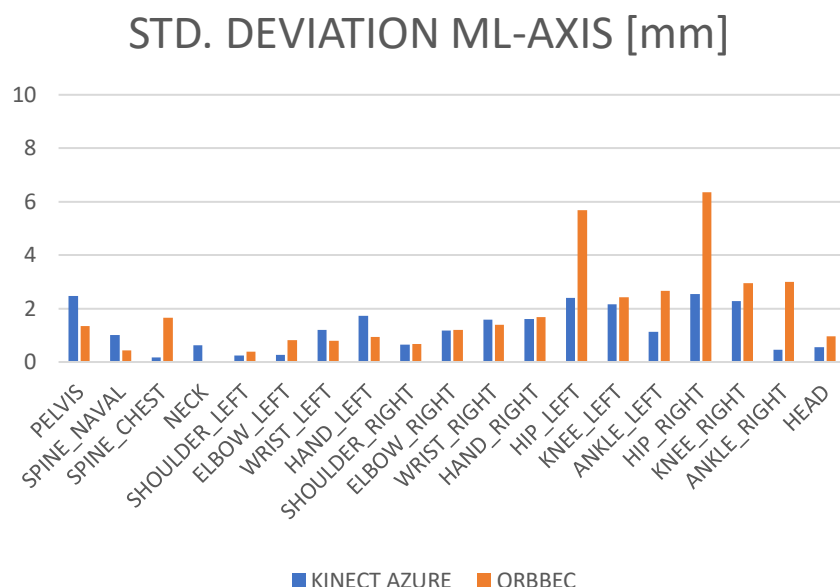


Figure 3.15-Standard deviation Bar Diagram ML-Axis static seated task

In the UD-Axis, as visible in **Figure 3.16**, the considerations about the lower limbs are much more evident, considered that the missing individuation of the floor makes it hard to fix the ankles and to follow them continuously.

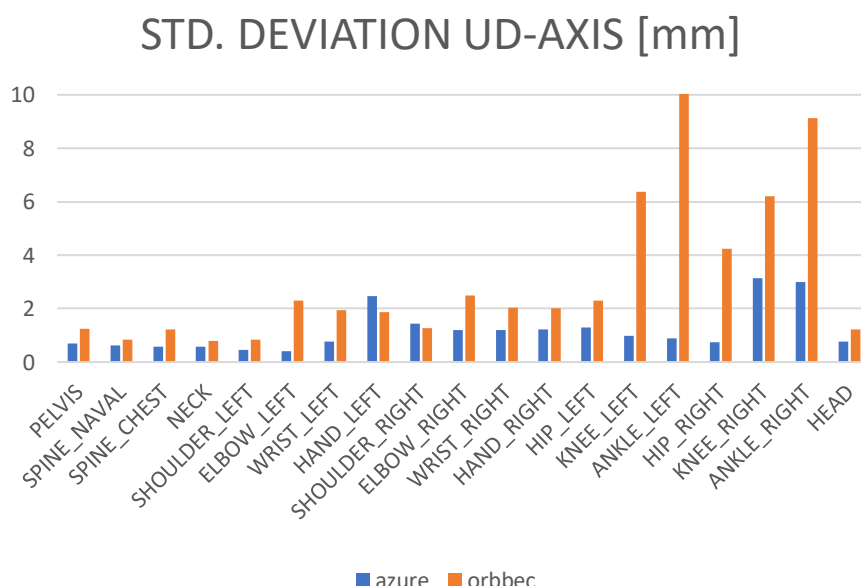


Figure 3.16-Standard deviation Bar Diagram UD-Axis static seated task Azure-Orbbec artificial light condition

3.3.4 Orbbec Astra Pro-Azure Kinect sitting dynamic task

In the sitting task, the detection of the angles of the upper limbs is high-correlated as shown in **Table 3.14**, with correlations near to one, but for the lower limbs the Orbbec results to have more difficulties in the correct tracking of the movements.

Table 3.14-Pearson's correlation coefficient seated dynamic task Azure-Orbbec artificial light condition

Parameter	Pearson's Correlation Coefficient r^a	
	Mean \pm Std. Dev.	p-value
Right Elbow Flexion	0.9866 \pm 0.0021	<0.05
Left Elbow Flexion	0.9656 \pm 0.0053	<0.05
Left Knee Flexion	0.8813 \pm 0.1051	<<0.05
Right Knee Flexion	0.5437 \pm 0.1951	<<0.05

Watching at the previous results we chose to validate both the setups, the Orbbec Astra Pro with the NuiTrack SDK and the Kinect Azure with his own SDK.

4.Validation results

In the following chapter, the results of all the tasks executed in order to validate the systems with the BTS Optitrack system will be exposed.

There will be exposed before the Orbbec results, with the consequent comments and subsequently the Kinect Azure results.

4.1 Orbbec Astra Pro results

The structure of the chapter follows the description of the tasks performed in [Chapter 2.5.2](#), introducing all the results highlighted by the validation analysis performed in the laboratory “*L. Divieti*” of Milan.

4.1.1 Static standing task

The original acquisitions have been saved in the *EMT* file and the *JSON* files respectively for the BTS and the Orbbec Astra Pro. After the down sample of the BTS file with the MATLAB function *resample*, passing from 100 to 30 fps, the observation window has been correctly found with the angles of the right arm, making the observation focused in 1000 frames, that is about 30 s.

It's necessary to reiterate that these acquisitions are made on a human model in a static position, so a real sway could be present. By the way, it is interesting, that the sways be comparable in the absolute, results that would be positive for the validation.

In **Figure 4.1**, the two bodies from the original raw points provided by the Orbbec Astra Pro and the BTS system, are represented.

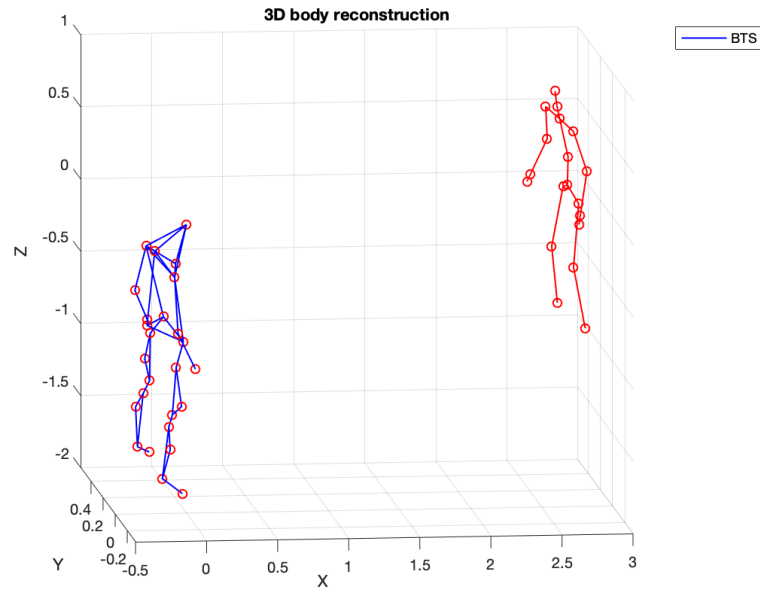


Figure 4.1-Bodies in the original reference system

In **Figure 4.2** the two bodies in axonometric view are represented, after the procedure of recalibration, showing a good realignment between the two bodies. This is a first positive result, showing how even if the captures are based on two completely different technologies, the body model extracted is highly comparable. The right limb joints are filled, in order to be discriminated against by the left side of the body. In **Figure 4.3**, the bodies are represented in a frontal view.



Figure 4.2-Axonometric view of bodies in the common reference system

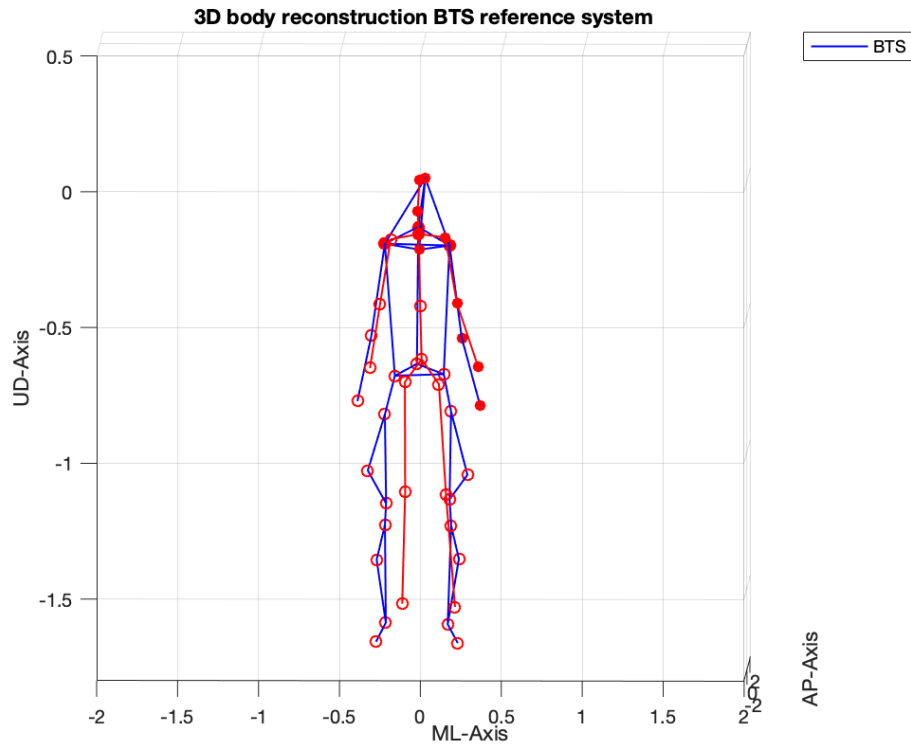


Figure 4.3-Frontal view of the bodies in the same reference system

In **Figure 4.4** are represented the CoP trend for the Orbbec and BTS system, with aligning of the reference system, showing the absolute sway in terms of centimeters.

The delta positions are slightly different, having an absolute value that is comparable, in the order of 3 cm for the AP and UD-axes and 0.5 cm for the ML-axes.

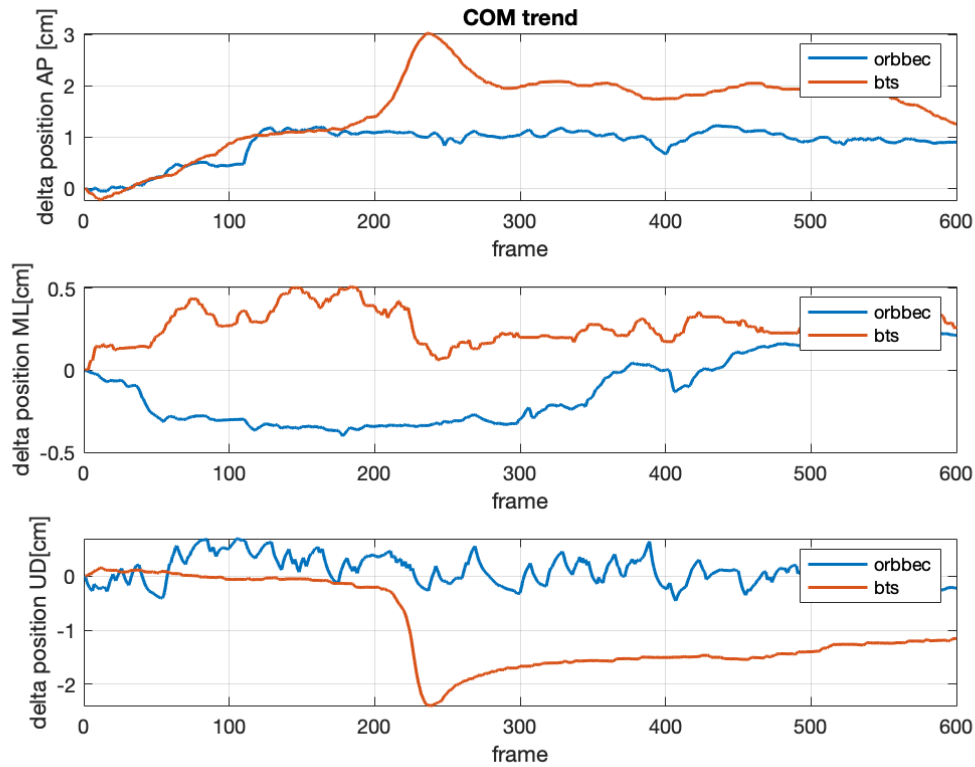


Figure 4.4-a) CoP trend BTS-Orbbec AP-Axis. (b) CoP trend BTS-Orbbec ML-Axis (c) CoP trend BTS-Orbbec UD-Axis

This first result is highly positive for the Orbbec that is much more variable but is concentrate around his mean value, while the trend of the BTS shows how the sway is smoother, but it deviates more than the Orbbec Astra results.

In **Figure 4.5** it's represented the trajectory of the CoP through the planes formed by the three axes, the Coronal plane, individuate by the ML-Axis/UD-Axis, the Sagittal plane, individuated by AP-Axis/UD-Axis and the Transverse plane, individuated by the ML-Axis/AP-Axis.

The results presented in **Figure 4.5** showed that there is a performance in the sway of the CoP that is in the same range for the two cameras, even if the Orbbec computation has much more variability around the mean value, confirming the representation of the absolute sway described in **Figure 4.4**.

The ML-axis presented by the Orbbec has a sway that goes in an absolute range of 0.25 cm while the BTS one has a range that goes in a range of 0.6 cm.

From the graphs it's highlighted how the behavior of the CoP computed it's similar. In the axes it's presented the trend that goes from the initial position of the CoP until the last position in order to give evidence of the sway.

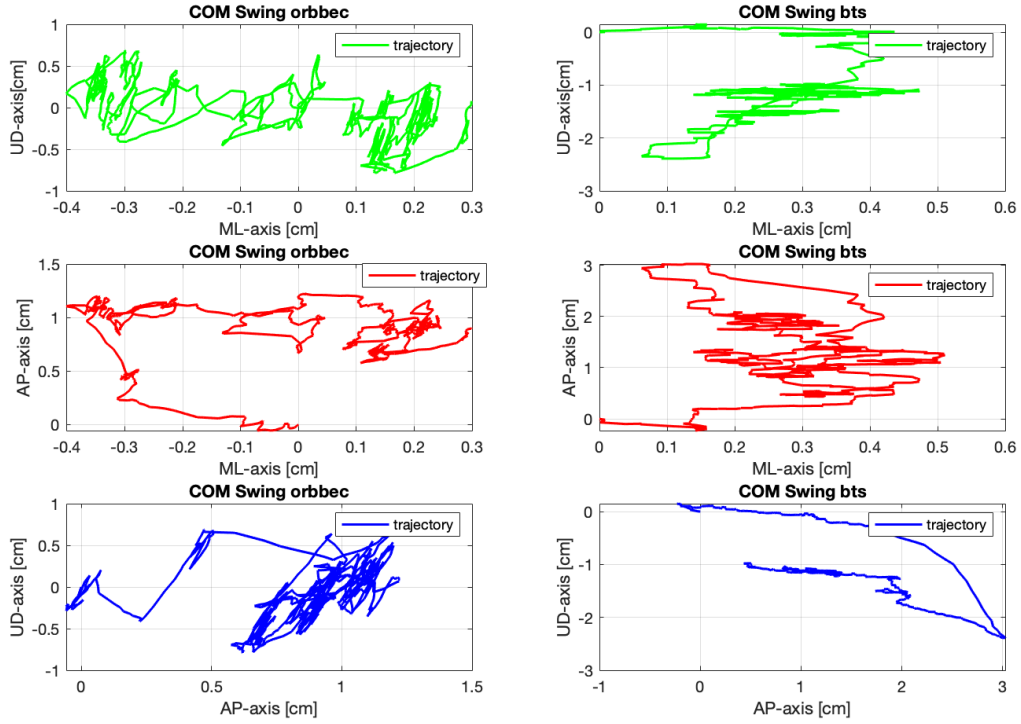


Figure 4.5-(a)CoP swing BTS-Orbbec AP-Axis. (b) CoP swing BTS-Orbbec ML-Axis (c) CoP swing BTS-Orbbec UD-Axis

In **Figure 4.6** are reported the boxplot of the different axes computed by the Orbbec and the BTS system. It's possible to examine the high number of outliers from the AP-axis of the Orbbec Astra Pro, and the optimal work of the ML and UD axes. The dimensions of the Boxes are about 0.5 cm, showing a good estimation of the CoP in his minimum and maximum value. The BTS system has a better behavior in the AP-axis, but definitely more outliers in the UD-Axis. Also, these considerations are coherent with the results obtained previously, highlighting again the high sway from the mean value of the BTS.

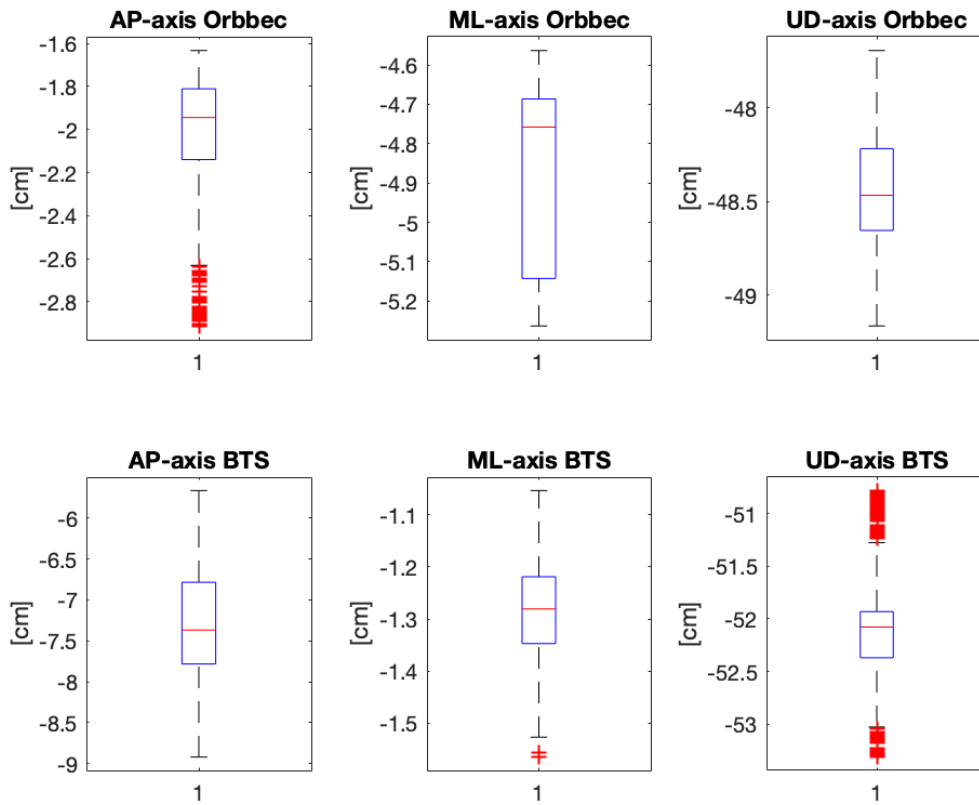


Figure 4.6-(a) Boxplot representation Orbbec. (b) Boxplot representation BTS.

In **Table 4.1** are expressed the Variations coefficients computed in the task, underlining a high percentage of variation in the AP-axes, reaching 52% of CV, results that are coherent with the Boxplot in **Figure 4.6**.

Table 4.1-Variation coefficient BTS-Orbbec

	BTS	ORBEC
	CV (%)	
AP-Axes	8.92	51.67
ML-Axes	8.66	3.41
UD-Axes	1.55	0.55

In **Table 4.2** there are exposed the means of the standard deviations with their sway during the three acquisitions made.

Table 4.2-CoP BTS-Orbbec Mean Standard Deviation

	BTS		ORBEC	
	Mean Std. Dev [cm]			
Coronal Plane (ML/UD Axes)	0.10 ±0.03	0.59 ±0.13	0.29 ±0.12	0.27 ±0.12
Sagittal Plane (AP/UD Axes)	0.6335 ±0.174	0.0194 ±0.025	0.2680 ±0.13	0.27 ±0.12
Transversal Plane (AP/ML Axes)	0.6335 ±0.174	0.0037 ±0.07	0.2680 ±0.13	0.29 ±0.12

The results in **Table 4.2**, allow observing the comparable values in all the axes. Indeed, the deviations stay in both the cases in the order of the millimeter.

These results allow saying that, even if the CoP computed by the Orbbec joints is much more variable, it remains around his mean value, giving a good estimation, while its drift is much more contained than the BTS one, that is less variable, but have a drift more appreciable.

4.1.2 Standing dynamic task:

The representations of all of the limbs' flexion angles are shown in **Figure 4.7** and **Figure 4.8**. The figures show the optimal realignment between the two angles, that are filtered in both the case, making evident the good smoothness of the BTS track, that is more stable, while the high-frequency interference in the Orbbec, although the filtering, is still visible in the traces of the curves.

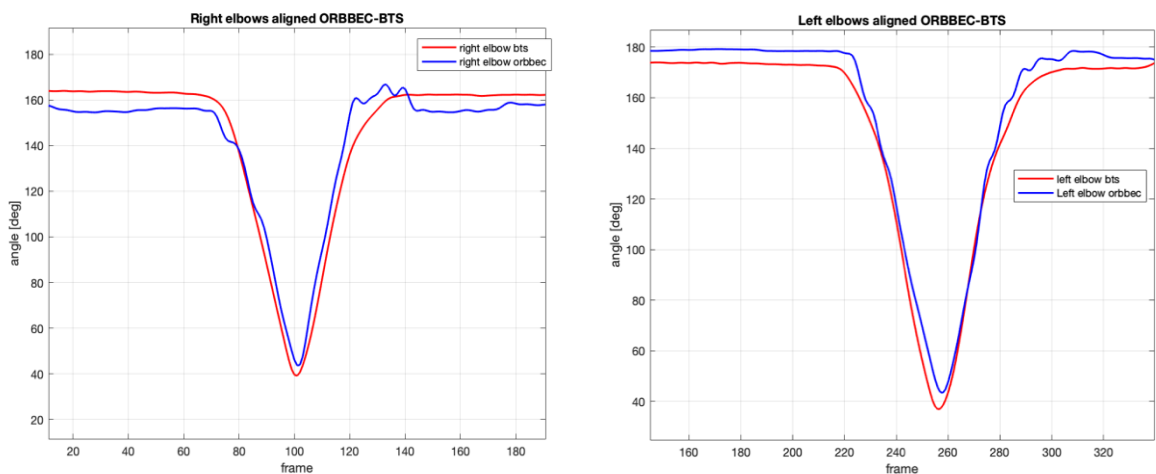


Figure 4.7-(a) Right elbows flexion angle BTS-Orbbec aligned. (b) Left elbows flexion angle BTS-Orbbec aligned

The left and right elbows have basically the same trajectory watching at the visible correlation and the realignment that is easily performed.

The Left and right knee as visible in **Figure 4.8** show how the BTS is seeing a deeper flexion of the knee during the squat movement of about 20° , while the Orbbec keeps tracking a similar movement, slightly more noisy, and less deep.

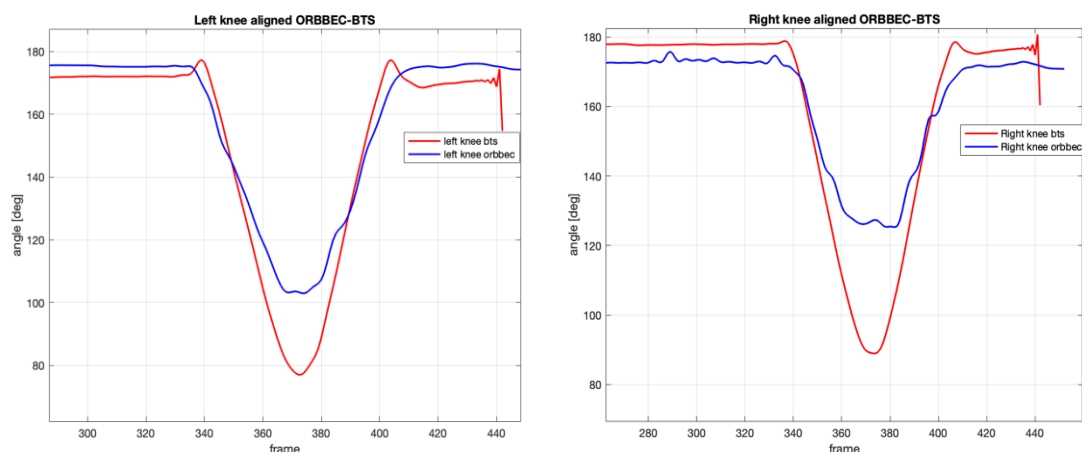


Figure 4.8-(a)Right Knee flexion angle BTS-Orbbec aligned. (b) Left Knee flexion angle BTS-Orbbec aligned

In **Table 4.3**, Pearson's Correlation coefficient are reported, for the three repetition tasks we have performed.

The initial indication visible by the plots of the limbs is confirmed by the values of the correlations.

Indeed, the limbs have a mean coefficient, computed on the three repetitions, that stands around the 0.95, while the knees, in an equal manner, stand around a mean coefficient of 0.85, results slightly inferior, but still very high.

The difference between the two representations of the limbs' angles can be explicated watching at the joints tracked by the two systems.

The upper limbs angles are computed using basically the same joints, that is, how explicated in chapter [2.5.2](#), the joint of the elbow, the joint of the shoulder and the joint of the wrist. So, considering some millimeters of difference, the position recovered by the two systems is similar.

Regarding the lower limbs, instead, the joints are lightly different in their original position. Indeed, for the Orbbec, the computation is performed using the joint of the hip, the joint of the knee and the joint of the ankle, while regarding the BTS are used the joints of the axis, positioned a little bit above the hip computed by NuiTrack, the joint of the Knee, and the joint of the Malleolus, again in a slightly position compared to the Ankle of NuiTrack.

Table 4.3- Pearson's correlation coefficients standing dynamic task BTS-Orbbec

Parameter	Test	Pearson's Correlation Coefficient r^a	
		Mean \pm Std. Dev.	p-value
Right Elbow Flexion	T1	0.8491 \pm 0.0387	<0.05
	T2	0.9816 \pm 0.0041	<0.05
	T3	0.9801 \pm 0.0051	<0.05
Left Elbow Flexion	T1	0.9981 \pm 0.005	<0.05
	T2	0.8018 \pm 0.0592	<0.05
	T3	0.9011 \pm 0.0336	<0.05
Left Knee Flexion	T1	0.7892 \pm 0.1961	<0.05
	T2	0.9513 \pm 0.0681	<0.05
	T3	0.8078 \pm 0.0674	<0.05
Right Knee Flexion	T1	0.8433 \pm 0.2809	<0.05
	T2	0.9374 \pm 0.0386	<0.05
	T3	0.8936 \pm 0.0298	<0.05

In **Figure 4.9** the computed velocities are represented. The waveforms are again highly correlated, showing an optimal capability of reconstruction of the kinematic information that derives from the acquisitions.

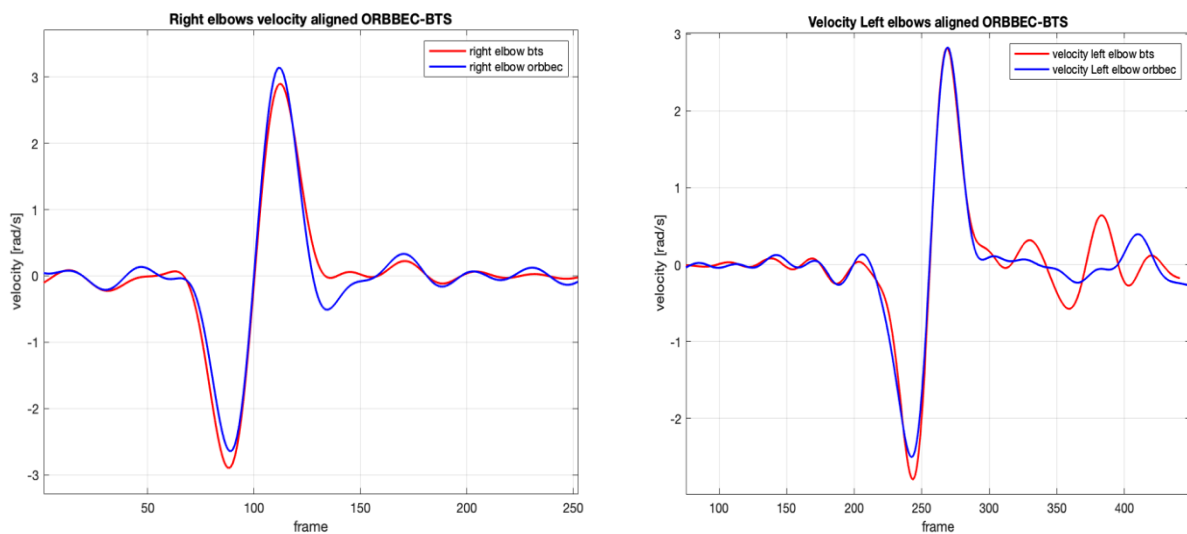


Figure 4.9-(a)Right Elbows flexion angular velocity BTS-Orbbec aligned. (b) Left Elbows flexion angular velocity BTS-Orbbec aligned

4.1.3 Seated static task

In **Figure 4.10** the two bodies reconstructed from the joints of the BTS system, and the Orbbec system before the procedure of recalibration, are showed.

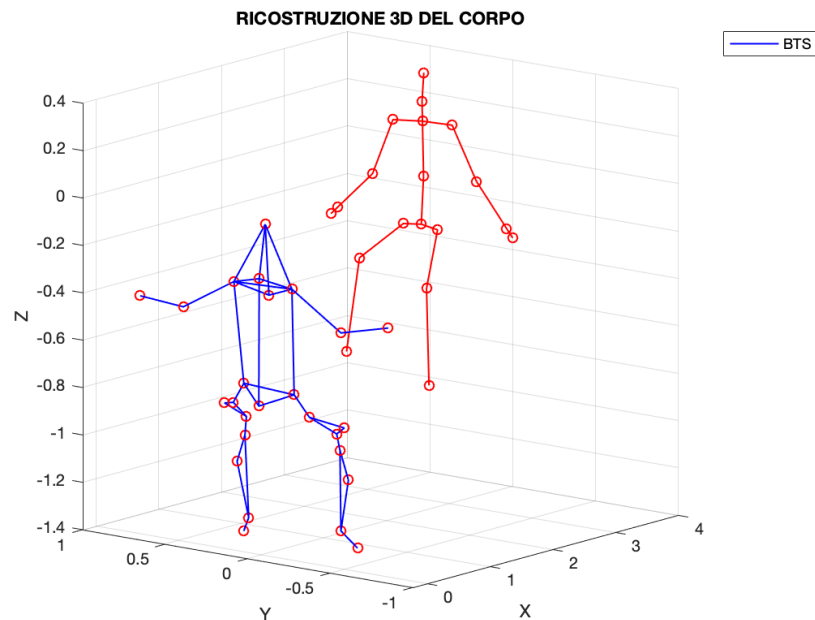


Figure 4.10-Bodies in the original reference systems

Computing the procedure of recalibration of the bodies to the new reference system, it's possible to observe the matching in **Figure 4.11** from the axonometric view and in a frontal view in **Figure 4.12**.

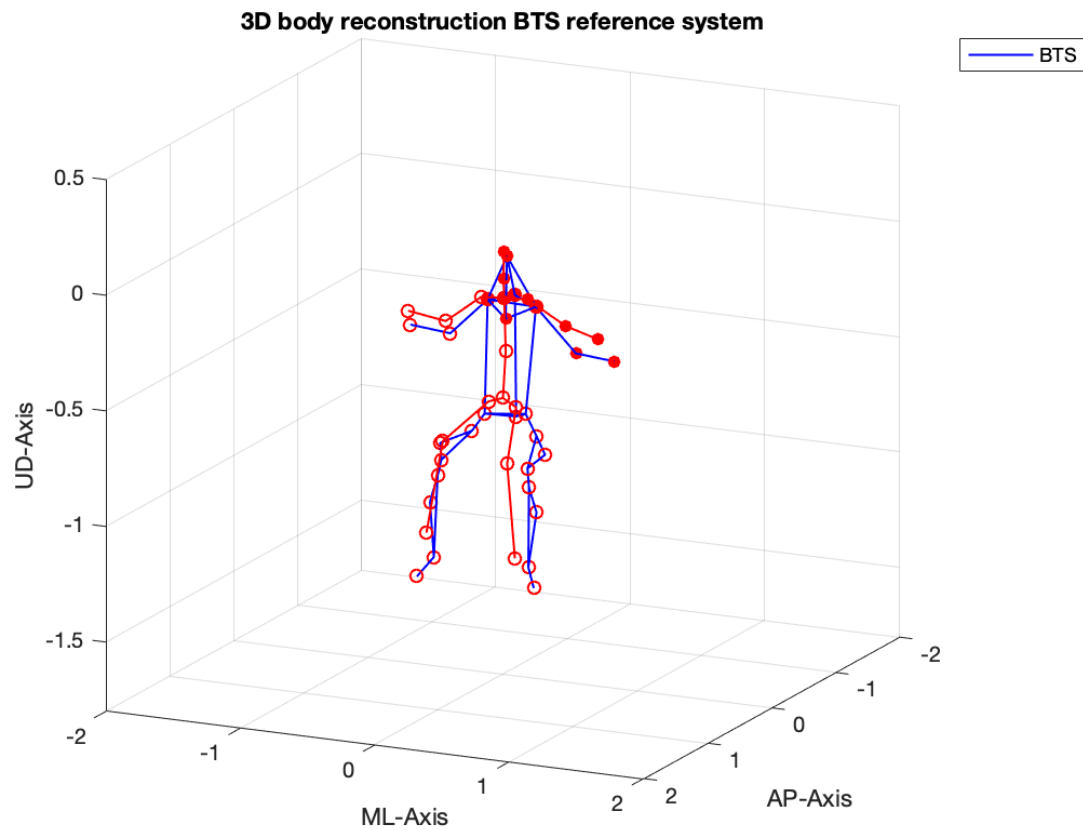


Figure 4.11-Axonometric view of the bodies in the common reference system

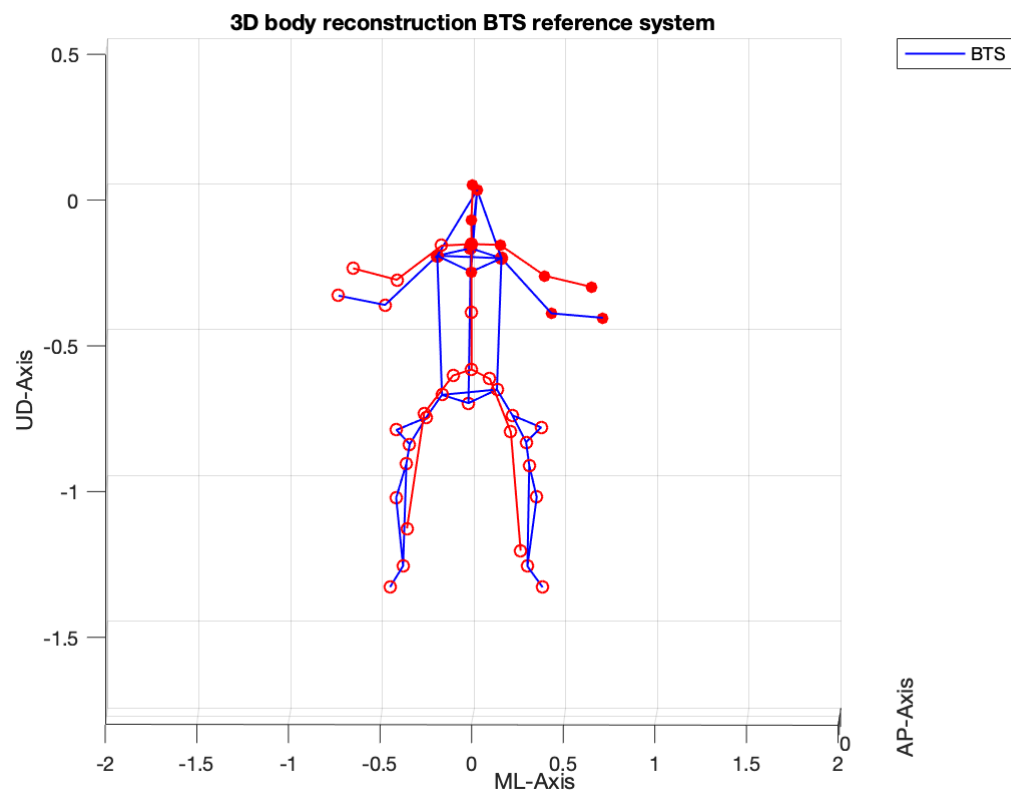


Figure 4.12-Frontal view of the bodies in the common reference system

In **Figure 4.13** it's presented the trend that goes from the initial position of the CoP until the last position in order to give evidence of the sway.

In the AP-axis the sway of the BTS system is much more evident than the Orbbec one, which keeps staying in an absolute range of 0.5 cm, while the BTS one reaches the 3 cm of sway.

The same observations are highlighted in the ML-axis and in the UD-axis where there are absolute sways of 0.5 cm for the BTS and 0.2 for the Orbbec.

It's necessary to reiterate that these acquisitions are made on a human model in a static sitting position, so the real sway could be present. By the way, the absolute values of the sways results are positive.

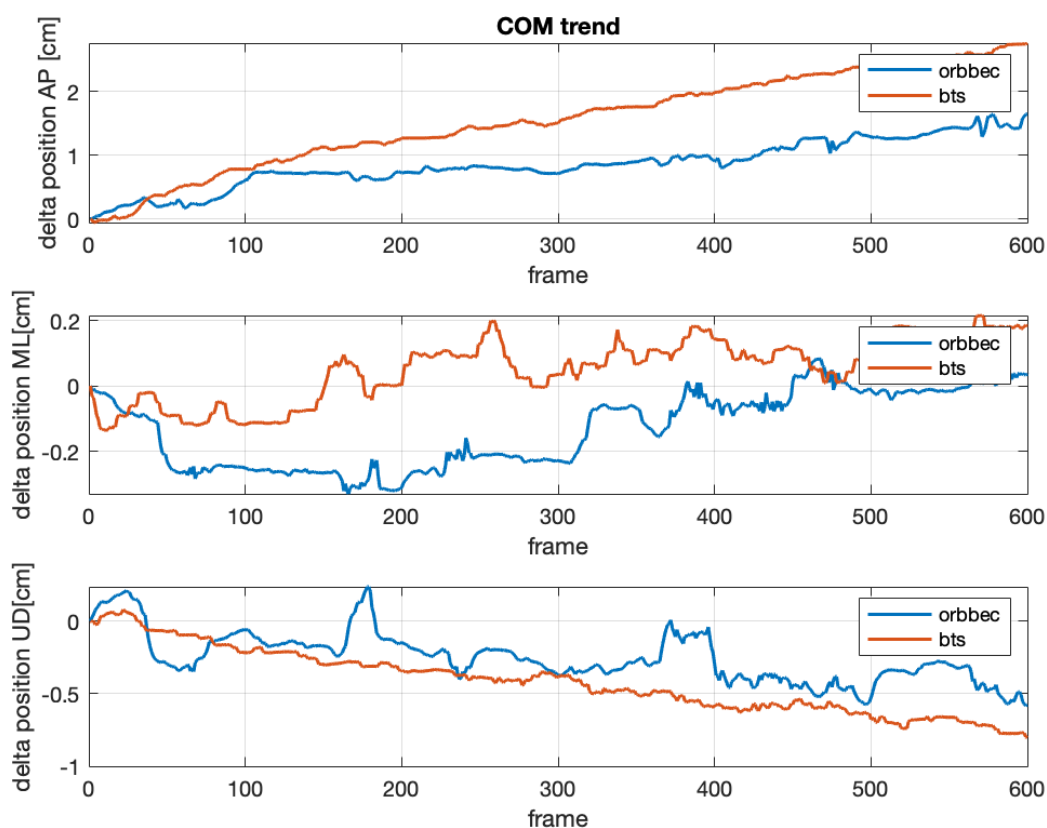


Figure 4.13-(a)CoP trend BTS-Orbbec AP-Axis Seated task. (b) CoP trend BTS-Orbbec ML-Axis seated task(c) CoP trend BTS-Orbbec UD-Axis seated task.

In **Figure 4.14** it's represented the trajectory of the CoP through the planes formed by the three axes, the Coronal plane, individuate by the ML-Axis/UD-Axis, the Sagittal plane, individuated by AP-Axis/UD-Axis and the Transverse plane, individuated by the ML-Axis/AP-Axis.

The results showed that there is a comparable performance in the sway of the CoP, where the ML-axis presented by the Orbbec has a sway that goes in a range of 0.3 cm while the BTS has a range that goes in the same range.

The same plane has a sway on the UD-Axis, for both the systems, that is representative of the problem due to the lower limbs. In the Orbbec results the sway goes in the range of 0.6 cm, while in the BTS, it goes in an absolute range of 1 cm being really comparable.

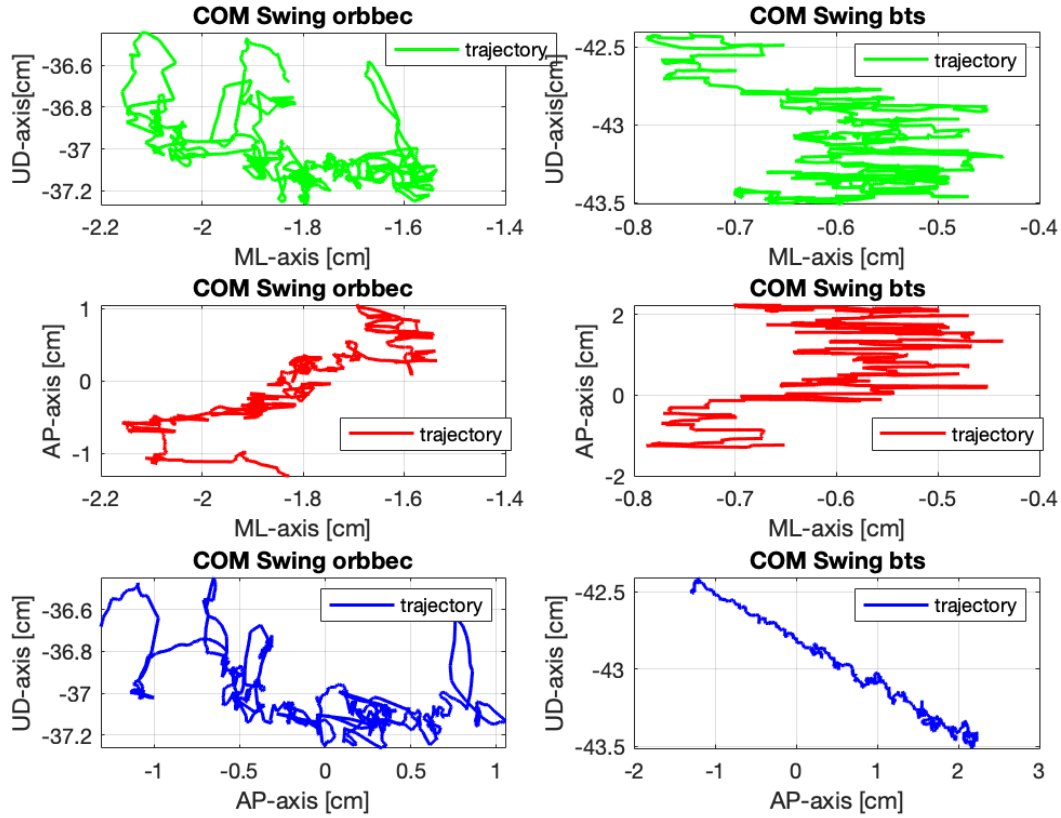


Figure 4.14-(a)CoP swing BTS-Orbbec AP-Axis seated task. (b) CoP swing BTS-Orbbec ML Axis seated task (c) CoP swing BTS-Orbbec UD-Axis seated task

In **Figure 4.15** the boxplot of the CoP values in the three axes, is reported highlighting how the seated position results to be more critical for the Orbbec compared to the BTS, increasing the number of the Outliers for both the AP-Axis and the UD-Axis.

In **Table 4.4** the CVs of the task are reported, that are comparable for both the cameras, results that is slightly different from the representation of the boxplots, where the Box of the BTS contains more values, about 0.7 cm, while the Orbbec has much more outliers but contained in the same space of the 0.7 cm. The values of the CVs are comparable, evidencing another time the optimal behavior of the Orbbec compared to the BTS performances.

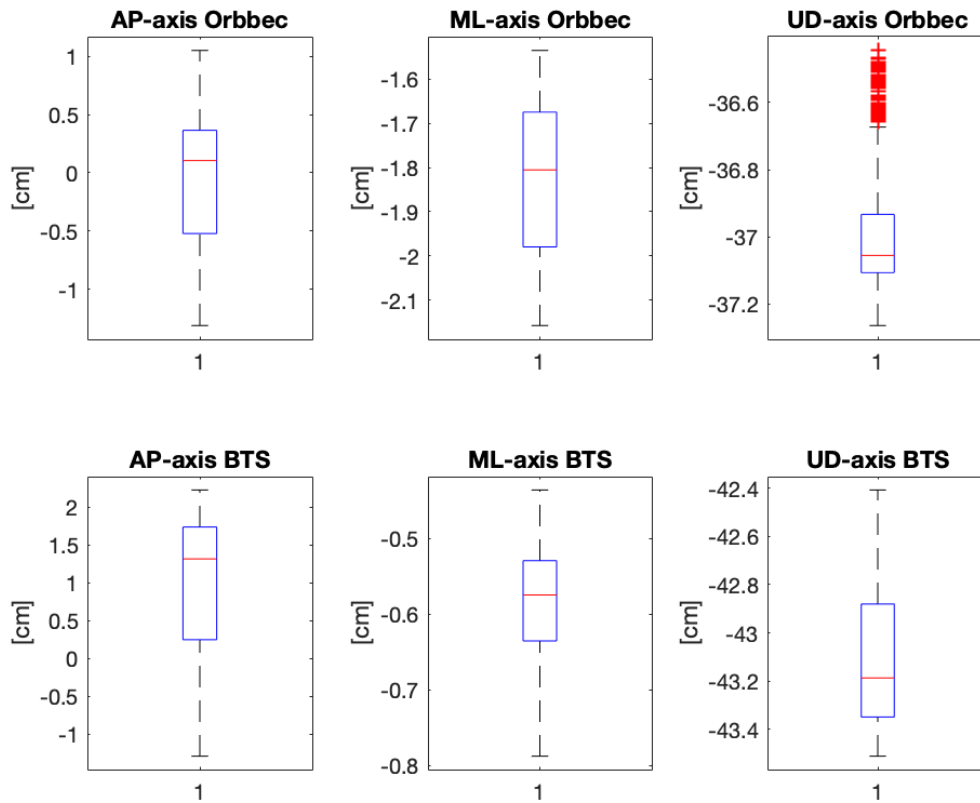


Figure 4.15-(a) Boxplot representation Orbbec. (b) Boxplot representation BTS.

Table 4.4-CoP BTS-Orbbec CV Seated task

	BTS	ORBEC
	CV (%)	
AP-Axes	6.72	4.62
ML-Axes	13.78	10.39
UD-Axes	0.66	18.33

In **Table 4.5**, the mean standard deviations computed on the three repetition of the task are reported. The results show values of the same order of deviation, representing again the UD-axis as the more critical axes.

Table 4.5-CoP BTS-Orbbec Mean Standard Deviation Seated task

	BTS		ORBEC	
	Mean Std. Dev [cm]			
Coronal Plane (ML/UD Axes)	0.14 ±0.08	0.25 ±0.12	0.09 ±0.03	0.13 ±0.03
Sagittal Plane (AP/UD Axes)	0.84 ±0.31	0.25 ±0.12	0.34 ±0.14	0.13 ±0.03
Transversal Plane (AP/ML Axes)	0.84 ±0.31	0.14 ±0.08	0.34 ±0.14	0.09 ±0.03

4.1.4 Seated dynamic task.

In **Table 4.6**, the coefficients show a slightly better performance in the seated position, than the standing position described in **Table 4.3**.

All the limbs, in this case, can keep a mean correlation of 0.95, resulting in a really high correlation between them.

Table 4.6-Pearson's correlation coefficients seated dynamic task BTS-Orbbec

Parameter	Test	Pearson's Correlation Coefficient r^a	
		Mean ± Std. Dev.	p-value
Right Elbow Flexion	T1	0.9767±0.0071	<0.05
	T2	0.9760±0.0073	<0.05
	T3	0.9722±0.0072	<0.05
Left Elbow Flexion	T1	0.9493±0.0137	<0.05
	T2	0.9855±0.0033	<0.05
	T3	0.9636±0.0127	<0.05
Left Knee Flexion	T1	0.8418±0.0667	<0.05
	T2	0.9673±0.0112	<0.05
	T3	0.9850±0.0127	<0.05
Right Knee Flexion	T1	0.8618±0.1490	<0.05
	T2	0.9646±0.0112	<0.05
	T3	0.9889±0.0188	<0.05

4.1.5 Increasing velocity task.

In this test, it has been let the subject free to perform ten movements with the request of increase progressively the velocity of the limbs, in order to verify the capability of the tracking of rapid movements.

In **Figure 4.16** and **Figure 4.17** the limb flexions are drawn, showing a good performance. The elbows keep having a good behavior following correctly the performances between the two cameras.

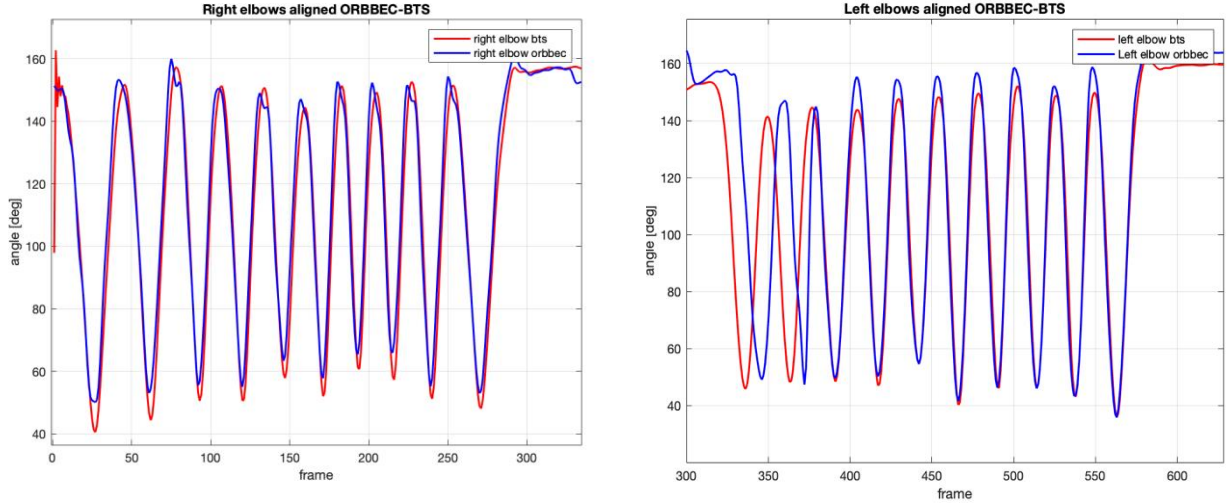


Figure 4.16-(a)Right elbows flexion angle increasing velocity BTS-Orbbec aligned. (b) Left elbows flexion angle increasing velocity BTS-Orbbec aligned

The plotting of the knee flexions has shown again the difference between the amplitude of the flexion seen by the BTS System and the Orbbec Astra Pro. Generally, we have assisted to one reduction of 10° of the upper position and 20° of the lower position as shown in **Figure 4.17**.

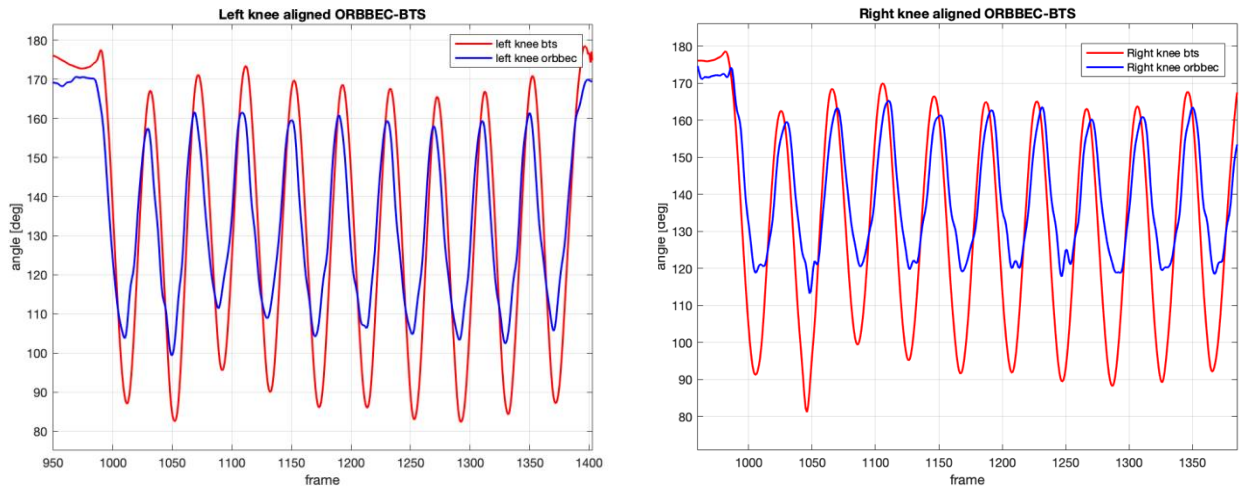


Figure 4.17-(a)Left knee flexion angle increasing velocity BTS-Orbbec aligned. (b) Right knee flexion angle increasing velocity BTS-Orbbec aligned

In **Table 4.7** are reported the Pearson's correlation coefficients of the task, making evident some problems in the left elbows flexions analysis.

It could be possible to explicate this behavior during the acquisition because we haven't kept the same initial position with respect to the different cameras of the BTS system.

During the task, it has been observed in the real-time viewer of NuiTrack that there was a hole in the depth map found correspondent to the position of the left elbow.

When the first two acquisition has been performed the left elbow, indeed, passed through the hole losing the coordinates. In this way, the angle analysis has given back a correlation coefficient of 0.50, results never found before.

Changing our relative position respect the BTS cameras, even if the hole kept being to stay in the depth map, we paid attention to executing the movement far from it, achieving to obtain a good analyzable movement with a high correlation of 0.82.

Regarding the right elbow, we found an error in the third acquisition of the right elbow, probably due to the same shift, that centered the left upper limb, and has occluded the right one. The knees flexions have given back good results, with a high coefficient of correlation.

Table 4.7-Pearson's correlation coefficients increasing velocity dynamic task BTS-Orbbec

Parameter	Test	Pearson's Correlation Coefficient r^a	
		Mean \pm Std. Dev.	p-value
Right Elbow Flexion	T1	0.9522 \pm 0.0075	<0.05
	T2	0.9648 \pm 0.0056	<0.05
	T3	0.5989 \pm 0.0681	<0.05
Left Elbow Flexion	T1	0.5177 \pm 0.0265	<0.05
	T2	0.332 \pm 0.081	<0.05
	T3	0.8209 \pm 0.0261	<0.05
Left Knee Flexion	T1	0.9489 \pm 0.0266	<0.05
	T2	0.9792 \pm 0.0029	<0.05
	T3	0.7785 \pm 0.1045	<0.05
Right Knee Flexion	T1	0.9498 \pm 0.0355	<0.05
	T2	0.9780 \pm 0.0029	<0.05
	T3	0.7763 \pm 0.1468	<0.05

In **Figure 4.18** and **Figure 4.19** are drawn the velocities of the flexion.

It's observable that, being good the framerate of the Orbbec, also the velocity is recovered comparably to the BTS one, that has a framerate much more detailed, having 100 fps. The amplitude of the lower limbs is affected by the initial amplitude of the angles, which are inferiors to the BTS ones, and by the filtering removing the high-frequency interferences.

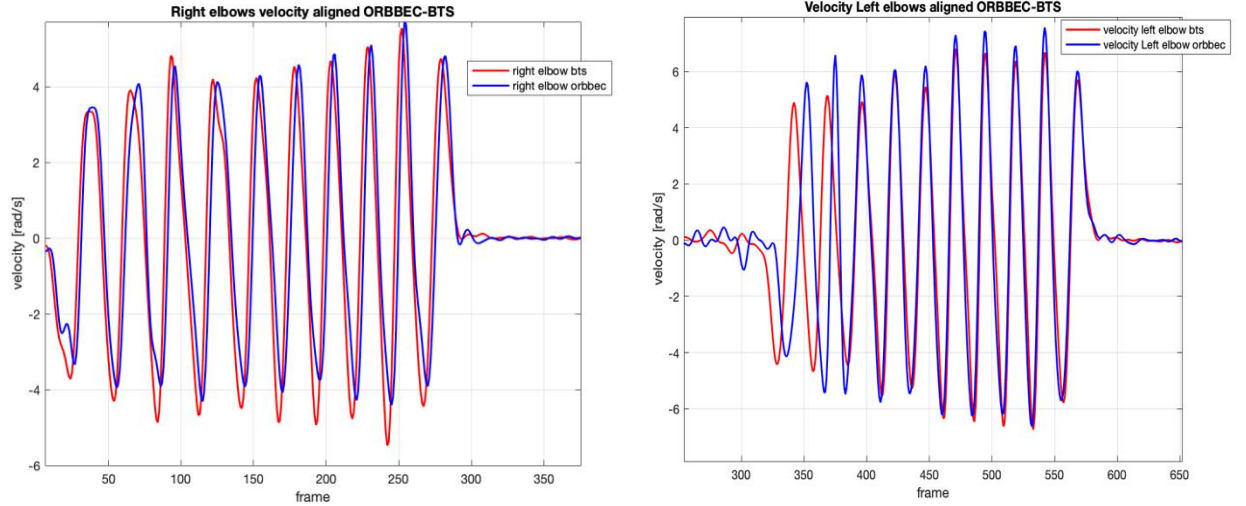


Figure 4.18-(a)Right Elbows flexion angular velocity BTS-Orbbec aligned. (b) Left Elbows flexion angular velocity BTS-Orbbec aligned

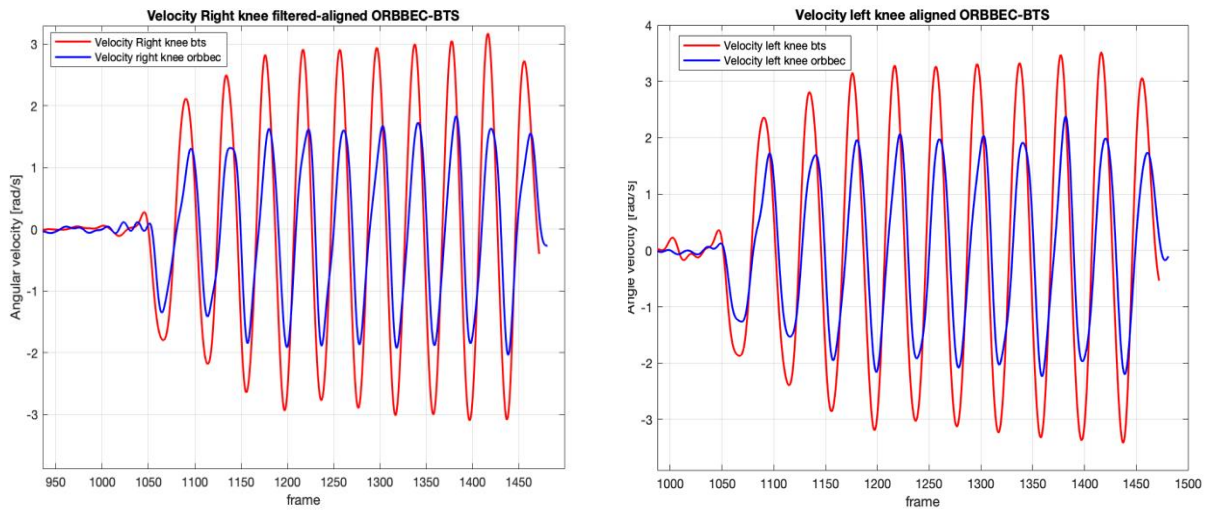


Figure 4.19-(a)Right Knee flexion angular velocity BTS-Orbbec aligned. (b) Left Knee flexion angular velocity BTS-Orbbec aligned

In **Figure 4.20**, are reported the time-frequency representations of the right elbow recovered by the cameras.

From the graphs, it's appreciable the variation of the frequency of the signals, coming from the acquisition, that is supposed to be variable, according to the design of the task.

Indeed, both the cameras have a signal that starts with the peak of the spectrum that is around 1 Hz, starting the task and reaches 1.5 Hz towards the end of the exercise, having made it faster the flexions of the elbows as required by the task.

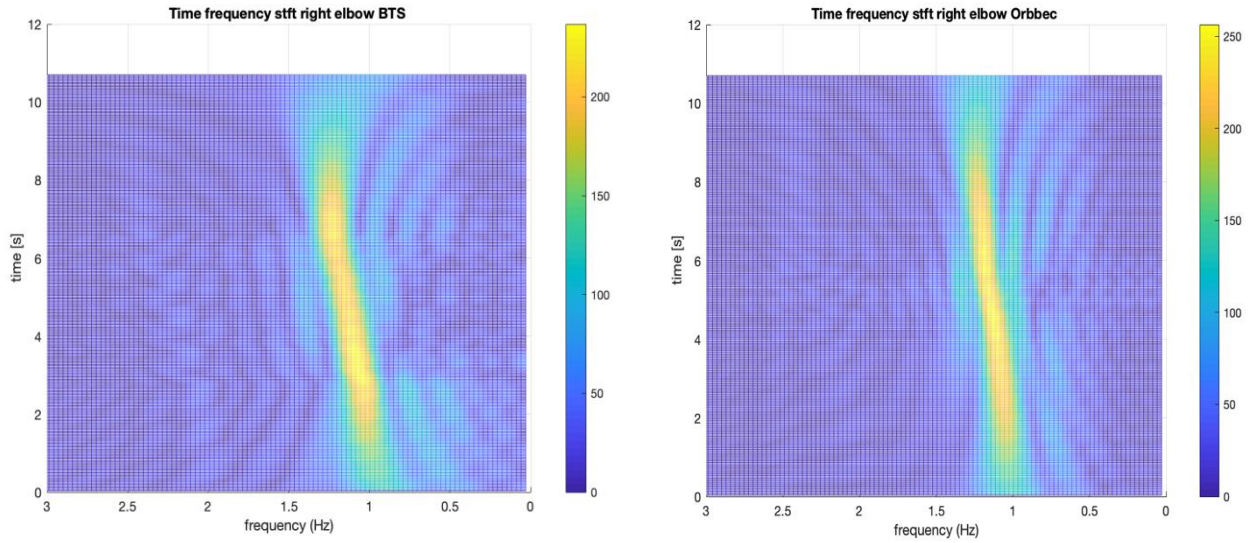


Figure 4.20-(a) Time-frequency mesh of the Orbbec recovered right elbow spectrum. -(b) Time-frequency mesh of the Orbbec recovered right elbow spectrum.

4.1.6 Leg-agility

The leg-agility task has been the most followed task in the analysis, having a great mean in the clinical consideration, explicating the dedication of a separate subchapter.

The initial analysis has followed the same approach of the previous results, giving the shreds of evidence of the correlation between the movements, and computing the coefficients.

In **Figure 4.21**, the leg flexions that have been rebuilt from the two cameras information. are plotted.

The right knee has basically the same amplitudes while the left knee has 10° of amplitude in less. The realigning, however, is performed with no particular problem, and the peaks are in the same positions.

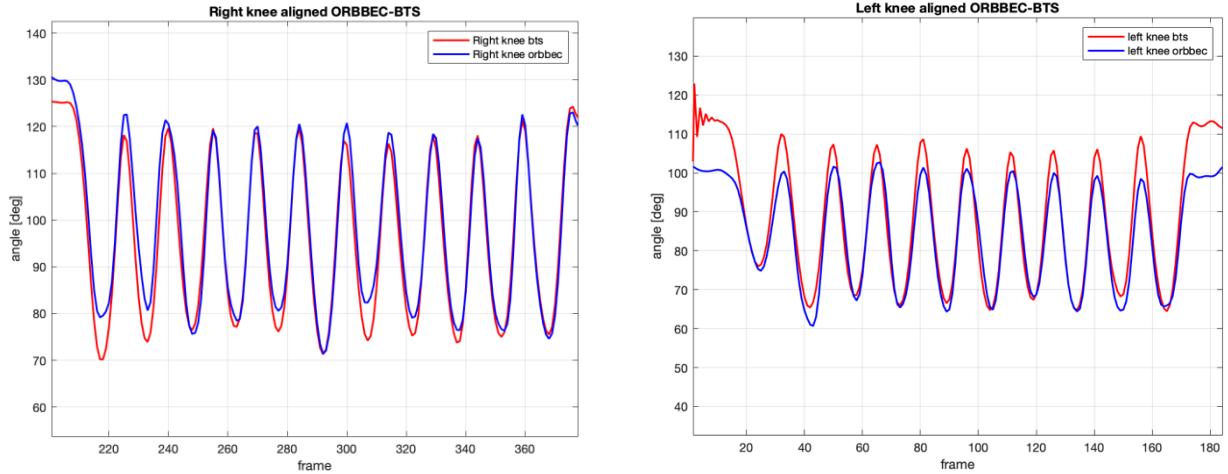


Figure 4.21-(a)Right Leg flexion BTS-Orbbec aligned. (b) Left Leg flexion BTS-Orbbec aligned

In **Table 4.8**, the results of Pearson's coefficients are reported, highlighting one corrupted acquisition, with the coefficient of 0.44 for the right knee in the first acquisition, a problem that is not proposed again in the subsequent acquisition, that have been tracked correctly.

Table 4.8-Pearson's correlation coefficients Leg-agility task BTS-Orbbec

Parameter	Test	Pearson's Correlation Coefficient r^a	
		Mean \pm Std. Dev.	p-value
Left Knee Flexion	T1	0.9733 \pm 0.1961	<0.05
	T2	0.8397 \pm 0.0681	<0.05
	T3	0.7559 \pm 0.0674	<0.05
Right Knee Flexion	T1	0.4466 \pm 0.2809	<0.05
	T2	0.9684 \pm 0.0386	<0.05
	T3	0.7867 \pm 0.0298	<0.05

Figure 4.22 and **Figure 4.23**, instead, point out the peaks found during the MATLAB analysis, that have been used in order to rate the parameters proposed in [chapter 2.6](#).

The peaks have been found for each of the three repetitions performed, but only the second one's graphs are reported.

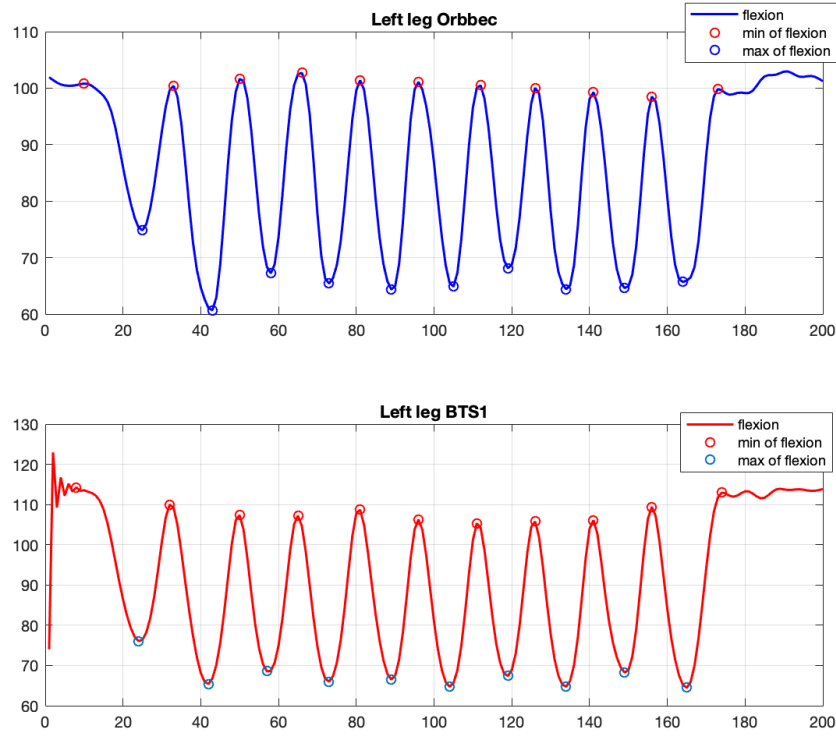


Figure 4.22-(a) Left leg flexion Orbbec recovered, with the peaks of the flexions. (b)Left leg flexions, BTS recovered with the peaks of the flexions.

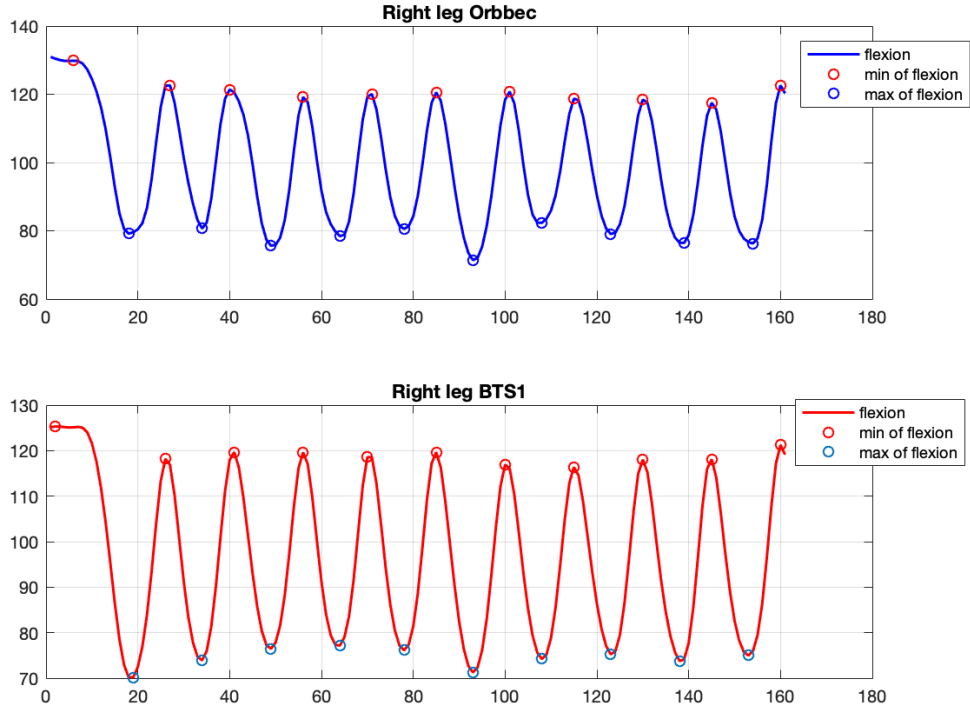


Figure 4.23-(a) Right leg flexion Orbbec recovered, with the peaks of the flexions. (b)Right leg flexions, BTS recovered with the peaks of the flexions.

In **Table 4.9**, the parameters we obtained from the two cameras are described.

Table 4.9-Kinematic results of the Leg-agility

	<i>ORBEC ASTRA PRO</i>		<i>BTS SMART-DX 400</i>	
	Left leg	Right leg	Left leg	Right leg
θ_m [deg]	34.56	42.53	40.7638	44.5019
ω_m [deg/s]	128.55	164.25	150.59	171.47
P_m [s]	16.30	15.40	16.6	15.8
R_m [s]	15.44	15.11	15.67	14.89
θ_{sd} [deg]	0.84	0.9706	0.71	0.69
ω_{sd} [deg/s]	5.37	3.3670	4.45	3.20
P_{sd} [s]	0.54	0.4533	0.68	0.55
R_{sd} [s]	0.27	0.13	0.25	0.07

From these parameters it's possible to deduct that, first of all, the mean amplitudes are calculated correctly from the Orbbec, having few degrees of deviations between them.

Furthermore, having similar results, from both the cameras it's possible to evince the dominant leg of the subject, that is to say, the right leg since the mean amplitudes are bigger than the left legs ones.

The velocity ω_m , indeed is on average, 20°/s, faster than the left one velocity, reaffirming the greatest capability of moving the right leg.

Also, the parameters as the regularity R_m and the P_{sd} are inferior between the two legs, and regarding the right one, there is much more precision and control in the movement, giving back a standard deviation much more reduced compared to the left one.

In **Figure 4.24**, **Figure 4.25**, **Figure 4.26** and **Figure 4.27** are reported both the Contour of the STFT, that the Mesh, in order to appreciate better the trend of the movements.

Both the systems, have obtained a mean frequency of the spectrum that it stays around the 1.90 Hz for all the time of the ten repetitions, for the left leg, and a mean frequency of the spectrum that stays around 2.10 Hz for all the time of the ten repetitions, for the right leg, reaffirming the major mastery of the movement of the dominant right leg.

These results are really interesting, thinking at the same task executed by a pathological subject: it could be easily found which leg has more critical issues, which regularity it has, which pause, in which measure the disease has affected the motion between the previous parameters and the newer.

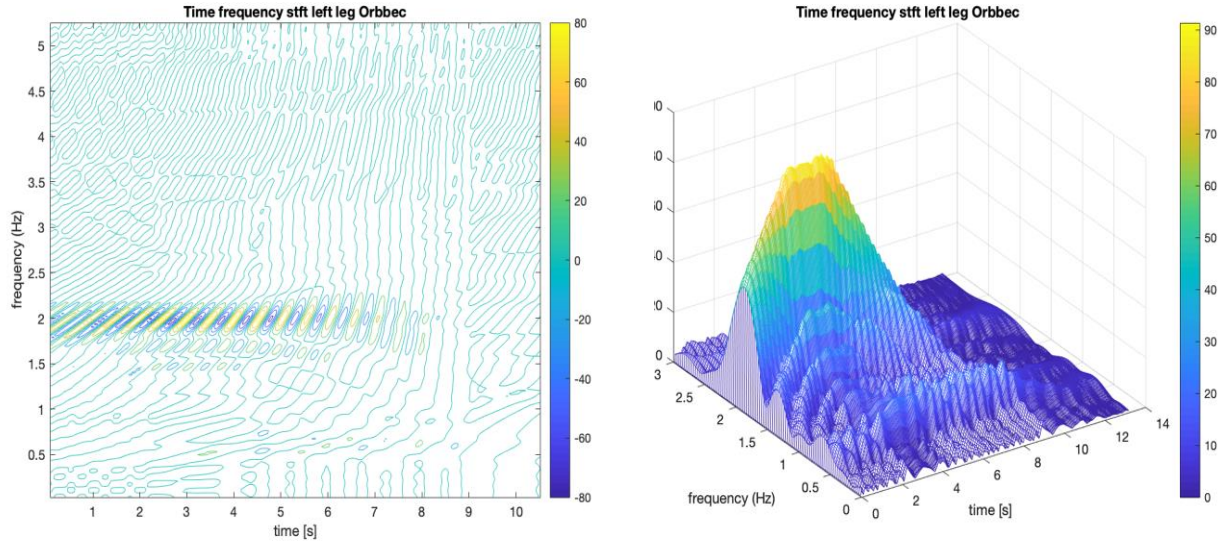


Figure 4.24-(a) Time-frequency contour of the Orbbec left leg spectrum. -(b) Time-frequency mesh of the Orbbec left leg spectrum. -(c) Time-frequency contour of the BTS left leg spectrum. -(d) Time-frequency mesh of the BTS left leg spectrum.

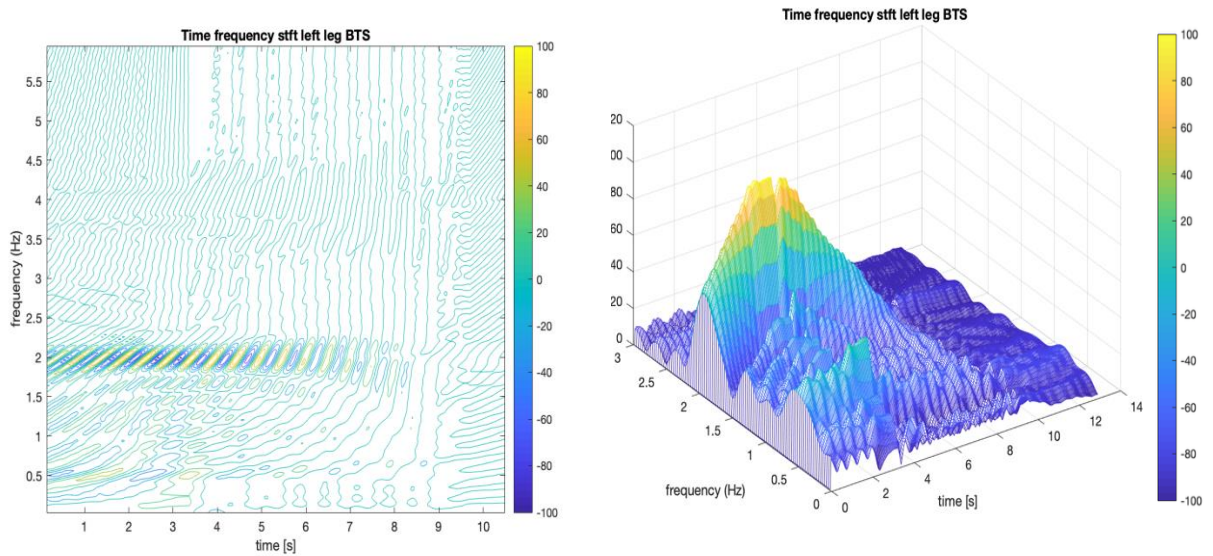


Figure 4.25-(a)Time-frequency contour of the Orbbec left leg spectrum. -(b)Time-frequency mesh of the Orbbec recovered left leg spectrum. -(c)Time-frequency contour of the BTS recovered left leg spectrum. -(d)Time-frequency mesh of the BTS recovered left leg spectrum.

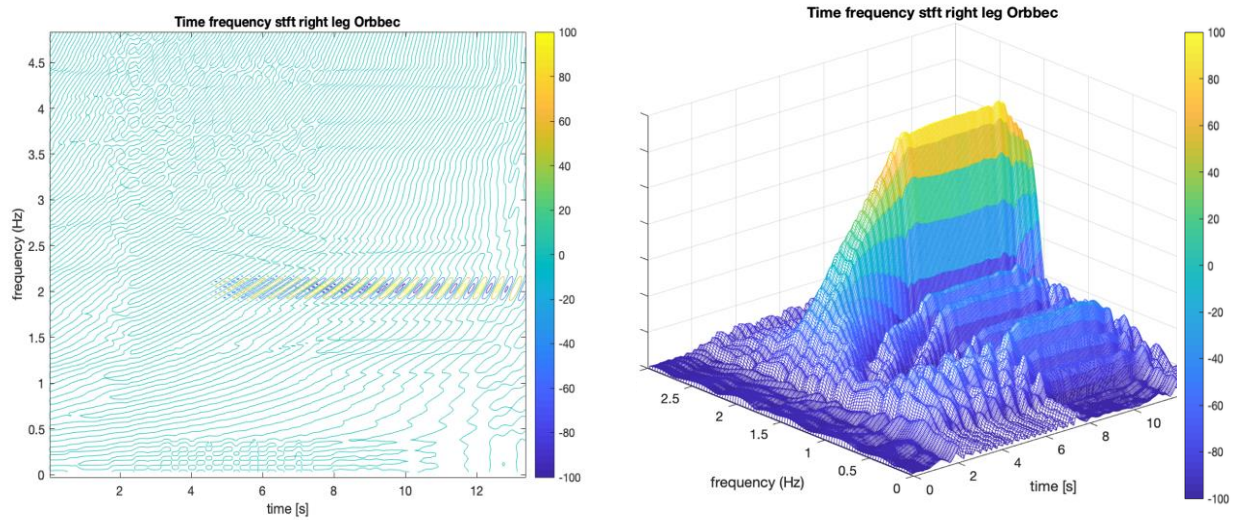


Figure 4.26-(a) Time-frequency contour of the Orbbec left leg spectrum. -(b) Time-frequency mesh of the Orbbec left leg spectrum. -(c) Time-frequency contour of the BTS left leg spectrum. -(d) Time-frequency mesh of the BTS recovered left leg spectrum

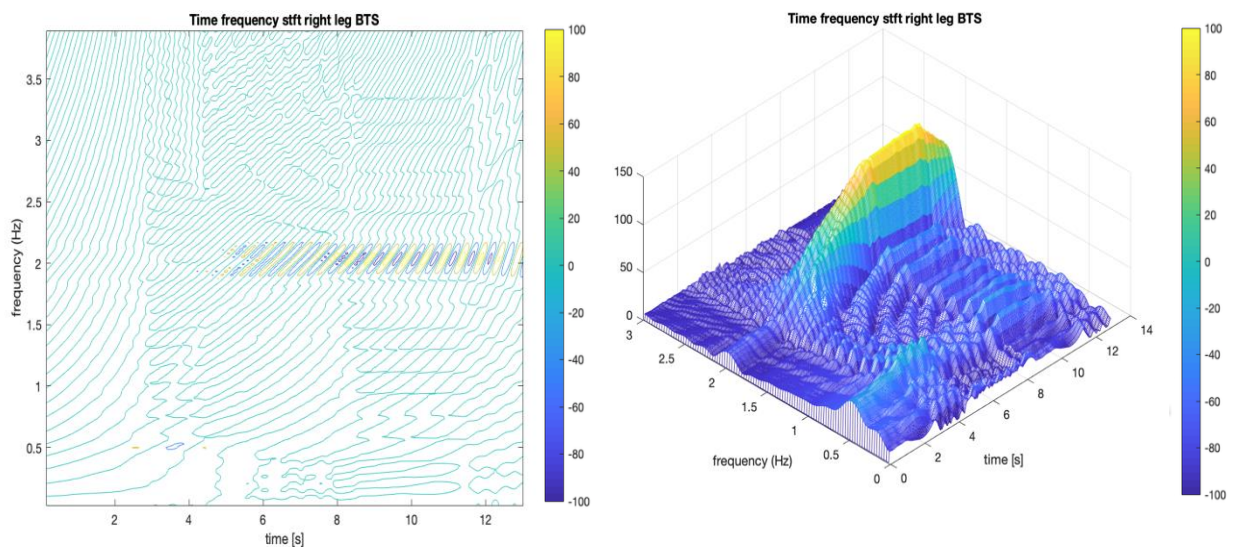


Figure 4.27-(a) Time-frequency contour of the Orbbec recovered right leg spectrum. -(b) Time-frequency mesh of the Orbbec recovered right leg spectrum. -(c) Time-frequency contour of the BTS recovered right leg spectrum. -(d) Time-frequency mesh of the BTS recovered right leg spectrum.

In **Figure 4.28** are reported the velocities of the flexions compared, for the right and left leg, showing, a good correlation between them, and a good realignment.

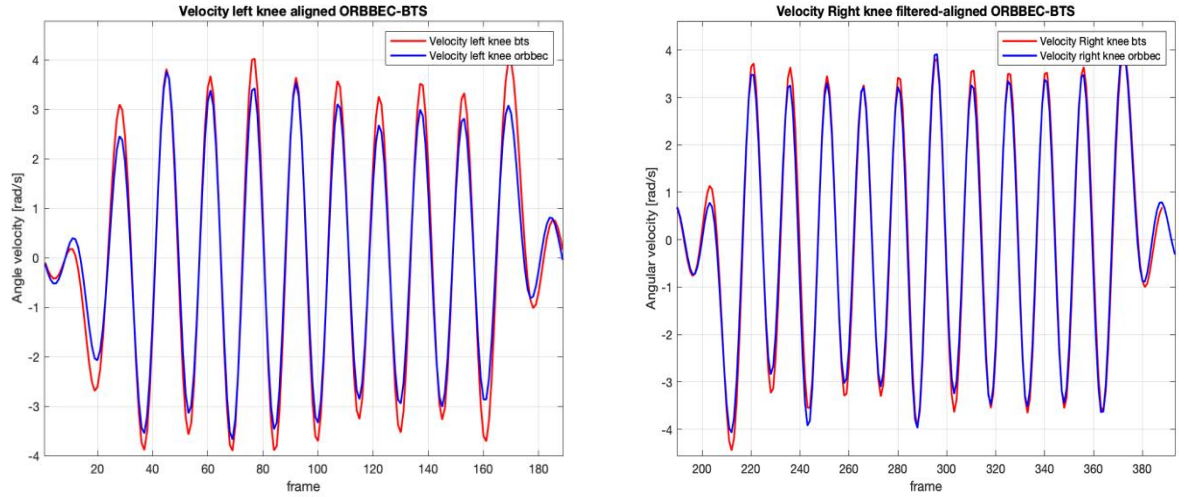


Figure 4.28-(a) Left Knee flexion angular velocity BTS-Orbbec aligned. (b) Right Knee flexion angular velocity BTS-Orbbec aligned task

4.2 Kinect Azure results.

The analysis of the Kinect Azure results, showed a great instability of the joints of the model as described in **Figure 4.29** making difficulty the extraction of the joints.

This behavior was never found in the preliminary tests showed in [chapter 2.7](#) and it was confirmed through analysis of the depth images.

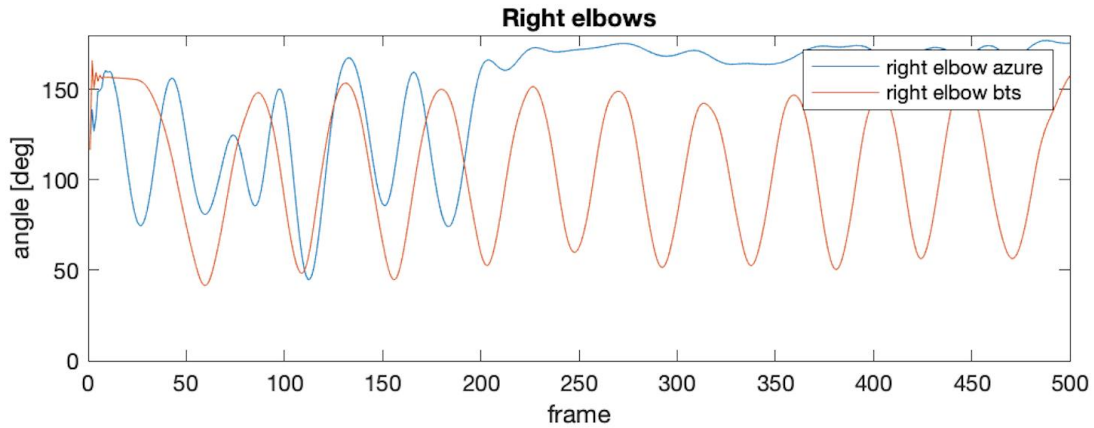


Figure 4.29-Right elbows angle flexion sway damaged

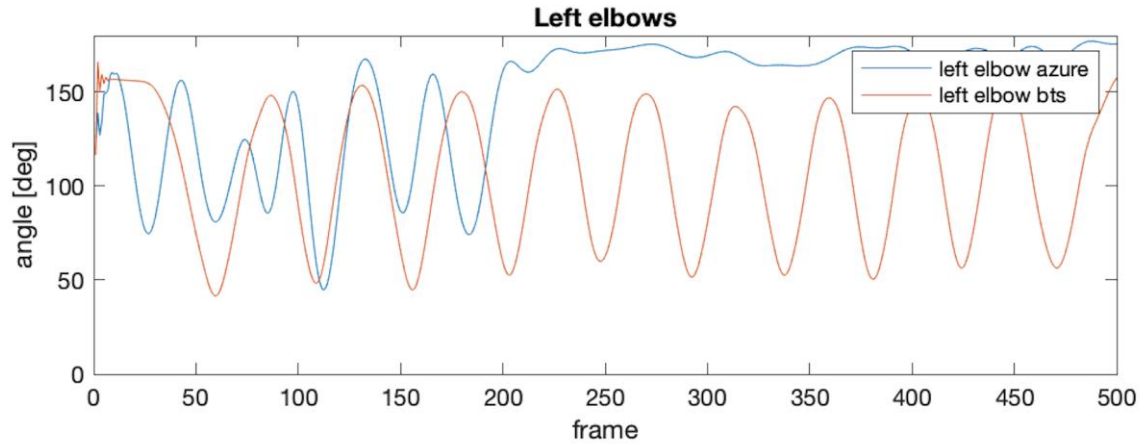


Figure 4.30-Left elbows angle flexion sway damaged

The BTS cameras are individuated in **Figure 4.31**, with three light blue squares and, three areas on the wall are individuated in order to evaluate the variation of Intensity in the IR field.

It has been computed the mean intensity in the IR field and the mean distance for the depth. The worsening of the depth Images and IR images when the BTS cameras are ON are showed

The task has a duration of 30 seconds and the analysis has been made with a 30 FPS acquisition.

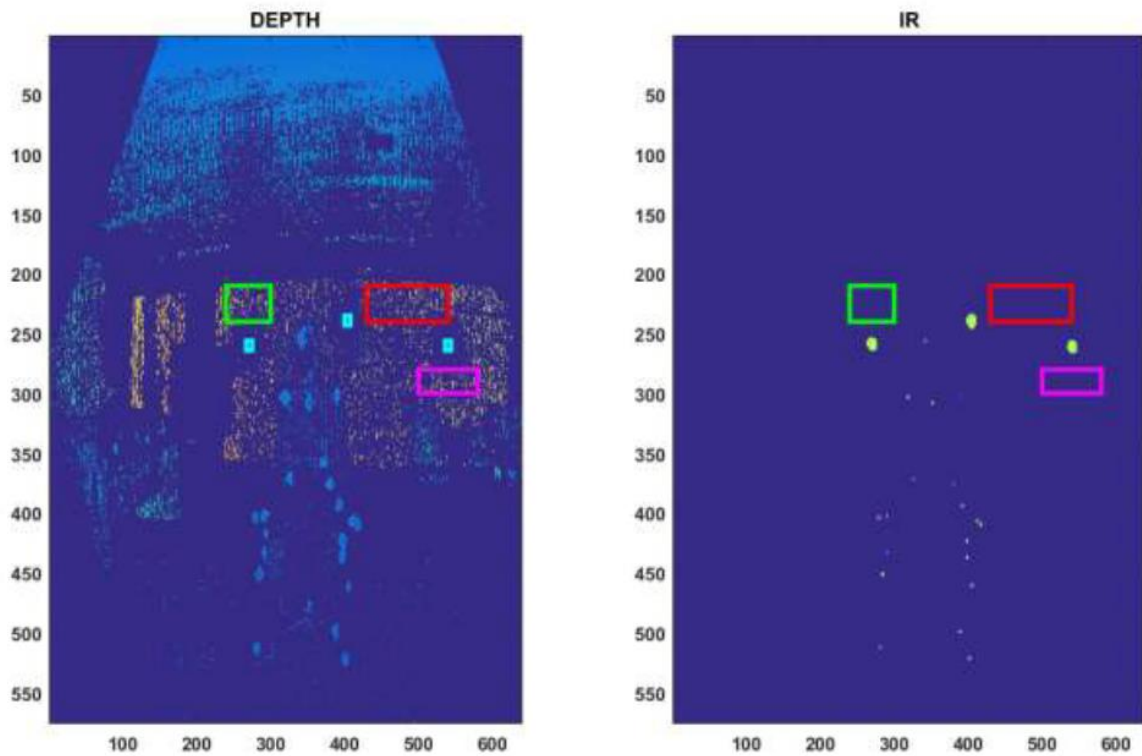


Figure 4.31-(a)Depth image of Kinect Azure (b) IR image of Kinect Azure acquisition

The signal of the BTS Camera has a frequency of 100 Hz with high magnitude luminous pulses that go on and off quickly (**Figure 4.32**).

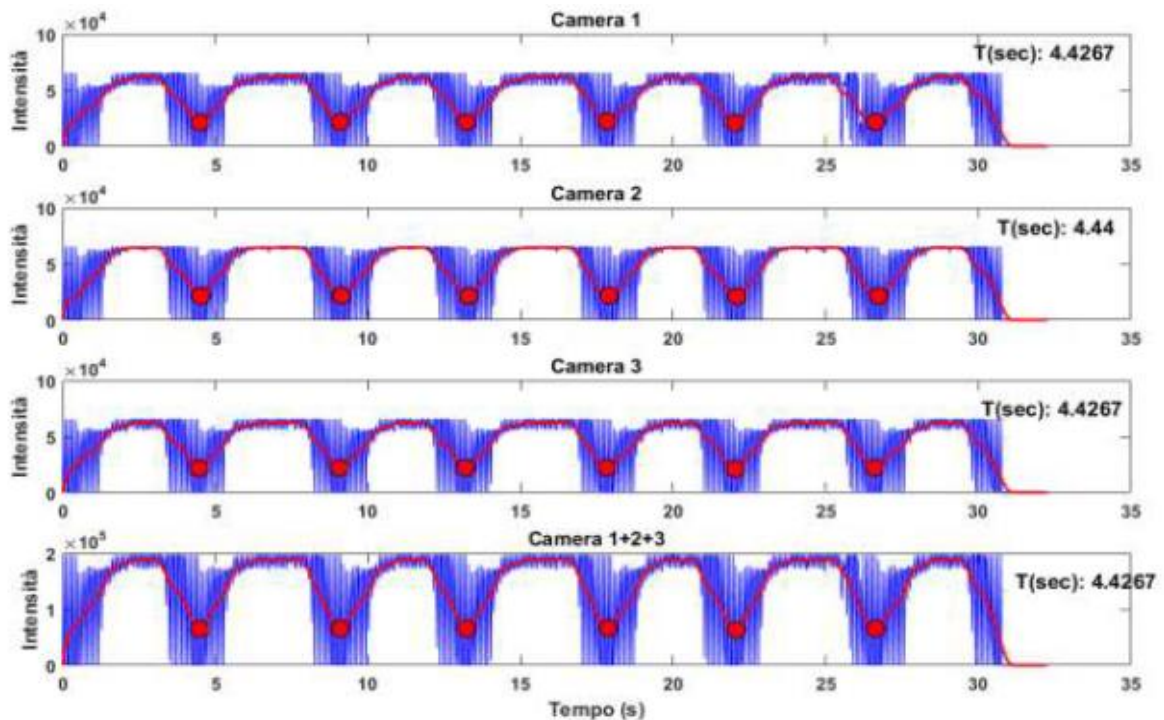


Figure 4.32- Kinect Intensity sway

The Kinect Azure, instead, has the sampling frequency of 30 Hz, that when is not synchronized takes to one down sampling of the start signal, that is, an oscillating trend of the intensity seen by the Kinect Azure.

When the BTS is off, it can be seen at the end of the acquisition in **Figure 4.32.**, where the IR intensity goes to 0. The BTS camera, furthermore, is synchronized, seeing at the period of 4.4 seconds in all the areas.

4.2.1 Depth Analysis: BTS Camera Area

Looking at the distances of the areas, it can be seen how the normal behavior, that should show a mean distance constant, while in the case of the BTS cameras in ON condition, there are periods of oscillating distances until distances computed as zero, where the sensor of the Kinect Azure is completely blinded by the BTS. (**Figure 4.33**).

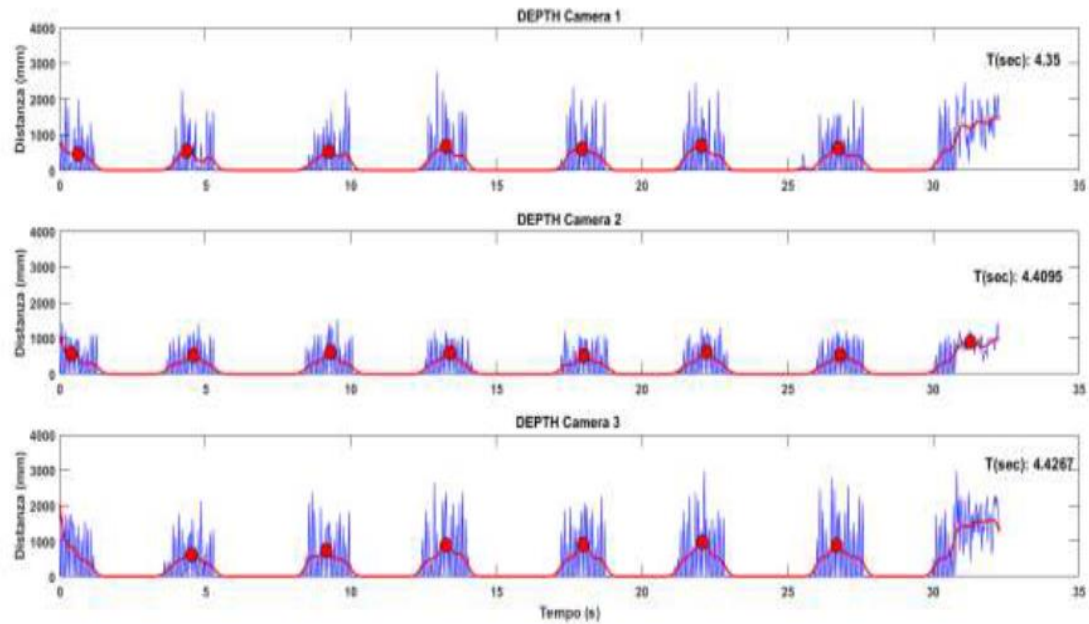


Figure 4.33- Kinect Measured Depth

4.2.3 Depth Analysis: Wall Area

The distance of the camera by the wall is fixed, and it should approximately nine or ten meters, and it should keep constant.

In the **Figure 4.34** it's possible to observe how the oscillating trends described in the previous sections are again present.

In this case, the distance goes again to zero when the Kinect can't observe anything of what it has in front.

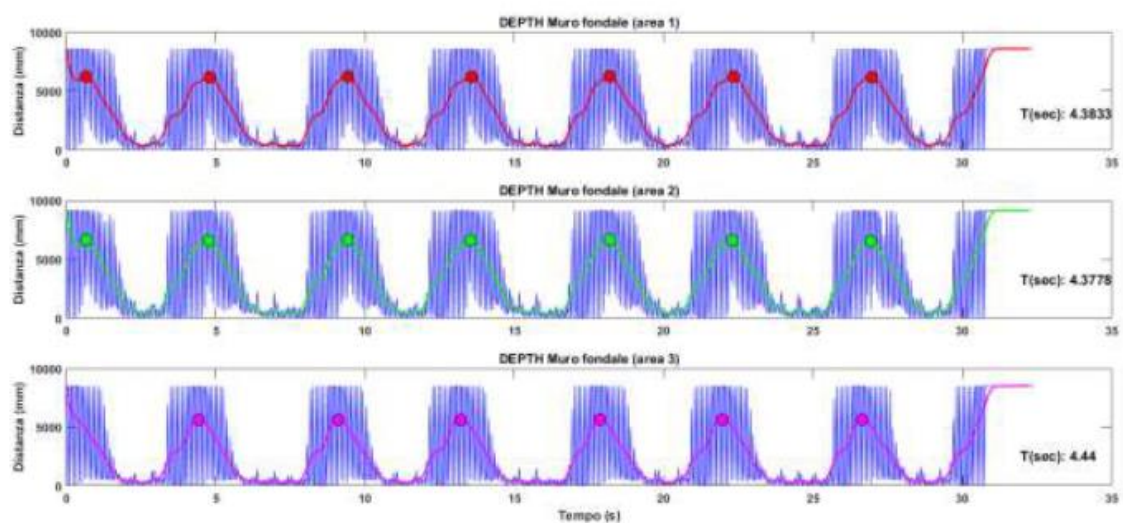


Figure 4.34-Kinect Depth Wall Area

At the final phase of the analysis, the depth is correctly recovered, underlining again the problem deriving by the simultaneous acquisition with the BTS systems.

After these analyses, we concluded that the illuminating of the BTS it's really impactful on the IR signal acquired by the Kinect Azure.

The Kinect acquisition at 30 Hz creates an IR artifact perceived by the Kinect as it there was a low-frequency signal in IR and Depth.

This behavior was analyzed on static parts of the scene, and it's observable in any part of the FoV of the camera, influencing negatively all the 3D reconstruction.

The skeletal joints are, indeed, really unstable and the SDK can't use the information provided by the camera in order to obtain correctly the information.

In this way, the validation of the Kinect Azure has not been possible to practice.

5. Conclusions

The results exposed in [Chapter 4](#), showed how the Orbbec Astra Pro can keep the performances reached by the BTS systems in terms of accuracy in the acquisition.

The experiment conducted relative to the Leg agility has evidenced how in one typical case of clinical rating scale task, the Orbbec can furnish optimal results for the assessment of the patient's condition. His main limitation derives from the concept of RGB-D camera that is: it can only acquire when the subject is positioned in front of the camera and his orientation does not cover any of the joints required for the analysis. Due to this limitation, there is just a percentage of tasks coverable with this system, avoiding the tasks where it is involved the turning or where the patient shows his back to the camera.

Furthermore, it has been captured the movement of a healthy subject in order to evaluate the parameters and there is no evidence of the same behavior of the camera in the recording of a pathological subject, which, however, should be plausible.

It is important to remark, that the Orbbec camera does not need any type of preparation, since it is necessary only the positioning and the turning on of the recording, making this type of tool interesting for a domiciliated system, with no presence of the professionals.

Regarding the Kinect Azure, it is necessary to remark how the validation has been influenced by the problems described in [chapter 4.2](#). In order to solve this impossibility of overlap, there are different possibilities, among which the use of only the cameras behind the Azure, assuming that the interference derives from the frontal cameras or the use of a synchronizing system that forces the acquisition of the Kinect when the BTS pulsation is surely in the Off-phase of its duty cycle.

The developments of this work foresee the test of pathological subjects including more clinical tasks in order to extract more parameters and have further validation of the cameras. Furthermore, the feasibility of including this camera in the medical analysis should be guided by neurologists that should evaluate the parameters provided, giving evidence of their correctness.

A further step is represented by the possibility of making evaluations automatized, collecting patient's data and building a robust classifier with the parameters.

In addition to this, it is essential to be assisted by the physicians that would help in the supervision of the data and their collection.

Different considerations, however, need to be performed about the Optitrack systems. The BTS system is a powerful tool, much more accurate than our systems, but not for this exempt from problematics.

During the acquisitions, different issues have come to light, about the loss of the markers during the movements or the finding of the optimal position in order to grant the capture of all of them.

Furthermore, the preparation that needs to be observed is long and ask the subject a great effort, in order to stay with the markers on the skin for different hours to be analyzed.

One last observation is represented by the cost and the maintenance of the optical systems: it has been used a model that costs about ten thousand euros, and it is enough for the tasks acquired, while the analyzed systems cost about five hundred euros, representing a tool comparable in terms of captures, and much more affordable for the large scale.

LIST OF SYMBOLS

Symbol	Description	Value	S.I.
μ_0	The vacuum permeability	$4\pi \cdot 10^{-7}$	$[\frac{H}{m}]$
i	The current in the circuit	-	[A]
ds	The infinitesimal element of the circuit	-	[m]
b	Coefficient of dumping	-	$[\frac{N}{m/s}]$
k	Coefficient of stiffness	-	$[\frac{N}{m}]$
$\Delta\varphi$	Delta phase	-	-
σ_{xy}	Covariance xy	-	-
R_{xy}	Cross-correlation xy	-	-
ω	Angular velocity	-	$[\frac{rad}{s}]$
\bar{x}	Mean value	-	-

BIBLIOGRAPHY

- [1] Patel V., D. Chisholm., T. Dua, R. Laxminarayan, and M. E. Medina-Mora, editors. 2015. *Mental, Neurological, and Substance Use Disorders*. Disease Control Priorities, third edition, volume 4, chapter 5. Washington, DC: World Bank. doi:10.1596/978-1-4648-0426-7. License: Creative Commons Attribution CC BY 3.0 IGO
- [2] Dugger, B. N., & Dickson, D. W. (2017). *Pathology of Neurodegenerative Diseases*. *Cold Spring Harbor perspectives in biology*, 9(7), a028035. doi:10.1101/cshperspect.a028035.
- [3] Beach T.G., 2017. A Review of Biomarkers for Neurodegenerative Disease: will they swing us across the valley? Banner Sun Health Research Institute, Sun City, AZ USA, doi: 10.1007/s40120-017-0072-x.
- [4] Gao H.M., Hong J.S.,2008. Why neurodegenerative diseases are progressive: uncontrolled inflammation drives disease progression. Neuropharmacology Section,Laboratory of Pharmacology, National Institute of Environmental Health Sciences/National Institutes of Health, Research Triangle Park, NC 27709, USA
- [5] Pal, G., & Goetz, C. G. (2013). Assessing bradykinesia in parkinsonian disorders. *Frontiers in neurology*, 4, 54. doi:10.3389/fneur.2013.00054
- [6] O.R. Pearson, M.E. Busse, R.W.M. van Deursen, C.M. Wiles,2004, Quantification of walking mobility in neurological disorders, QJM: An International Journal of Medicine, [\[academic\]](#).
- [7] Cronin T, Arshad Q and Seemungal BM (2017) Vestibular Deficits in Neurodegenerative Disorders: Balance, Dizziness, and Spatial Disorientation. *Front. Neurol.* 8:538. doi: 10.3389/fneur.2017.00538
- [8] Homann, B., Plaschg, A., Grundner, M., Haubenhofer, A., Griedl, T., Ivanic, G.,Hofer E., Fazekas F. and Homann, C. N. (2013). *The impact of neurological disorders on the risk for falls in the community dwelling elderly: a case-controlled study*. *BMJ open*, 3(11), e003367. doi:10.1136/bmjopen-2013-003367
- [9] Young A. B. (2009). *Four decades of neurodegenerative disease research: how far we have come!*. *The Journal of neuroscience: the official journal of the Society for Neuroscience*, 29(41), 12722–12728. doi:10.1523/JNEUROSCI.3767-09.2009
- [10] Dickerson B.C.,2014, New tools for the evaluation of patients with neurodegenerative disease, *Neurodegenerative Disease Management*, vol.4 no.6., Future Medicine Ltd., <https://doi.org/10.2217/nmt.14.48>
- [11] Chen X., Pan W., 2014, The treatment strategies for neurodegenerative diseases by integrative medicine, *Integrative Medicine International*, Vol.1, No.4, <https://doi.org/10.1159/000381546>
- [12] Veronese, Simone and Gallo, G. and Valle, A. and Cugno, C. and Chio, A. and Calvo, A. and Cavalla, P. and Zibetti.M. and Rivoiro, C. and Oliver, David J. (2017) *Specialist palliative care improves the quality of life in advanced neurodegenerative disorders: Ne-PAL a pilot randomized controlled study*. *BMJ Supportive and Palliative Care*, 7 (2). ISSN 2045-435X.
- [13] Vogel H.P., Influence of additional on interrater reliability in the neurologic examination, 1992, Influence of additional information on interrater reliability in the neurological examination, 42(11) 2076, DOI: 10.1212/WNL.42.11.2076

- [14] Al-Hameed S, Benaissa M, Christensen H, Mirheidari B, Blackburn D, et al. (2019) A new diagnostic approach for the identification of patients with neurodegenerative cognitive complaints. PLOS ONE 14(5): e0217388. <https://doi.org/10.1371/journal.pone.0217388>
- [15] Muilwijk, D., Verheij, S., Pel, J.J. et al. Changes in Timing and kinematics of goal directed eye-hand movements in early-stage Parkinson's disease. Transl Neurodegener 2, 1 (2013) doi:10.1186/2047-9158-2-1
- [16] Brown, R. C., Lockwood, A. H., & Sonawane, B. R. (2005). Neurodegenerative diseases: an overview of environmental risk factors. Environmental health perspectives, 113(9), 1250–1256. doi:10.1289/ehp.7567
- [17] Francisco-Ángel Moreno, José Antonio Merchán-Baeza, Manuel González-Sánchez 2,3, Javier González-Jiménez 1 and Antonio I. Cuesta-Vargas, Experimental Validation of Depth Cameras for the Parameterization of Functional Balance of Patients in Clinical Tests,(2017)
- [18] Peter Berlit , McGraw-Hill Libri Italia, Clinica Neurologica, chapt.7, pg.145-173,[88-386-2235-3]
- [19] Côté R1, Battista RN, Wolfson C, Boucher J, Adam J, Hachinski V., The Canadian Neurological Scale: validation and reliability assessment.
- [20] Peter Berlit , McGraw-Hill Libri Italia, Clinica Neurologica, chapt.8,pg.195-211, ,[88-386-2235-3]
- [21] Perlmutter JS. Assessment of Parkinson disease manifestations. Curr Protoc Neurosci. 2009;Chapter 10:Unit10.1. doi:10.1002/0471142301.ns1001s49
- [22] http://www.movementdisorders.org/MDS-Files1/PDFs/MDS-UPDRS-Rating-Scales/MDS_UPDRS_Italian_Offical_Working_Document.pdf
- [23] Wilson, Braunwald, Isswlbacher, Pedersdorf, Martin, Fauci, Root, Principi di medicina interna, McGraw-Hill Libri Italia, chapt.162, ,[88-386-2417-8]
- [24] https://www.acmt-rete.it/uplds/BERG_ACMT-Rete.pdf
- [25]https://www.cdc.gov/steady/pdf/TUG_test-print.pdf
- [26] David A. Winter, Biomechanics and motor control of human movement, chapt. 2, Pg.50, John Wiley and sons, Inc., 2009, ISBN: 978-0-470-39818-0
- [27] David A. Winter, Biomechanics and motor control of human movement, chapt. 2, Pg.48, John Wiley and sons, Inc., 2009, ISBN: 978-0-470-39818-0
- [28] Seedahmed G., Schenk A. ,Direct linear transformation in the context of different scaling criteria, 10.13140/2.1.3600.4644
- [29] Position and orientation in space of bones during movement: anatomical frame definition and determination. Cappozzo A1, Catani F, Croce UD, Leardini A.
- [30] Alhwarin, Faraj & Ferrein, Alexander & Scholl, Ingrid. (2014). IR Stereo Kinect: Improving Depth Images by Combining StructuredLight with IR Stereo. 10.1007/978-3-319-13560-1_33.
- [31] <https://www.intelrealsense.com/depth-camera-d415/>
- [32] <https://www.intelrealsense.com/depth-camera-d435/>
- [33] <https://orbbec3d.com/product-astra-pro/>
- [34] <https://docs.microsoft.com/it-it/azure/Kinect-dk/hardware-specification>
- [35] <https://nuitrack.com>
- [36] David A. Winter, Biomechanics and motor control of human movement, chapt. 4, Pg.86, Table 4.1, John Wiley and sons, Inc., 2009, ISBN: 978-0-470-39818-0

- [37] <https://p5js.org/reference/#/p5/loadJSON>
- [38] L.Mesin, Introduction to biomedical signal processing, chapt.2, pag.45, L.Mesin, 978-88-92332-48-5
- [39] G.Vicario, R.Levi, Calcolo delle probabilità e statistica per ingegneri, chapt.4, pag.140,Progetto Leonardo, ISBN: 88-86524-16-1
- [40] Wilhelmus Johannes Andreas Grooten,Lisa Sandberg , John Ressiman, Nicolas Diamantoglou, Elin Johansson, and Eva Rasmussen-Barr, Reliability and validity of a novel Kinect based software program for measuring posture, balance and side-bending
- [41] Erik E. Stone, Member, IEEE, and Marjorie Skubic, Member, IEEE, Fall Detection in Homes of Older Adults Using the Microsoft Kinect.
- [42] Chuang-Yuan Chiu¹ , Michael Thelwell¹, Terry Senior¹, Simon Choppin¹ , John Hart¹ and JonWheat², Comparison of depth cameras for three-dimensional reconstruction in medicine
- [43] Calin A.,Coroiu A., Interchangeability of Kinect and Orbbec Sensors for Gesture Recognition, 978-1-5386-8445-0/18/ © 2018 IEEE
- [44] Monica Carfagni, Rocco Furferi , Lapo Governi , Chiara Santarelli, Michaela Servi, Francesca Uccheddu and Yary Volpe ,Department of Industrial Engineering, University, Metrological and Critical Characterization of the Intel D415 Stereo Depth Camera (2019)
- [45] <https://www.btsbioengineering.com/it/prodotti/smart-dx-2/>
- [46] Philip R. Evans, Rotations and rotation matrices, MRC Laboratory of Molecular Biology, Hills Road, Cambridge CB2 2QH, England
- [47] G.Vicario, R.Levi, Calcolo delle probabilità e statistica per ingegneri, chapt.4, pag.142,Progetto Leonardo, ISBN: 88-86524-16-1
- [48] Matteo Giuberti, Student Member, IEEE, Gianluigi Ferrari, Senior Member, IEEE, Laura Contin, Veronica Cimolin, Corrado Azzaro, Giovanni Albani, and Alessandro Mauro, Assigning UPDRS Scores in the Leg Agility Task of Parkinsonians: Can It Be Done through BSN-based Kinematic Variables?, IEEE INTERNET OF THINGS JOURNAL, SPECIAL ISSUE ON “INTERNET OF THINGS FOR SMART AND CONNECTED HEALTH,” JUNE 2014
- [49] Mukaka MM. Statistics corner: A guide to appropriate use of correlation coefficient in medical research. *Malawi Med J.* 2012;24(3):69–71.
- [50] L.Mesin, Introduction to biomedical signal processing, chapt.3.2, pag.96, L.Mesin, 978-88-92332-48-5
- [51] <https://www.ffmpeg.org>
- [52] L.Mesin, Introduction to biomedical signal processing, chapt.4.1, pag.102, L.Mesin, 978-88-92332-48-5